1-2-2013

Characterization Of High-Voltage-Activated Calcium Channels In Retinal Bipolar Cells

Qi Lu
Wayne State University,

CHARACTERIZATION OF HIGH-VOLTAGE-ACTIVATED CALCIUM CHANNELS IN RETINAL BIPOLAR CELLS

by

QI LU

DISSERTATION

Submitted to the Graduate School

of Wayne State University,

Detroit, Michigan

in partial fulfillment of the requirements

for the degree of

DOCTOR OF PHILOSOPHY

2013

MAJOR: ANATOMY & CELL BIOLOGY

Approved by:

_____

Advisor Date

_____

_____

_____

ACKNOWLEDGMENTS

First of all, I want to thank my mentor, Dr. Zhuo-Hua Pan. I was never so committed to research until I joined Dr. Pan's lab. Dr. Pan not only taught me how to do patch clamp recordings, he also triggered my passion for vision research. He helped me develop critical thinking skills, generate ideas, and design feasible experiments. During the four years working with Dr. Pan, gradually I establish a stubborn attitude toward experimental failures and learned to keep on fighting.

I would like to thank my dissertation committee members: Dr. Rodrigo Andrade for your enlightened ideas, generously providing of the 5HTR2a-GFP mouse line and your suggestions, Dr. Rodney Braun for challenging me and strengthening me critical thinking, and Dr. Ryan Thummel for pointing our those important details and aspects I overlooked. I would also like to thank Dr. Paul Walker for pushing me and providing me great help.

I owe my deepest gratitude to Dr. Elena Ivanova. Elena devoted so many time and energy to train me in immunostaining, patch clamp recordings and virus injection. Elena always gave me great knowledge and guidance. I am also grateful to Jingjuan Cui, Yi Zhang, Chaowen Wu, Tushar Ganjawala, Jie Feng, and Zhifei Zhang, for all your kind help during these years. And I enjoyed the time with all of you.

Finally, but by no means least, thanks go to my mom Zheng-Ming Dou, my dad Shipan Lu and my husband Kai Liu for truly unbelievable support. I want to dedicate this thesis to them.

PREFACE

Voltage-gated calcium channels play a key role in many neuronal functions, including controlling electrical excitability and triggering neurotransmitter release. Retinal bipolar cells have been known to possess both LVA and HVA calcium currents. Previous immunostaining and electrophysiological recordings suggest a heterogeneous expression of different types of calcium channels among different bipolar cells. The detailed molecular and electrophysiological properties of the calcium currents in specific bipolar cell types, however, remain largely unknown. In this study, I investigated the electrophysiological and molecular properties of HVA calcium currents in bipolar cells, especially rod bipolar cells, in the mouse retina.

TABLE OF CONTENTS

LIST OF TABLES

LIST OF FIGURES

LIST OF SCHEMES

CHAPTER 1 Background and rationale

Roles of retinal bipolar cells in visual information processing

It is well known that visual information is processed through the retina in parallel fashion (Wu et al., 2000; Wassle, 2004). Retinal bipolar cells (BCs), the second order cells in the retina, not only relay visual signals from rod and cone photoreceptors to retinal third order neurons, amacrine and ganglion cells, but also play an important role in parallel visual processing in the retina. In mammals, there is one type of rod bipolar cell (RBC) and at least nine types of cone bipolar cells (CBCs) based on their terminal stratification at the inner plexiform layer (IPL) (Ghosh et al., 2004; Pignatelli and Strettoi, 2004). More recently, additional subtypes of CBCs have been revealed based on the expression of intrinsic membrane channels and other molecular markers (Jakobs et al., 2003; Fyk-Kolodziej and Pourcho, 2007; Mataruga et al., 2007; Cui and Pan, 2008).

The existence of multiple BC types is believed to be the important anatomical substrate for segregating visual information into parallel pathways. For example, at the BC level, visual signals are segregated into ON and OFF pathways, carried by ON- and OFF-BCs with ON-BCs responding to light increase with membrane depolarization and OFF-BCs to light increase with membrane hyperpolarization.

BCs are also divided into RBCs and CBCs for processing scotopic and photopic visual signals, respectively. Furthermore, the light response waveforms from BCs to third order cells become ever more diversified (Euler and Masland, 2000). The appearance of the diversified response properties in BCs and third order neurons is believed to relate to increasing complexity of visual processing from photoreceptors to ganglion cells. The occurrence of the diversified

light responses in inner retinal neurons (second and third order retinal neurons) has been reported to originate in part at the level of BCs, possibly due to their diversified response waveforms and neurotransmitter release (Awatramani and Slaughter, 2000; Berntson and Taylor, 2000; Euler and Masland, 2000).

Indeed, previous studies have reported that BCs of different types use multiple subtypes of glutamate receptors at their dendrites to filter the visual signal from photoreceptors into different functional groups of BCs (DeVries, 2000). For example, in the primate retina OFF type BCs contacting medium wavelength (M) and long wavelength (L) sensitive cones, express AMPA glutamate receptors. At the other hand, those BCs receiving information of short wavelength (S), express kainite-type glutamate receptors.

In addition, increasing evidence suggests that voltage-dependent membrane channels contribute to the diverse physiological properties of BCs (Burrone and Lagnado, 1997; Mao et al., 1998; Protti et al., 2000; Ma et al., 2005). The BCs of different types have been known to express heterogeneous properties of voltage-gated membrane currents, including voltage-gated Ca^{2+} currents (Pan, 2000), potassium (K^+) currents (Hu and Pan, 2002), sodium (Na^+) currents (Pan and Hu, 2000), inwardly rectifying K^+ currents and hyperpolarization-activated cyclic nucleotide-gated inward currents (HCN or h-currents) (Ma et al., 2003; Muller et al., 2003). Voltage-gated Ca^{2+} channels could be particularly important in governing the physiological properties of retinal BCs, because the influx of Ca^{2+} current can be directly involved in regulating synaptic signal integration, shaping response waveform, as well as triggering neurotransmitter release.

Molecular composition and functions of voltage-gated Ca^{2+} channels

Voltage gated Ca^{2+} channels selectively mediate Ca^{2+} influx, being involved in numerous physiological processes such as muscle contraction, hormone secretion, gene transcription, and synaptic transmission. Voltage-gated Ca^{2+} channels are heteromultimeric protein complexes consisting of a α1 subunit, as well as auxiliary β, α2δ, and possibly γ subunits (Scheme 1A) (Hofmann et al., 1994). Ten α1, four β (β_{1-4}), four α2δ ($\alpha2\delta_{1-4}$), and eight γ (γ_{1-8}) subunits have been cloned (Scheme. 1A). The α1 subunit of 190 to 250 kDa, forms the ion flowing pore and contains the ion selectivity filter and voltage sensors which gate the channels in response to changes in membrane potentials and primarily determines biophysical and pharmacological properties of the channel (Catterall, 2000). Moreover, the α1 subunit is the major target of regulatory molecules, drugs and toxins (Catterall et al., 2007). Auxiliary subunits facilitate membrane targeting of the α1 subunit and influence channel kinetics such as voltage-dependent activation and inactivation (Neely et al., 1993; Tareilus et al., 1997; Yasuda et al., 2004). Intracellular β subunit is a hydrophilic protein, composed of a SH3 (Src homology-3) domain and a guanylate kinase (GK) domain. The β subunit binds with α subunit via a GK domain interaction (Catterall et al., 2013). The α2δ subunit is encoded by a single gene. After it is post translationally cleaved, forms disulfide-bond to the plasma membrane and is anchored, the α2δ subunit is mature. Each of subunits also could be subject to unique modulation by endogenous modulators.

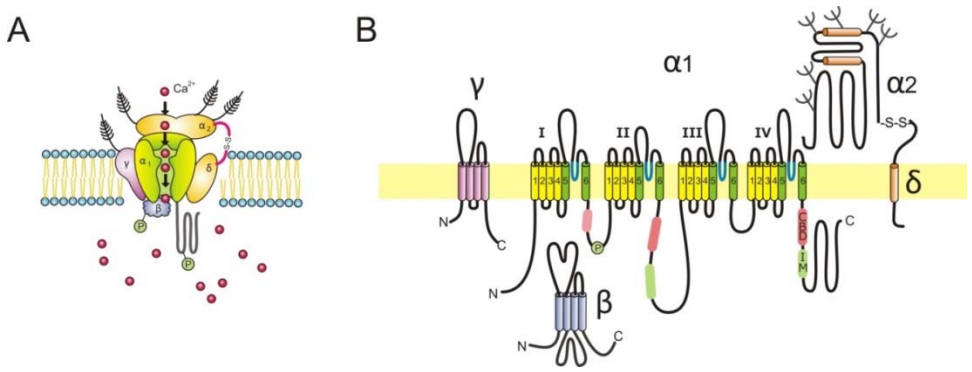

Scheme 1. Schematic illustration of structure of voltage-gated Ca^{2+} channels. *A,* The principal α1 subunit is a transmembrane protein containing a conducting pore, through which Ca^{2+} ions can pass upon opening. The α1 subunit is further regulated by auxiliary subunits: intracellular β subunit, transmembrane γ subunit and a complex of extracellular α2 subunit and transmembrane δ subunit, connected by a disulphide bridge. modified from (Lacinova, 2005). *B,* Diagrammatic representation of the topology of subunits of voltage-gated Ca^{2+} channels. Yellow and green cylinders indicate transmembrane segments of α1 subunit. Green cylinders indicate the charged S4 segment and yellow indicates the pore region. Orange cylinder represents transmembrane segment of δ subunit. Glycosylation is indicated by fork shapes. Modified from (Dolphin, 2003).

Matching percentage	Snutch	Ca_V	Tsien	Ligands		Divalent Block	Relative Conductance	Activation	Inactivation
80% / 90% / 50%	α1S	$Ca_V1.1$	L	DHP (Antagonist: nimodipine) (Agonist: BayK8644)		$Cd^{2+} > Ni^{2+}$	$Ba^{2+} > Ca^{2+}$	HVA > -30 mV	Very Slow (τ > 500 ms)
	α1C	$Ca_V1.2$							
	α1D	$Ca_V1.3$							
	α1F	$Ca_V1.4$							
90% / 50%	α1A	$Ca_V2.1$	P/Q	DHP-insensitive	ω-agatoxin IVA			HVA > -20 mV	Partial (τ ≈ 50-80 ms)
90%	α1B	$Ca_V2.2$	N		ω-conotoxin GVIA				
	α1E	$Ca_V2.3$	R		SNX 482				
30% / 90%	α1G	$Ca_V3.1$	T	DHP-insensitive	mibefradil	$Cd^{2+} < Ni^{2+}$	$Ba^{2+} = Ca^{2+}$	LVA >-70 mV	Complete (τ ≈ 20-50 ms)
	α1H	$Ca_V3.2$							
	α1I	$Ca_V3.3$							

Table 1. Classification, nomenclature and comparison of voltage gated Ca^{2+} channels. Modified from Hille, Ion Channels of Excitable Membrane, Chapter 4, p117) (Hille, 2001; Dolphin, 2003; Lacinova, 2005).

Voltage-gated Ca^{2+} channels are divided into low-voltage-activated (LVA) and high-voltage activated (HVA) Ca^{2+} channels based on their activation threshold (Carbone and Lux, 1984; Ertel et al., 2000). The HVA Ca^{2+} channels are further classified into L-type and non-L-type HVA Ca^{2+} channels based on pharmacological properties. Low-voltage-activated (LVA) Ca^{2+} channels are also named T-type.

T-type Ca^{2+} channel family is encoded by α 1G (Cav3.1), α 1H (Cav3.2) and α 1I (Cav3.3) Ca^{2+} channel subunits (Perez-Reyes, 2003). T-type Ca^{2+} channels are well known for their roles in burst firing and oscillatory behavior in neurons. In chromaffin cells and retinal BCs, T-type Ca^{2+} channels could also mediate transmitter release (Carbone et al., 2006; Pan et al., 2001).

Based on their sensitivity to 1, 4-dihydropyridine (DHP) class of compounds, HVA Ca^{2+} channels are further divided into two subgroups: L-type and non-L-type HVA Ca^{2+} channels. L-type Ca^{2+} channel family is sensitive to DHP antagonists and agonists, such as nifedipine, nimodipine, and BayK8644. They are encoded by α 1S (Cav1.1), α 1C (Cav1.2), α 1D (Cav1.3), and α 1F (Cav1.4). L-type Ca^{2+} channels are present in skeletal muscle, heart, smooth muscle, and neurons (Hess et al., 1984; Nowycky et al., 1985). In most neurons in the CNS, L-type voltage-gated Ca^{2+} channels are primarily targeted to dendrites and the cell soma (Catterall, 2000) and are responsible for Ca^{2+} signals for controlling cell excitability, gene transcription, and neural plasticity (Graef et al., 1999; West et al., 2001). For example, NMDA receptor-independent long-term potentiation (LTP) most often requires the activation of L-type Ca^{2+} channels (Grover and Teyler, 1990). L-type Ca^{2+} channels mediated gene expression and neural plasticity are known to be carried through CREB (cyclic AMP response element binding protein), a calcium-regulated transcription factor. Specifically, L-type Ca^{2+} channels trigger phosphorylation of CREB through activation of the calmodulin (CaM) kinases and CaM kinase

IV (CaMKIV) (Calin-Jageman and Lee, 2008). Thus, through the regulation of CREB, L-type Ca^{2+} channels can potentially regulate a host of genes responsible for a wide range of cellular functions, including activity-dependent synaptic plasticity and tropic factor-dependent neuronal survival (West et al., 2001).

The non-L-type HVA Ca^{2+} channels were subclassified with the aid of several invaluable toxins. They are named P/Q (Cav2.1), N (Cav2.2) and R (Cav2.3). N-type Ca^{2+} channels are blocked by ω-conotoxin GVIA (McCleskey et al., 1987). Mintz's group found that P-type Ca^{2+} channels are blocked by ω-agatoxin IVA and later another subtype, Q-type, were found to be sensitive to ω-agatoxin IVA too (Mintz et al., 1992; Wheeler et al., 1995). These two components are combined as P/Q. R-type Ca^{2+} channels are resistant to DHPs, ω-conotoxin GVIA and ω-agatoxin IVA (Wheeler et al., 1995). P/Q and N type Ca^{2+} channels are expressed on presynaptic terminals and dendrites in CNS to trigger rapid synaptic transmission (Wheeler et al., 1995; Evans and Zamponi, 2006) and mediate dendritic transient Ca^{2+} influx (Catterall, 2000). In particular, the P/Q Ca^{2+} channel is expressed in the cerebellum, particularly in Purkinje and granule cells (Lonchamp et al., 2009). R type Ca^{2+} channel is primarily found to be expressed in hippocampus (Westenbroek et al., 1992; Weiergraber et al., 2007), trigeminal ganglion nociceptive neurons and dorsal root ganglion neurons (Fang et al., 2010). The functions of non-L-type HVA Ca^{2+} channels are considered to trigger action potential as well as neurotransmitter release (Catterall, 2000; Weiergraber et al., 2007). HVA (L-type and DHP-insensitive HVA) and LVA Ca^{2+} channels differ in their distinct biophysical and pharmacological properties (Table 1).

Biophysical and pharmacological properties of L-type voltage gated calcium channels

A hallmark of L-type Ca^{2+} channels is their slow voltage-dependent inactivation. However, the detailed biophysical properties, such as activation threshold, voltage-dependent inactivation, calcium-dependent inactivation, and voltage-dependent facilitation are different among L-type Ca^{2+} channels formed by different α1 subunits (Hess et al., 1984; Koschak et al., 2003). First, among α1C, α1D, and α1F, the α1D exhibits the lowest activation threshold, followed by α1F, while the α1C has the highest activation threshold (Koschak et al., 2003). Second, these three Ca^{2+} channels also show different voltage- and Ca^{2+}-dependent inactivation. α1C exhibits the fastest voltage- and Ca^{2+}-dependent inactivation followed by α1D. Voltage- and Ca^{2+}-dependent inactivation is not apparent in α1F. Finally, these three L-type Ca^{2+} subunits also display different voltage-dependent facilitation (Koschak et al., 2003).

Also, although all L-type Ca^{2+} channels are sensitive to DHP compounds, their sensitivity to DHP antagonists and agonists has been reported to be different among different subunits (Hess et al., 1984; Nowycky et al., 1985) (Table 1). The α1F shows the lowest sensitivity to DHP compared to α1C and α1D. This is because DHPs bind preferentially to the inactivated state of channels. The lack of inactivation of α1F Ca^{2+} channels decreases the apparent affinity to DHP compounds. On the basis of their biophysical characteristics and intermediate DHP sensitivity, α1D and α1F have also been thought to be classified as a functional low-voltage-gated Ca^{2+} channel subgroup.

It should be noted that most studies of the biophysical and pharmacological properties of L-type Ca^{2+} channels was carried out in heterologous expression systems, such as in the HEK cell line (Koschak et al., 2003). Although these studies provide important insights into the

properties of L-type Ca^{2+} channels, the properties of native L-type Ca^{2+} channels could be different. First, it remains unclear whether or what auxiliary subunits are associated with L-type Ca^{2+} channels *in vivo*. The presence of auxiliary subunits could alter the properties of L-type Ca^{2+} channels (Koschak et al., 2003). Furthermore, the central nervous system also utilizes alternative splicing to support an astounding level of structural and functional diversity in the voltage-gated Ca^{2+} channel family. In different tissue types, there are different L-type Ca^{2+} channel α1 subunit mRNA alternative splicing isoform products (Chien and Hosey, 1998; Lipscombe et al., 2002; Tang et al., 2004; Shen et al., 2006; Tang et al., 2007). For example, Doering *et al* 's study revealed that alternative splicing enables functional α1F subunits to be expressed at low levels in the α1F mutant strain (Doering et al., 2008). The presence of multiple alternative splicing variants of L-type Ca^{2+} channel subunits could also alter the properties of L-type Ca^{2+} currents.

Modulation of high voltage gated calcium channel

Ca^{2+} plays an essential role in many normal cellular functions, but Ca^{2+} overloading could also induce toxic effects and cell death. Therefore, Ca^{2+} channels are under restricted regulation by multiple mechanisms (Calin-Jageman and Lee, 2008). One type of regulation is feedback regulation, mainly Ca^{2+}-dependent inactivation and Ca^{2+}-dependent facilitation (Calin-Jageman and Lee, 2008). Both Ca^{2+}-dependent inactivation and Ca^{2+}-dependent facilitation depend on the ubiquitous Ca^{2+}-binding protein calmodulin (CaM). CaM can also facilitate trafficking of α1C in neurons through binding with the C-terminal of the L-type α1 channel (Wang et al., 2007).

Voltage-gated Ca^{2+} channels in general and L-type Ca^{2+} channels in particular are also subject to modulation by many endogenous modulators. The classic modulation is phosphorylation, which might be mediated by G-protein coupled receptors (Dascal et al., 1986;

Fisher and Johnston, 1990; Dolphin, 2003). For example, Gα can mediate voltage-independent Ca^{2+} channel phosphorylation or dephosphorylation to increase or decrease Ca^{2+} current. Gα/PKA and Gq/PLCβ second messenger pathways could up-regulate N and P/Q Ca^{2+} currents by direct channel phosphorylation. In addition, PKA modulates L-type Ca^{2+} channel proteins through interacting with A-kinase anchoring protein (AKAP), which binds with the L-type Ca^{2+} channel protein C-terminal via a leucine zipper motif. Synaptic proteins, such as syntaxin 1A and SNAP-25 bind to the intracellular linker between domains II and III of L-type Ca^{2+} channel proteins (Wiser et al., 1996). Single synaptic proteins inhibit L-type Ca^{2+} channel function, but co-binding of syntaxin 1A and SNAP-25 can induce an activation effect on L-type Ca^{2+} channel proteins (Wiser et al., 1999).

High voltage gated calcium channels in retinal BCs

The presence of L-type Ca^{2+} channels in retinal BCs has been demonstrated by electrophysiological recordings based on their sensitivity to DHP compounds (Maguire et al., 1989; Kaneko et al., 1991; Pan, 2000, 2001). L-type Ca^{2+} currents have been observed in both RBCs and CBCs (Pan, 2000). In particular, the L-type Ca^{2+} currents in RBCs in rodents were found to be located only at the axon terminals (Hartveit, 1999; Pan, 2001), suggesting that they are involved in neurotransmitter release in BCs. Indeed, the involvement of L-type Ca^{2+} channels in the transmitter release in BCs has been demonstrated in Mb-1 BCs in goldfish and in RBCs in rodents (Heidelberger and Matthews, 1992; Singer and Diamond, 2003; Oltedal and Hartveit, 2010). In gold fish Mb1 BCs, the L-type Ca^{2+} channels can generate Ca^{2+} spikes in the dark-adapted retina (Protti et al., 2000).

Interestingly, the involvement of L-type Ca^{2+} channels in neurotransmitter release in retinal neurons (both in BCs and photoreceptors) contrasts to that in the other regions of the CNS

where neurotransmitter release is primarily controlled by non-DHP sensitive HVA Ca^{2+} channels. From a functional point of view, this is not surprising. Retinal BCs and photoreceptors belong to a small class of sensory neurons, including inner ear hair cells, which mainly use graded potential to control neurotransmitter release rather than spikes for signal coding (Barbour et al., 1994). In contrast to spiking neurons in which the Ca^{2+} currents are activated by large depolarization and then rapid inactivation, the Ca^{2+} currents of photoreceptors and BCs are activated at relatively hyperpolarized potentials and do not significantly inactivate (de la Villa et al., 1998; Protti and Llano, 1998). Furthermore, sustained signals, exhibiting little inactivation, and a relatively narrow range of membrane potentials are prominent features of this kind of sensory cell signals (Wilkinson and Barnes, 1996). Thus, L-type Ca^{2+} channels with slow inactivation would be especially suitable to control graded and sustained neurotransmitter release in BCs.

L-type Ca^{2+} currents at the axon terminals of the Mb-1 BCs in goldfish and in mammalian BCs have also been reported to contribute to the stereotypical spontaneous and/or light-evoked waveforms (Heidelberger and Matthews, 1992; Ma and Pan, 2003).

I am particularly interested in the molecular properties of voltage-gated Ca^{2+} channels in retinal information processing. A differential expression of L-type Ca^{2+} channel subunits among different BCs could have important functional implications for visual signal processing in the retina. First, different L-type Ca^{2+} channels are known to have distinct biophysical properties which could result in distinct Ca^{2+} signaling in different BCs. In addition, different L-type Ca^{2+} channels could be subject to distinct modulation by endogenous modulators, which could result in differential regulation of Ca^{2+} signaling in different BCs, thus the information processing pathways at the level of BCs. Furthermore, whether retinal BCs express non-L-type L-type Ca^{2+}

channels remains unknown. Thus, a detailed knowledge of the properties of HVA Ca^{2+} channels, including L-type Ca^{2+} channels, in different types of retinal BCs could provide important insights into the mechanisms of visual information processing in the retina. In addition, the knowledge we gain from these studies could also provide insight into Ca^{2+} signaling and Ca^{2+} channel deficit-related diseases of the visual system.

Molecular properties of HVA Ca^{2+} channels in retinal BCs

Although BCs is known to express only L-type Ca^{2+} channels, the molecular properties of L-type Ca^{2+} channels in different retinal BCs are largely unclear. Previous studies of the molecular properties of the L-type voltage-gated Ca^{2+} channels in the retina in general and in retinal BCs in particular were mainly carried out by immunostaining. The expression of all four Ca^{2+} channel α1 subunits, α1S, α1C, α1D, and α1F, was reported in the retina (Morgans, 1999; Morgans et al., 2001; Xu et al., 2002; Berntson et al., 2003).

The expression of the α1F Ca^{2+} channel subunit in the retina has been well documented. Particularly, α1F is the primary Ca^{2+} channel in controlling photoreceptor transmitter releasing in rod photoreceptors (Berntson et al., 2003). Consistently, mutation of α1F in human can cause incomplete X-linked congenital stationary night blindness, a recessive, nonprogressive visual disease characterized by poor night vision and decreased visual acuity (Miyake et al., 1986). One early study also suggests that α1F subunits are expressed in rod BCs, especially at the axon terminals (Berntson et al., 2003).

α 1D is known to be predominantly expressed in cochlea hair cells (Kollmar et al., 1997). In the retina, Ca^{2+} channels in cone photoreceptors were suggested to be α 1D (Morgans et al., 2005). Abundant L-type Ca^{2+} channel α1D subunit mRNA expression was confirmed in most cells of the inner nuclear layer in the mouse retina (Xiao et al., 2007). The peak of the

electroretinogram was reported to be altered in α1D subunit knockout mice (Wu et al., 2007). It remains unknown whether α1D contribute to the L-type Ca^{2+} currents in BCs.

Immunostaining studies also reported the expression of the α1C Ca^{2+} channel subunit in retinal BCs (Xu et al., 2002; Specht et al., 2009). Especially, the whole RBCs, including dendrites, the cell soma and axon terminals, show immunoactivity against α1C Ca^{2+} channels antibody. Interestingly, this contrasts to the electrophysiological results in which L-type Ca^{2+} currents were only observed in the axon terminals. The reasons for the discrepancy between the immunostaining and electrophysiological results remain to be investigated.

The expression of α1S was recently reported to be expressed on dendritic terminals of ON-BCs (Specht et al., 2009), suggesting it could be involved in synaptic signal integration of BCs.

It also remains largely unclear whether auxiliary subunits are associated with L-type Ca^{2+} channels in retinal BCs *in vivo*. The expression, biophysical and pharmacological properties could be significantly influenced by the auxiliary subunits, notably the β subunits. For example, co-expression of β subunits can increase DHP agents' binding and affinity. The key role of the β2 subunit has been demonstrated by a recent study showing that elimination of this subunit in mouse retina produces a phenotype similar to X-linked congenital stationary night blindness in humans (Ball et al., 2002). The finding indicates that the β2 subunit is obligatorily required for the formation of native retinal L-type Ca^{2+} channels. On the other hand, no retinal phenotype has been reported so far for other β subunit-deficient mice.

The detailed biophysical and pharmacological properties of L-type Ca^{2+} channels in retinal BCs have not been investigated. In retinal BCs of different species, DHP-sensitive Ca^{2+} currents were found to possess properties not typically found for L-type currents in cardiac

myocytes (Adachi-Akahane et al., 1999) or neurons (Sinnegger-Brauns et al., 2009). These were described as faster activation, slower inactivation, negative activation thresholds, and intermediate DHP sensitivity. These properties were thought to be the properties of α1D. However, the more recently discovered α1F also exhibits similar properties.

The heterogeneous properties of L-type Ca^{2+} currents among different BCs were observed in previous results in our laboratory from isolated BCs (Pan, 2000). This together with immunostaining results reported by others led us to hypothesize that there is a differential expression of L-type Ca^{2+} channels among different types of BCs. To test the hypothesis, I will investigate the biophysical properties of HVA Ca^{2+} channels among different BCs. In particular, I will investigate the molecular identity of Ca^{2+} channels in RBCs.

Using L-type Ca^{2+} channel KO mice

The characterization of the properties of L-type Ca^{2+} channels in BCs has been hampered by several factors. First, although a number of antibodies have been available for L-type Ca^{2+} channels, most of the antibodies for L-type Ca^{2+} channels, except α1F, have not been validated in knockout animals and thus make the interpretation of the immunostaining data inconclusive. Second, multiple splicing variants of L-type Ca^{2+} channels could exist, and some of them may not display the conventional biophysical and pharmacological properties of known L-type (Murbartian et al., 2002). Furthermore, since there are about ten types of BCs, the lack of biomarkers for specific BC types makes the electrophysiological studies of a specific BC type difficulty.

The recent availability of several L-type Ca^{2+} channel KO or mutant mice and several BC type specific GFP transgenic mice has provided valuable tools for the study of the properties and functions of L-type Ca^{2+} channels (Moosmang et al., 2007). First, a spontaneous α1F mutant

mouse is available from Jackson Laboratory. In addition, conventional α1D KO and conditional α1C KO mice have been produced (Platzer et al., 2000; White et al., 2008). Both mice are viable and did not show gross abnormality of retinal anatomy. In these studies, I will take advantage of these L-type Ca^{2+} channel knockout and mutant mice. The L-type Ca^{2+} channel KO and mutant mice could enable us to validate the molecular composition of L-type Ca^{2+} channel α1 subunits in the retina and in retinal BCs.

Characterization of fluorescence protein-expressing retinal BCs in transgenic mouse lines

The second factor that hampers the study of Ca^{2+} current in BCs is the lack of BC specific markers. In particular, markers that can be used to identify BC types for *in vitro* electrophysiological studies are lacking.

Several immunocytochemical markers for BCs are discovered to label specific BC types (Wassle et al., 2009). However, most of them are not suitable for *in vitro* labeling except CD15, which labels type 2 BCs of mice. For example, protein kinase C (PKCα) is RBC marker. Synaptotagmin 2 (Syt2) is type 2 and type 6 CBC marker.

Recently, the generation of transgenic mice with green fluorescence protein (GFP) expression has become an alternative approach to identify cell types in the CNS and the retina (Gong et al., 2003). Several transgenic mouse lines in which specific retinal BC type (s) labeled with fluorescence proteins have been previously described, such as ON BCs (Morgan et al., 2006; Dhingra et al., 2008), type 7 CBCs (Wong et al., 1999; Huang et al., 2003), and type 9 CBCs (Haverkamp et al., 2005), and, more recently, type 5 CBCs (Wässle et al., 2009). The development of more BC type specific GFP or Cre transgenic mouse line will facilitate the *in*

vitro electrophysiological recordings of specific retinal BC types. In this study, we have characterized a GFP transgenic mouse line, 5HTR2a-GFP. In this line, type 4 CBCs are selectively labeled by GFP.

CELL TYPE	MARKER			TRANSGENE	
type 1	NK3R				
type 2	NK3R	Recoverin	Syt2		
type 3a	HCN4				
type 3b	PKARIIβ				
type 4	Csen			5HT2aR-EGFP	
type 5				5HT3R-EGFP	Grm6-tdTOMATO
type 6			Syt2		Grm6-tdTOMATO
type 7				GUS-GFP	Grm6-tdTOMATO
type 8					Grm6-tdTOMATO
type 9					Grm6-tdTOMATO
RBC	PKCα			GUS-GFP	Grm6-tdTOMATO

Table 2. BC types of the mouse retina and the markers and transgenic mouse lines used in the present study modified from (Wassle et al., 2009).

Characterization of Cre recombinase expressing pattern in transgenic mouse lines

The third factor that hampers the study of Ca^{2+} current in BCs is the lack of BC specific knockout systems for *in vitro* electrophysiological studies. There are two reasons for us to further characterize Cre-transgenic animal lines such as follows: (1) This provides another approach for BC identification. (2) Cre recombination can be used to knockout genes in specific cell types.

The manipulation of gene expression in specific BC type (s) in the retina is able to investigate the molecular mechanisms of physiological and pathological properties of BCs. The powerful Cre/LoxP recombination system has become one of the approach to control gene expression *in vivo* (Nagy, 2000; Branda and Dymecki, 2004), especially with the increasing availability of cell- and tissue-specific Cre transgenic mouse lines (Gaveriaux-Ruff and Kieffer, 2007; Gong et al., 2007). A widely used conditional gene-targeting approach is to cross cell- and tissue-specific Cre transgenic mouse lines with Cre-dependent reporter or conditional mouse

lines. Cre transgenic lines, especially those produced by conventional methods (via pronuclear injection), are subject to the local chromatin environment (i.e., position effect), which could lead to transgene silencing or variable ectopic expression (Milot et al., 1996; Williams et al., 2008; Le, 2011; Smith, 2011). To specialize and evaluate the utility of Cre-mediated reporter gene expression require *in vivo* screen of the expression pattern and recombination efficiency in detail. Cre-dependent virus-mediated gene delivery is another powerful approach that can be used to target a transgene to Cre-expressing cells in transgenic mouse lines (Schnutgen et al., 2003; Atasoy et al., 2008; Kuhlman and Huang, 2008).

Recombinant adeno-associated virus (rAAV) vectors have been particularly widely used in retinal gene transfer (Surace and Auricchio, 2008). Due to their anatomical location in the middle of the retina, however, retinal BCs are the most inaccessible cell types in the retina to virus transduction. The ability of the Cre-dependent rAAV vector-mediated transgene delivery to retinal BCs in Cre transgenic mouse lines has not been examined.

So far, only a small number of retinal BC-expressing Cre transgenic mouse lines have been reported (Barski et al., 2000; Rowan and Cepko, 2004; Saito et al., 2005; Zhang et al., 2005; Ivanova et al., 2010; Nickerson et al., 2011). Most of them were driven by the Pcp2 (Purkinje cell protein 2) promoter, a gene that is known to target Purkinje cells in the cerebellum as well as in retinal RBCs (Oberdick et al., 1990). Few Cre transgenic lines have been reported to target retinal cone BCs. One of them is Chx10-cre, which was reported to target the Cre recombinase in multiple retinal BC types (Rowan and Cepko, 2004).

In this study, we examined the Cre-mediated recombination expression profiles of three retinal BC-expressing Cre-transgenic lines, 5-HTR2a-cre, Pcp2-cre, and Chx10-cre, by crossing these lines to a strong Cre reporter mouse line. We characterized the Cre-mediated expression

patterns in multiple BC types in the 5-HTR2a-cre and Pcp2-cre mouse lines. We also examined the ability and transduction efficiency of Cre-dependent rAAV-mediated transgene delivery to BCs of the BC-expressing transgenic lines. We found that a Cre-dependent rAAV2/2 vector using cytomegalovirus (CMV) promoter and containing a capsid mutation of Y444F is capable of achieving Cre-mediated transgene expression in retinal BCs.

CHAPTER 2 Characterization of GFP-expressing retinal cone bipolar cells in a 5-HTR2a transgenic mouse line

SUMMARY

Retinal BCs relay visual information from photoreceptors to ganglion cells. The various types of BCs are involved in the segregation of visual information into multiple parallel pathways within the retina. Finding molecular markers that can label specific retinal BCs could greatly facilitate the investigation of BC functions in the retina. The transgenic approaches of expressing green fluorescence protein (GFP) in specific cell type(s) enable studies for the morphology and function of specific cell types in the CNS and the retina. In this study, we report a 5-hydroxytryptamine-2a (5-HTR2a) transgenic mouse line in which the expression of GFP fluorescence was observed in two populations of BCs in the retina. Based on the terminal stratification and immunostaining, the majority of the GFP labeled BCs were found to be type 4 CBCs. In addition, a small number of weakly labeled BCs were also observed, which might be type 8 or 9 CBCs. The expression of GFP in retinal CBCs was seen as early as on postnatal day 5. In addition, despite the severe retinal degeneration due to carrying an rd1 (or Pde6brd1) gene in this transgenic line, the densities of the GFP labeled CBCs were stable up to at least six months of the age. This transgenic mouse line will be a useful tool for the study of type 4 cone BCs in the retina under normal as well as different disease conditions.

Key words: Green fluorescence protein, type 4 cone bipolar cell, retina, 5-HTR2a, transgenic mouse.

INTRODUCTION

Retinal BCs, the second order neurons in the retina, relay visual information from photoreceptors to retinal third-order neurons. BCs comprise multiple types which are essential for segregating visual information into multiple parallel pathways in the retina (Wu et al., 2000; Wassle, 2004). BCs are subdivided into ON- and OFF-types based on their light response polarity and are also subdivided into rod and cone BCs based on their synaptic inputs. In mammals, a single type of RBC (Dowling and Boycott, 1969; Boycott and Kolb, 1973; Dacheux and Raviola, 1986) and about nine types of CBCs have been described primarily based on their terminal stratification at the inner plexiform layer (Famiglietti, 1981; Kolb et al., 1981; Pourcho and Goebel, 1987; Euler and Wassle, 1995; Ghosh et al., 2004; Pignatelli and Strettoi, 2004; Wassle et al., 2009). In addition to their distinct morphological properties and, likely, unique synaptic connections with photoreceptors and third order retinal neurons, increasing evidence also suggests that BCs of each type express a distinct array of membrane channels and receptors (DeVries, 2000; Pan and Hu, 2000; Hu and Pan, 2002; Muller et al., 2003; Ma et al., 2005; Ivanova and Muller, 2006; Fyk-Kolodziej and Pourcho, 2007). Thus, the detailed characterization of the anatomical and physiological properties of individual BC types could provide important insights into the functional roles of retinal BCs in retinal processing. Finding BC specific markers could facilitate such studies.

The transgenic approaches of expressing green fluorescence protein (GFP) in specific cell type(s) enable studies for the morphology and function of specific cell types in the CNS and the retina (Gong et al., 2003). Several transgenic mouse lines in which specific retinal BC type (s) labeled with fluorescence proteins have been previously described, such as ON BCs (D'Hooge et al., 2003; Morgans et al., 2006), type 7 CBCs (Miller et al., 1999; Huang et al., 2003), and type 9 CBCs (Haverkamp et al., 2005), and, more recently, type 5 CBCs (Wassle et al., 2009) . In this

study, we report a 5-hydroxytryptamine-2a receptor (5-HTR2a) transgenic mouse line in which strong GFP expression was found in type 4 cone BCs.

METHODS

Animals

5-HTR2A-EGFP transgenic mice were obtained from Mutant Mouse Regional Resource centers (MMRRC; Line: DQ118). The transgenic mice were generated by homologous recombination with a bacterial artificial chromosome (BAC) containing the promoter of 5-HTR2A receptor with the 5-HTR2A receptor coding sequence being replaced by a sequence encoding the EGFP reporter gene (Gong et al., 2003). All animal-handling procedures were approved by the Institutional Animal Care and Use Committee at Wayne State University and were in accord with the NIH Guide for the Care and Use of Laboratory Animals. Most of the experiments were carried out on mice at the age of one month unless otherwise indicated.

Immunocytochemical staining

Mice were deeply anesthetized with CO_2 and decapitated. The retinas were fixed in the eyecups with 4% paraformaldehyde in 0.1 M phosphate buffer (PB) for 20 minutes. The GFP fluorescence without enhancement by antibody staining was sufficient to visualize the GFP labeled cells. The expression of GFP in the retina was examined in retinal whole-mounts and vertical sections. For whole-mounts, after fixation the retina was dissected free in PB solution, flat mounted on slides, and cover slipped. For retinal vertical sections, the retinas were cryoprotected in a sucrose gradient (10%, 20%, and 30% w/v in PB, respectively), and cryostat sections were cut at 20 μm.

To identify the GFP expressing cell types, the GFP fluorescence was enhanced by applying antibodies against GFP and the GFP labeled cells were co-stained with other retinal cell

specific antibodies. The following antibodies were used in this study: rabbit anti-GFP (1:2000; Molecular Probes); mouse anti-GFP (1:2000; Neuromab); goat anti-choline acetyl transferase (CHAT, 1:2000; Chemicon); rabbit anti-HCN4 (1:500; Alomone Labs); mouse anti-protein kinase A (1:80000; BD); mouse anti-calsenilin (1:2000; W. Wasco, Harvard Medical School); mouse anti-synaptotagmin II (Syt-2; 1:600; Nalgene); rabbit anti-serotonin 2A receptor (1:800; Immunostar).

For immunostaining, retinal whole-mounts or sections were blocked for 30 mins in a solution containing 5% Chemiblocker (membrane-blocking agent, Chemicon), 0.5% Triton X-100 and 0.05% sodium azide (Sigma). The primary antibodies were diluted in the same solution and the whole mount retinas were immersed in overnight followed by incubation (1 h), and in the secondary antibodies which were conjugated to Alexa 555 (1:600; red fluorescence, Molecular Probes) and Alexa 488 (1:600, green fluorescence, Molecular Probes). All steps were carried out at room temperature (RT).

All images were made under a Zeiss Axioplan 2 microscope with the Apotome oscillating grating to reduce out-of-focus stray light. Individual cells were selected and Z-stacks images were captured using the Zeiss Apotome microscope. Image projections were made by collapsing individual z-stacks of optical sections into a single plane unless otherwise specifically indicated. The brightness and the contrast were adjusted to acquire optimal signals with Adobe Photoshop CS4.

Primary Antibody	Cell type	Source	Dilution
NK3, neurokinin-3 receptor	Type1	Dr. Hirano, Geffen School of Medicine at University of Los Angeles, Los Angeles, CA	1:500
Syt2, mouse anti-synaptotagmin II	Type2	Type6 Zebrafish International Resource Center, University of Oregon, Eugene, OR.	1:200
Recoverin, rabbit anti recoverin	Type2	Gift from Dr. Dizhoor and also available in Chemicon	1:1000
HCN4, rabbit anti hyperpolarization activated cyclic nucleotide-gated channels 4	Type 3A	Alomone Labs	1:500
Alpha1H, goat anti T-type Ca^{2+} channels	Type 3B	Santa Cruz	1:50
Csen, mouse anti-calsenilin	Type4	Dr. Wasco, Harvard Medical School, Charlestown, MA	1:2000
PKARIIβ, anti-protein kinase A, regulatory subunit IIβ	Type 3B	BD Biosciences	1:3000
PKC, mouse anti-protein kinase C	RBC	Santa Cruz	1:20000
GoA, rabbit/mouse anti Goalpha	All ON-type	Millipore	1:20000
CHAT, goat anti choline acetyl transferase	Starburst amacrines	Chemicon	1:2000
Calretinin, mouse anti calretinin	Amacrines	Chemicon	1:10000

Secondary antibody	Antiserum type Coupled	Company	Dilution
Donkey -anti- Rabbit	Alexa488	Molecular probe	1:500
Donkey-anti-Rabbit	Alexa555	Molecular probe	1:500
Goat-anti- Rabbit	Alexa488	Molecular probe	1:500
Donkey-anti- Mouse	Alexa488	Molecular probe	1:500
Donkey -anti- Mouse	Alexa555	Molecular probe	1:500
Donkey -anti- Mouse	AMCA	Jackson	1:200
Goat-anti- Mouse	Alexa488	Molecular probe	1:500
Donkey -anti- Goat	Alexa555	Molecular probe	1:500
Donkey -anti- Goat	Alexa488	Molecular probe	1:500

Table 3. Primary and secondary antibody lists

RESULTS

GFP expression was observed in the retina of the GFP-transgenic mouse line under the control of 5-HTR2a promoter. In retinal whole-mounts, GFP labeled cell somas were observed throughout the entire retina with the focal plane at the inner nuclear layer (INL) (Fig. 1A). Most of the cell somas were brightly labeled. Some weakly labeled cells were also observed. When examined in retinal vertical section, the labeled cells located in the (INL) were found to be BCs based on their morphological characteristics (Fig. 1B). The somas of the labeled cells were located in the distal portion of the INL with their dendrites and axon terminals extending into the outer plexiform layer (OPL) and the inner plexiform layer (IPL), respectively. The vast majority of the labeled axon terminals ramified in the distal portion of the IPL. Some axon terminals were found to ramify in the inner portion of the IPL but they are barely visible without antibody staining (see below). In addition, some weakly labeled cells located in the retinal ganglion cell layer were observed (see Fig. 1B).

It should be noted that since the 5-HTR2a transgenic mice were generated in a FVB/N-Swiss Webster hybrid background which carries an rd1 (or Pde6brd1) gene (Bowes et al., 1990), these mice displayed rapid retinal degeneration. Only a single layer of photoreceptor cell bodies remained at the age of one month (see the Nomarski micrograph in the left panel of Fig. 1B).

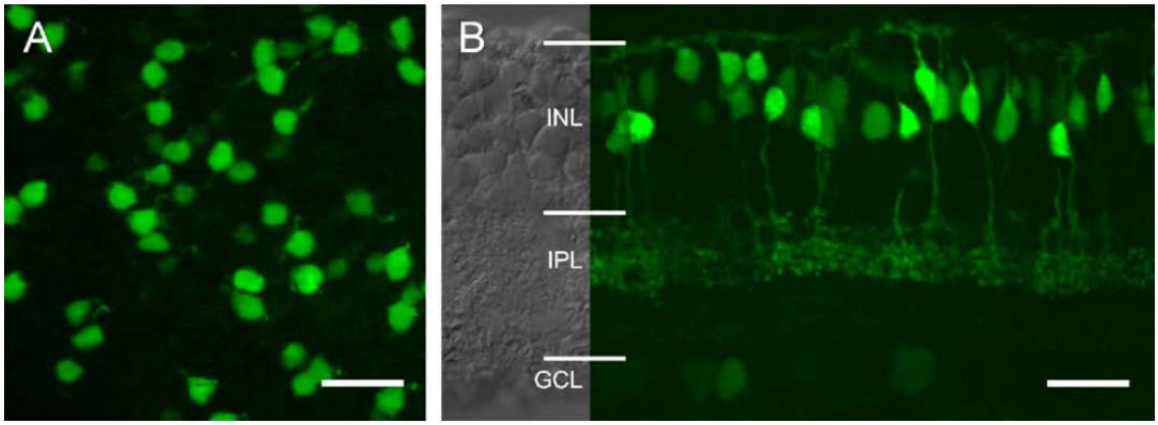

Figure 1. GFP labeled cells in the 5-HTR2a transgenic mouse line. *A*, GFP labeled cells viewed in retinal whole-mount. *B*, GFP labeled cells viewed in retinal vertical section. Left panel in B shows the Nomarski micrograph. Scale bars: 25 μm.

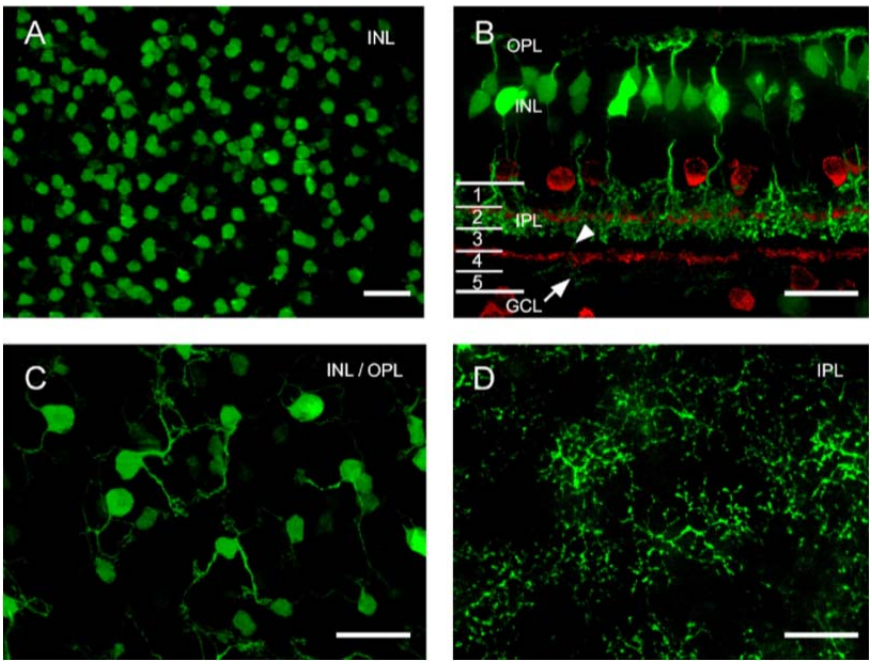

Figure 2. GFP labeled retinal BCs after the enhancement by anti-GFP antibody. *A*, GFP labeled cells viewed in retinal whole-mount with the focal plane at the INL. *B*, GFP labeled cells were co-labeled with anti-CHAT antibody (red) viewed in retinal vertical section. The weakly GFP labeled axon terminals located in the proximal portion of the IPL are identified by an arrow the axon is identified by an arrowhead. *C*, Whole-mount view of the dendritic trees of the GFP labeled CBCs with stacked image that captured both cell somas and dendrites. *D*, Whole-mount view of the axon terminals of the labeled CBCs with the focal plane at the IPL. The images of C and D were taken at the same field. Scale bars: 25 μm.

To examine the labeled BCs in more detail, GFP fluorescence was enhanced by an antibody to GFP. Again, cell somas with strong and weak GFP expression were observed in retinal whole-mounts with the focal plane at the INL (Fig. 2A). Figure 2B shows the double staining with an antibody to choline acetyltransferase (CHAT) in retinal vertical section. Clearly, the strongly GFP-labeled axon terminals ramified in sublamina 1 and 2 of the IPL. The weakly GFP-labeled axon terminals stratified in sublamina 4 and 5 (an axon is identified by an arrowhead the axon terminals are identified by an arrow in Fig. 2B). Figure 2C shows a stacked image in retinal whole-mount that captured both cell somas and dendrites. Each cell soma sends out several dendritic branches with distal apical terminals, presumably forming contacts with photoreceptor cells. Figure 2D shows a stacked image focusing on the distal portion of the IPL that was taken at the same field as in figure 2C. The terminal arborizations of individual BCs are clearly visible.

Based on the previously reported classification of retinal BCs (Ghosh et al., 2004) , the strongly GFP labeled BCs with their axon terminals ramifying in sublamina 1 and/or 2 should be OFF type CBCs whereas those weakly labeled BCs with their axon terminals ramifying in sublamina 4 and 5 should be ON type BCs. To identify the BC types, we co-stained GFP-positive cells with several BC-specific antibodies. First, the GFP-labeled BCs were not found to be stained by an anti-recoverin antibody (Fig. 3A-C) which labels type 2 CBCs in the mouse retina (Haverkamp et al., 2003). Second, the GFP-labeled BCs were not co-stained with an anti-HCN4 antibody (Fig. 3D-F). In addition, the GFP labeled BCs were not co-stained with an anti-PKARIIβ antibody (Fig. 3G-I) with the exception of a few cells (such as the cell identified by an arrow in Fig. 3G and H). HCN4 and PKARIIβ were reported to label two subtypes of type 3 CBCs (Mataruga et al., 2007). Furthermore, the GFP labeled BCs were negative to an anti-

synaptotagmin II (Syt-2) antibody (Fig. J-L). The anti-Syt 2 antibody has been reported to label type 2 (Fox and Sanes, 2007) and type 6 BCs (Wassle et al., 2009). The enlarged images in the insertions of Figure J-L show the lack of co-localization of the Syt-2 positive axon terminals and the weakly GFP labeled axon terminals in the lamina 5 and 6. These results suggest that the GFP expressing BCs are not type 2, 3, or 6.

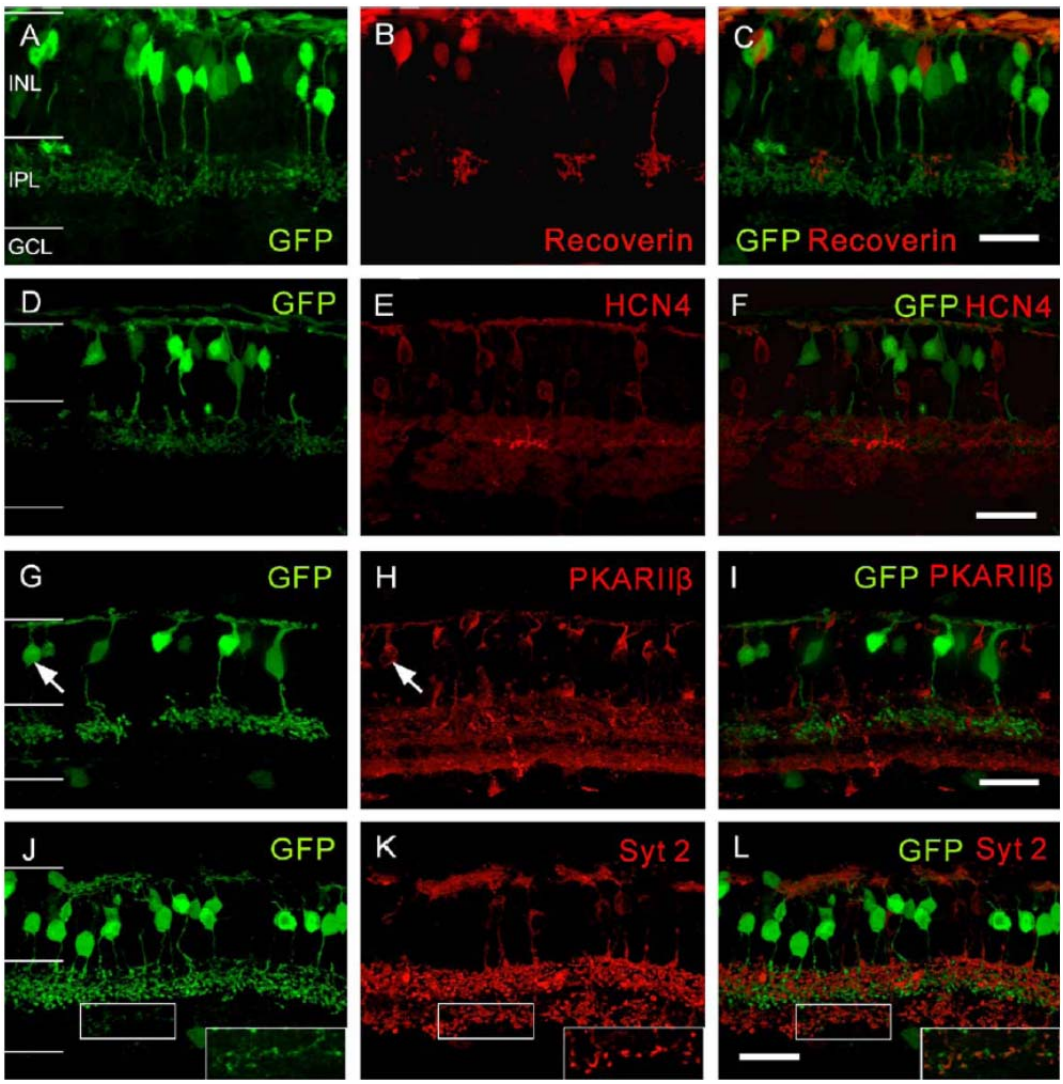

Figure 3. Double immunostaining using GFP and retinal BC specific antibodies. *A-C,* Retinal vertical section was immunostained for GFP in *A* and recoverin in *B*. The superimposition of *A* and *B* in *C*. The double immunostaining for GFP and HCN4 in *D-F*, for GFP and PKARIIβ in *G-I* and for GFP and Syt-2 in *J-L*. The enlarged insertions in the bottom-right of *J-L* are single z-section images. Scale bars: 25 μm.

On the other hand, we found that the majority of the GFP-labeled BCs were stained by an anti-calsenilin antibody, which was reported to stain type 4 CBCs (Haverkamp et al., 2008). Figure 4A-C shows the co-staining of GFP-positive cells with calsenilin in retinal whole-mount with the focal plane at the INL. The majority of the GFP labeled cells including all the strongly labeled cell somas and a small portion of the weakly labeled cell somas were positive for

calsenilin. The co-localization of the GFP and calsenilin positive BCs (cell soma) was also apparent in vertical section (Fig. 4D-F). This result indicates that the majority of the GFP-label BCs, including all strong GFP-labeled BCs, are type 4 CBCs. In addition, in both whole-mounts and retinal vertical sections, all calsenilin-positive cells were found to express GFP, suggesting that all type 4 cells are labeled by GFP. The cell densities for the calsenilin positive and negative cells at the ages of one month and 6 months were counted and the values are shown in Table 4. The cell densities for the calsenilin-positive (type 4) and negative cells were not found to be significant different between the ages of 1 month (wholemount retina; n = 12 retinas; n = 6 mice) and 6 months (wholemount retina; n = 10 retinas; n = 5 mice).

To examine the developmental and age-dependent expression of GFP in this transgenic line, the expression of GFP was examined from postnatal day 5 to 6 months of age. As shown in Figure 5A, the expression of GFP in the INL was already observed at postnatal day 5, although only a few GFP labeled cells were observed in the INL at this time point. At P7, many GFP labeled cone BCs were clearly seen (Fig. 5B). As a note, the photoreceptor cells were present at these early postnatal ages. Figure 5C-D shows the expression of GFP in the retinas at the ages of two weeks, one month, and 6 months. The expression was persistent up to at least at the age of 6 months, the oldest animals that were checked in this study.

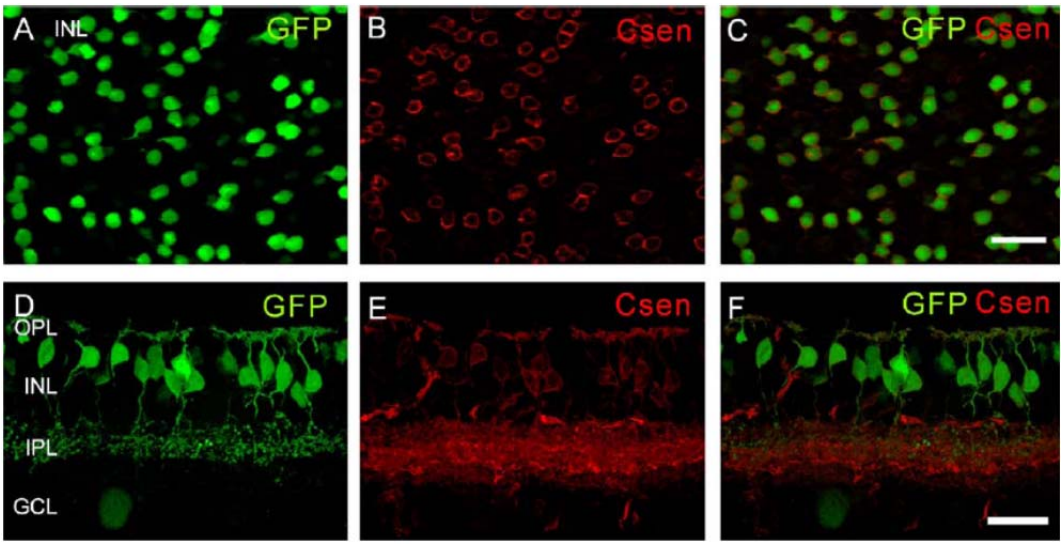

Figure 4. Double immunostaining with anti-GFP and anti-calsenilin antibodies. *A-C,* Co-staining of GFP in *A* and calsenilin in *B* viewed in retinal whole-mount. The superimposition of *A* and *B* in *C*. *D-F*, Co-staining of GFP in *D* and calsenilin in *E* viewed in retinal vertical section. The superimposition of *D* and *E* in *F*. Scale bars: 25 μm.

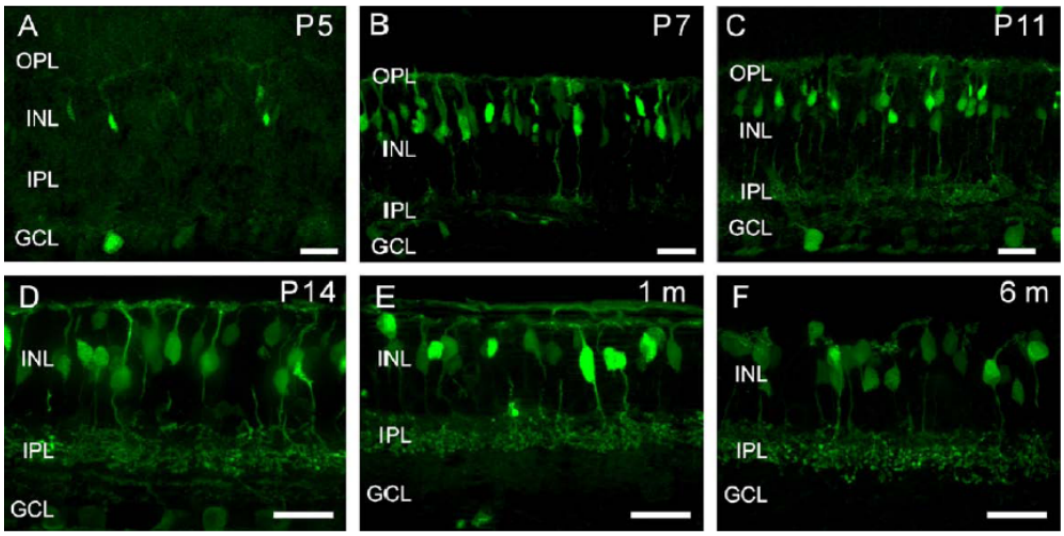

Figure 5. The age-dependent expression of GFP in retinal BCs. The expression of GFP viewed in retinal whole-mounts and vertical sections at the ages of postnatal *A* day 5, *B* 7, *C* 11, *D* two weeks, *E* one month, and *F* 6 months. Scale bars: 25 μm.

	1 month	6 months
Calsenilin-positive CBCs	3,561 ± 333 / mm^2	3,659 ± 780 / mm^2
Calsenilin-negative CBCs	1,564 ± 619 / mm^2	1,543 ± 757 / mm^2

Table 4. Comparison of Calsenilin-positive and negative CBCs at the ages of 1 and 6 months. The cell numbers are the average of eight 40X pictures (0.0037 mm^2 per image; four images are taken from central portion of the retina and the other four are taken from peripheral areas; n = 12 retinas for 1 month; n = 10 retinas for 6 months)

DISCUSSIONS

This study revealed GFP labeled BCs in a 5-HTR2a transgenic mouse line. Our results show that the majority of the GFP labeled BCs are type 4 CBCs. This is based both on their terminal stratification pattern and immunostaining. First, the axon terminals of the strongly GFP labeled BCs were found to ramify in sublamina 1 and 2 of the IPL. Based on the classification of BCs in rodents, type 1-4 BCs have been described to have their axon terminals ramifying in sublamina 1 and/or 2 (Ghosh et al., 2004). However, among them, only type 4 CBCs have their axon terminals ramifying in both sublamina 1 and 2. Second, the GFP labeled cells were immunoreactive to anti-calsenilin antibody, an antibody that has been shown to stain type 4 CBCs in the mouse retina (Haverkamp et al., 2008). Furthermore, the GFP labeled BCs were found to be negative to antibodies against recoverin and Syt-2. Both of these antibodies label type 2 CBCs in the mice. In addition, the GFP labeled BCs were not found to co-localize with HCN4-positive cells and PKARIIβ positive cells, with the exception of a few cells for the latter. HCN4 and PKARIIβ antibodies have been reported to label two subtypes of type 3 CBCs (Mataruga et al., 2007). The reason for the localization of very few GFP labeled cells and PKARIIβ positive cells is not clear. It might be possible that very few GFP labeled BCs were type 3 CBCs or the anti-PKARIIβ antibody could occasionally label type 4 CBCs.

In addition, we found that the axon terminals of a small portion of GFP labeled BCs, albeit weakly labeled, ramified in sublamina 4 and 5. Because the diffuse nature of their axon terminals in the proximal portion of the IPL, they are unlikely to be type 7 CBCs which are restricted their axon terminal stratification restricted to sublamina 4 (Huang et al., 2003) or RBCs which have their axon terminals stratifying in sublamina 5, close to the ganglion cell layer. Also, since neither the GFP labeled BC somas nor the weakly labeled axon terminals were stained by an anti Syt-2 antibody which stains type 2 and 6 CBCs, the CBCs with their weakly labeled axon terminals in the proximal portion of the IPL cannot be type 6 CBCs. Taken together, our results suggest that the weakly labeled axon terminals likely belong to type 8 or 9 CBCs. Unfortunately, currently no antibodies are available that can label type 8 or 9 CBCs.

The expression of GFP in CBCs in this transgenic mouse were observed as early as postnatal day 5 and the expression is stable at least up to the age of 6 months. The cell densities for both the calsenilin positive and negative CBCs at the age of 1 and 6 months were not found to be significantly changed. The value for the calsenilin positive cells is ~3600/mm^2, which is slightly higher than the value of ~3,000/mm^2 in type 4 CBCs reported by a recent study (Wassle et al., 2009). The discrepancy could be due to different mouse strains used in these studies (FVB/N-Swiss vs. C57BL/6J). The cell density for calsenilin negative cells is ~1,500/mm^2. The cell density of the type 9 CBCs was reported to be around 600/mm^2. So far, the cell density of the type 8 CBCs remains unknown.

It is worth to point out that since the mouse strain used in this study carries an rd1 (or Pde6brd1) gene, the un-altered cell density observed for both types of GFP labeled BCs between the ages of one month and 6 month suggests that retinal remodeling did not cause significant cell death of these CBCs in this rd1 mouse strain up to 6 months of age. However, a dramatic

morphological remodeling of second order cells after the death of photoreceptors has been previously reported (Strettoi and Pignatelli, 2000). Thus, it would be interesting to examine how the retinal degeneration affects the synaptic circuits. The transgenic mouse line with GFP labeled BCs could be used for such a purpose.

So far, whether mammalian retinas express 5-HTR2a immunoactivity remains unclear. An early study reported 5-HTR2a immunoactivity in the retinas of rabbit (Pootanakit et al., 1999). The staining was found to be in photoreceptor terminals and RBCs. Using two different anti-5-HTR2a antibodies, a recent study showed the 5-HTR2a immunoactivity in glia cells and some amacrine cells in the bullfrog retina but not in the rat retina (Han et al., 2007). Since the antibody used by Pootanakit and colleague (1999) was the only one that has been reported to show immunoactivity in the mammalian retina so far, we examine the expression pattern of this same antibody in this 5-HTR2a transgenic mouse line. Interestingly, our results show this antibody stained a certain population of CBCs, but these BCs were not found to co-localize with the GFP labeled CBCs. It remains unknown whether the discrepancy of the 5-HTR2a immunoactivity and the GFP expression is due to a non-specificity of this 5-HTR2a receptor antibody in the mouse retina or the non-specificity of the GFP targeting of this transgenic mouse line, or both. Nevertheless, the targeting expression of GFP to the specific CBCs in this transgenic mouse line will be a useful tool for retinal research.

Transgenic mouse lines expressing GFP in RBCs (Morgans et al., 2006; Dhingra et al., 2008), and type 5, 7, and 9 CBCs (Wong et al., 1999; Huang et al., 2003; Haverkamp et al., 2005; Haverkamp et al., 2009; Wassle et al., 2009) have been previously reported. These BC specific GFP transgenic mouse lines have been used in the study of BC development (Morgans et al., 2006), synaptic circuits (Han and Massey, 2005; Lin et al., 2005; Wassle et al., 2009),

physiological properties (Duebel et al., 2006) and molecular biology (Huang et al., 2003; Dhingra et al., 2008). The revelation of GFP expression in type 4 CBCs and possibly also type 8 or 9 CBCs in this transgenic line expended further this valuable tool to include these CBCs. In particular, the expression of GFP in type 4 BC bodies is sufficiently bright without the enhancement of antibody. Therefore, this mouse line can be used for *in vitro* electrophysiological recordings of type 4 CBCs in retinal slices or dissociated preparations. It should be noted that although the type 4 CBCs in the mouse can be stained by anti-calsenilin antibody (Haverkamp et al., 2008), this antibody also labels the processes of third order neurons in the IPL, which excludes the use of this antibody to label the axon terminals of this BC type. Therefore, this mouse line will also be useful for examining the synaptic circuits of type 4 CBCs with retinal third order neurons. Furthermore, as shown in this study, the expression of GFP in BCs was detected in early postnatal retinas as well as in aged retinas. Therefore, this transgenic mouse line could be used to study the development and aging of retinal BCs. Finally, crossing this mouse with wild-type and other transgenic lines with retinal diseases will allow the study of effects on retinal BCs during disease processes.

CHAPTER 3 Cre-mediated recombination efficiency and transgene expression patterns of three retinal bipolar cell-expressing Cre transgenic mouse lines

SUMMARY

Retinal bipolar cells play an essential role in segregating visual information into multiple parallel pathways in the retina. The ability to manipulate gene expression in specific BC type (s) in the retina is important for understanding the molecular basis of their normal physiological functions and diseases/disorders. The Cre/LoxP recombination system has become an important tool for allowing gene manipulation *in vivo*, especially with the increasing availability of cell- and tissue-specific Cre transgenic mouse lines. Detailed *in vivo* examination of the Cre/LoxP recombination efficiency and the transgene expression patterns for cell- and tissue-specific Cre transgenic mouse lines is essential for evaluating their utility. In this study, we investigated the Cre-mediated recombination efficiency and transgene expression patterns of retinal BC-expressing Cre transgenic mouse lines by crossing them with a Cre reporter mouse and through Cre-dependent recombinant adeno-associated virus (rAAV) vector-mediated transgene delivery.

INTRODUCTION

Retinal BCs, the second-order neurons with multiple types in the retina, transmit visual information from photoreceptors to third-order retinal neurons and segregate visual information into multiple parallel pathways in the retina (Wassle, 2004). BCs are subdivided into ON- and OFF-types, based on their light- response polarity, and into rod and CBCs, based on their

synaptic inputs. In mammals, a single type of RBC (Dowling and Boycott, 1969; Dacheux and Raviola, 1986) and about nine types of CBCs have been characterized based on their terminal stratification in the inner plexiform layer (IPL) and cell-type-specific molecular markers (Famiglietti, 1981; Kolb et al., 1981; Pourcho and Goebel, 1987; Euler and Wassle, 1995; Ghosh et al., 2004; Pignatelli and Strettoi, 2004; Wassle et al., 2009; Light et al., 2012). BCs of different types are known to exhibit diverse physiological properties (Awatramani and Slaughter, 2000; DeVries, 2000; Euler and Masland, 2000; Wu et al., 2000); however, less is known about the molecular basis of this diversity.

Gene manipulation in specific BC types in the retina offer an approach to investigate BC physiological and pathological properties. In addition, BC diseases animal models can be generated for further gene therapy. The Cre/LoxP recombination system has become a powerful tool for allowing gene manipulation *in vivo* (Nagy, 2000; Branda and Dymecki, 2004), especially with the increasing availability of cell- and tissue-specific Cre transgenic mouse lines (Gaveriaux-Ruff and Kieffer, 2007; Gong et al., 2007). A widely used conditional gene-targeting approach is to cross cell- and tissue-specific Cre transgenic mouse lines with Cre-dependent reporter or conditional mouse lines. Cre transgenic lines, especially those produced by conventional methods (via pronuclear injection), are subject to the local chromatin environment (i.e., position effect), which could lead to transgene silencing or variable ectopic expression (Milot et al., 1996; Williams et al., 2008; Le, 2011; Smith, 2011). Detailed *in vivo* examination of the expression pattern and recombination efficiency of Cre-mediated reporter gene expression in targeted tissues is essential for evaluating their utility. Cre-dependent virus-mediated gene delivery is another powerful approach that can be used to target a transgene to Cre-expressing cells in transgenic mouse lines (Schnutgen et al., 2003; Atasoy et al., 2008; Kuhlman and Huang,

2008). Recombinant adeno-associated virus (rAAV) vectors have been particularly widely used in retinal gene transfer (Surace and Auricchio, 2008). Due to their anatomical location in the middle of the retina, however, retinal BCs are the most inaccessible cell types in the retina to virus transduction. The feasibility of the Cre-dependent rAAV vector-mediated transgene delivery to retinal BCs in Cre transgenic mouse lines has not been examined.

So far, only a small number of retinal BC-expressing Cre transgenic mouse lines have been reported (Barski et al., 2000; Rowan and Cepko, 2004; Saito et al., 2005; Zhang et al., 2005; Ivanova et al., 2010; Nickerson et al., 2011). Most of them were driven by the Pcp2 (Purkinje cell protein 2) promoter, a gene that is known to target Purkinje cells in the cerebellum as well as retinal RBCs (Oberdick et al., 1990). Few Cre transgenic lines have been reported to target retinal CBCs. One of them is Chx10-cre, which was reported to target the Cre recombinase in multiple retinal BC types (Rowan and Cepko, 2004).

In this study, we examined the Cre-mediated recombination expression profiles of three retinal BC-expressing Cre-transgenic lines, 5-HTR2a-cre, Pcp2-cre, and Chx10-cre, by crossing these lines to a strong Cre reporter mouse line. We characterized the Cre-mediated expression patterns in multiple BC types in the 5-HTR2a-cre and Pcp2-cre mouse lines. We also examined the ability and transduction efficiency of Cre-dependent rAAV-mediated transgene delivery to BCs of the BC-expressing transgenic lines. We found that a Cre-dependent rAAV2/2 vector using cytomegalovirus (CMV) promoter and containing a capsid mutation of Y444F is capable of achieving Cre-mediated transgene expression in retinal BCs.

METHODS

Animals

All animal handling procedures were approved by the Institutional Animal Care and Use Committee at Wayne State University and were in accordance with the NIH Guide for the Care and Use of Laboratory Animals. Three Cre transgenic lines were used in this study: (1) Tg(Htr2a-cre)KM207Gsat/Mmcd (referred to as 5-HTR2a-cre), produced by the expression of Cre under the control of the BAC 5-hydroxytryptamine (serotonin) receptor 2A promoter (Gong et al., 2003; Gong et al., 2007); (2) Tg (Pcp2-cre)1Amc/J (referred to as Pcp2-cre), generated by driving Cre recombinase and GFP under the control of a modified mouse Pcp2 (Purkinje cell protein 2) promoter enhancer (Lewis et al., 2004); (3) Tg (Chx10-EGFP/cre-ALPP)2Clc/J (referred to as Chx10-cre), produced by the expression of a green fluorescent protein (GFP)/Cre fusion transgene under the control of a BAC clone containing the mouse transcription factor Chx10 (C. elegans ceh-10 homeodomain-containing homolog) promoter (Rowan and Cepko, 2004). The 5-HTR2a-cre line was chosen because a previous study showed that a 5-HTR2a-GFP line produced by the expression of GFP under the control of the same BAC 5-HTR2a promoter predominantly expressed GFP in type 4 CBCs (Lu et al., 2009). The transgenes of both Pcp2-cre and Chx10 mouse lines contain GFP, but the GFP fluorescence signal is relatively weak (Ivanova et al., 2010). These mice were crossed with a strong Cre reporter line, B6.Cg-Gt(ROSA)26Sortm9(CAG-tdTomato)Hze/J (referred to as tdTomato reporter line), which harbors a combination of the CMV early enhancer element and chicken beta-actin (CAG) promoter-driven red fluorescent protein (RFP) variant, tdTomato, at the Gt (ROSA)26Sor locus with a loxP-flanked STOP sequence (Madisen et al., 2010). When bred to mice with a Cre recombinase gene under the control of a promoter of interest, the STOP sequence is deleted in Cre-expressing cells, and tdTomato is expressed. The 5-HT2a-cre mice were purchased from

Mutant Mouse Regional Resource Center (MMRRC; University of California, Davis, CA, USA); all other mice were purchased from Jackson Laboratory (Bar Harbor, ME, USA).

AAV virus construct and virus injection

The construct that conferred the rAAV2-mediated expression of a double-floxed inverted open-reading frame (DIO) encoding channelrhodopsin-2-mCherry (ChR2-mCherry) with a ubiquitous neuronal promoter Elongation factor I alpha (EF1α), rAAV2-EF1α-DIO-ChR2-mCherry, was kindly provided by Karl Deiserroth at Stanford University. The construct of rAAV2-CMV-DIO-ChR2-mCherry was made by replacing EF1α with the ubiquitous viral promoter, CMV. Virus vectors of rAAV2-EF1α-DIO-ChR2-mCherry were produced in normal rAAV2, and virus vectors of rAAV2-CMV-DIO-ChR2-mCherry were made in Y444F capsid mutation at the virus core facility of University of Pennsylvania. Virus vectors were injected intravitreally into the eyes of Cre-transgenic mouse lines, as previously described (Ivanova et al., 2010). Briefly, one- to two-month-old mice were anesthetized by intraperitoneal injection of a mixture of 120 mg/kg ketamine and 15 mg/kg xylazine. Under a dissecting microscope, a small perforation was made in the temporal sclera region with a needle. A total of 1.5 µl of viral vector suspension in saline at a concentration of 1.3 x 10^{12} GC/ml and 5.6 x 10^{12} GC/ml for rAAV2 (Y444F)-CMV-DIO-ChR2-mCherry and rAAV2-EF1α-DIO-ChR2-mCherry, respectively, was injected into the intravitreal space through the perforation with a Hamilton syringe. The expression of ChR2-mCherry was examined one month after the injection.

Immunohistochemical staining

Mice were deeply anesthetized with CO_2 and decapitated. The retinas were fixed in the eyecups with 4% paraformaldehyde in 0.1 M phosphate buffer (PB, pH7.4) for 20 min. For retinal whole-mounts, the fixed retina was dissected free in PB solution, flat-mounted on slides,

and coverslipped. For retinal vertical sections, the retinas were cryoprotected in a sucrose gradient (10%, 20%, and 30% w/v in PB), and cryostat sections were cut at 14 μm.

The expression of tdTomato fluorescence in the retina was examined in retinal whole-mounts and/or vertical sections. For retinal vertical section imaging, tdTomato fluorescence was sufficient to visualize the tdTomato signal. Therefore, the tdTomato fluorescence was not enhanced with an antibody. For retinal whole-mount imaging, to stabilize the fluorescence signal and reduce bleaching, the tdTomato fluorescence was enhanced using an anti-mCherry antibody, which recognizes tdTomato, followed by a secondary antibody conjugated to Alexa 555 or Alexa 594.

For immunostaining, retinal whole-mounts or vertical sections were blocked for 1 h in a solution containing 5% Chemiblocker (membrane-blocking agent; Chemicon, Brica, MA, USA), 0.5% Triton X-100 and 0.05% sodium azide (Sigma). The primary antibodies were diluted in the same solution and applied overnight, followed by incubation (1 h) in the secondary antibodies, which were conjugated to Alexa 594 (1:600, red fluorescence, Molecular Probes), Alexa 555 (1:600, red fluorescence, Molecular Probes), Alexa 488 (1:600, green fluorescence, Molecular Probes), or AMCA (1:200, blue fluorescence). The following antibodies were used in this study: rabbit anti-mCherry (1:500, 632496, Clontech); mouse anti-calsenilin (1:2,000; kindly provided by W. Wasco, Harvard Medical School, Boston, MA, USA); rabbit anti-PKC (1:20,000, catalog number 2056, Cell Signal); mouse anti-PKC (1:10000, catalog number sc8393, Santa Cruz); mouse anti–synaptotagmin II (Syt-2; 1:600; Zebrafish International Resource Center, Eugene, OR); rabbit anti-HCN4 (1:500; Alomone Labs); mouse anti–protein kinase A (PKA) RIIβ (1:80,000; BD Biosciences).

All steps were carried out at room temperature (RT). All images were made using a Zeiss Axioplan 2 microscope with the Apotome oscillating grating to reduce out-of-focus stray light. Most images were acquired at an approximate optical thickness of 0.4 µm for vertical sections and 0.7 µm for whole-mount tissues. Z-stack images (0.5 µm step size, 20 to 30 sections) were captured and displayed as maximum intensity projections. The full image size is 1388 x 1040 pixels. The excitation light source is mercury short-arc HXP 120. The following filter sets (excitation, dichroic mirror, and emission) were used: Alexa 555 or 594 (BP 546/12, FT 580, LP 590); Alexa 488 (BP 470/40, FT 510, and BP 540/50); AMCA (labeling, BP 365/12, FT 395, LP 397). Brightness and contrast of the final images were adjusted using Adobe Photoshop CS4 to enhance visibility.

RESULTS

Three retinal BC-expressing Cre transgenic lines, 5-HTR2a-cre, Pcp2-cre, Chx10-cre, were crossed with a strong Cre-dependent reporter line that expresses a RFP variant, tdTomato for examining the Cre-medicated recombination pattern in the retina and, especially in BCs. The expression of tdTomato fluorescence in the retina was examined in retinal vertical sections without antibody enhancement, and in retinal whole-mounts with antibody enhancement (see Methods).

5HTR2a-cre mouse line

For the 5HTR2a-cre line, in retinal whole mounts, bright tdTomato-expressing cells were observed throughout the retina, especially in the focal plane at the distal portion of the inner nuclear layer (INL) (Fig. 6A). In retinal vertical sections, the majority of these cells appeared to be BCs, with their somas located in the distal portion of the INL (Fig. 6B). The tdTomato-

labeled cell processes were observed through the entire inner plexiform layer (IPL), although the fluorescence signal was more intense in the distal half of the IPL. In addition, some sparse axon terminals located in the proximal portion of the IPL were also apparent (marked by arrows in Fig. 6B). These terminals resemble the axon terminals of RBCs with their characteristic terminal buttons and their location in the proximal margin of the IPL. Furthermore, tdTomato-expressing cells with their somas located in the proximal portion of the INL and ganglion cell layer were also observed (Fig. 6B). These cells were most likely ganglion cells or displaced amacrine cells (Perez De Sevilla Muller et al., 2007).

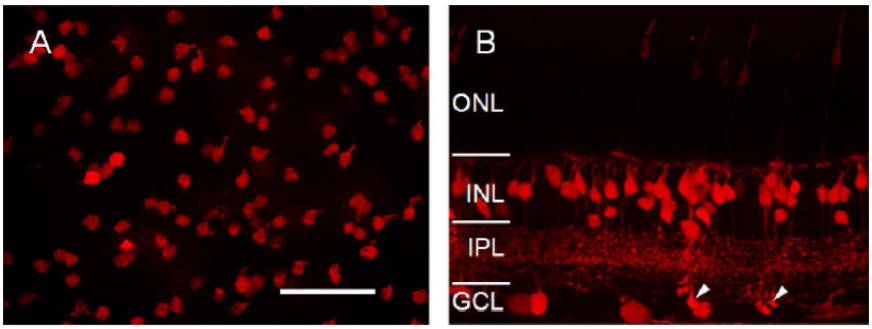

Fig. 6. tdTomato-expressing cells in the 5-HTR2a-cre transgenic mouse line. *A,* tdTomato-expressing cells viewed in a retinal whole-mount with the focal plane at the distal portion of the INL. *B,* tdTomato-expressing cells viewed in a retinal vertical section. The arrowhead points to the BCs with their axon terminals located in the proximal portion of the IPL. ONL, outer nuclear layer; INL, inner nuclear layer; IPL, inner plexiform layer; GCL, ganglion cell layer. Scale bar 50 μm in *A* (applies to *B*).

To identify the BC types in the 5-HTR2a-cre line, we co-labeled tdTomato-expressing cells with several BC type-specific antibodies. Our previous studies showed that the GFP-expressing cells in a 5-HT2aR-GFP transgenic animal line are predominantly type 4 BCs (Lu et al., 2009). Therefore, we first labeled the retina with an antibody to calsenilin, a type 4 BC marker (Haverkamp et al., 2008). Indeed, in retinal vertical sections, the majority of the tdTomato-expressing cells were found to be immunoreactive for calsenilin (Fig. 7A-C; marked

by stars at the somas). The labeling with calsenilin in the majority of the tdTomato-expressing BCs was also observed in retinal whole mounts with the focal plane at the distal portion of the INL (Fig. 7D-F), but there were also a small number of tdTomato-expressing cells that were negative for calsenilin staining (marked by arrows). In retinal whole mounts, approximately 69.5 ± 8.9% (Mean ± SEM; n = 6 retinas) of the tdTomato-expressing cells that were located in the distal portion of the INL were immunoreactive for calsenilin. Next, we labeled the retina with an antibody against PKCα, a RBC marker. In retinal vertical sections, some tdTomato-expressing cells (4.5 ± 2.5%; n = 6 retinas) were found to be immunoreactive for PKCα (Fig. 7G-I; marked by arrows at the somas and arrowheads at the terminals). Furthermore, we labeled tdTomato-expressing cells with other bipolar-cell-specific markers. We found that a small number of the tdTomato-expressing cells were immunoreactive for PKAIIβ (Fig. 7J-L; marked by stars at the somas) but none were immunoreactive for HCN4 (Fig. 7M-O). HCN4 and PKAIIβ antibodies are known to label type 3a and type 3b CBCs, respectively (Mataruga et al., 2007). In addition, the tdTomato-expressing cells were not found to be labeled with synaptotagmin2 (Syt-2) (Fig. 7P-R), an antibody that labels both type 2 and type 6 CBCs (Fox and Sanes, 2007; Wassle et al., 2009).

Taken together, these results indicate that the majority of the tdTomato-expressing BCs in the 5-HTR2a-cre line are type 4 CBCs. In addition, the tdTomato-expressing cell population includes RBCs and type 3b CBCs (see Table 1).

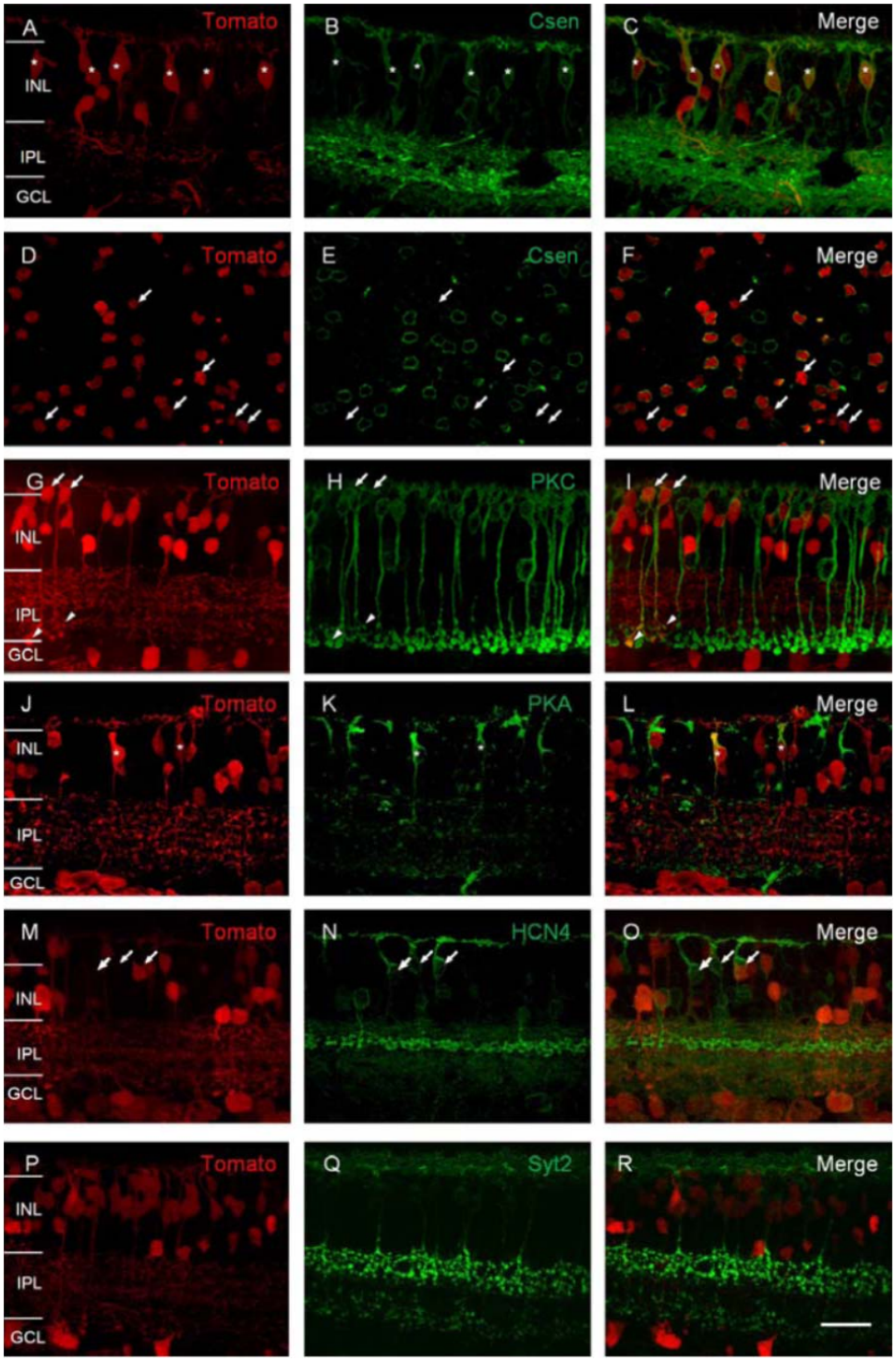

Figure 7. Immunolabeling of the tdTomato-expressing retinal BCs in the 5-HTR2a-cre mouse line with BC-type specific antibodies. *A-C,* in a retinal vertical section, the tdTomato-expressing retina *A* was immunostained for calsenilin in *B*. The overlay of *A* and *B* is shown in *C*. The double-positive BCs are marked with stars. *D-F,* in a retinal whole mount with the focal plane at the distal portion of the INL, the tdTomato-expressing retina *D* was immunostained for calsenilin in *E*. The overlay of *D* and *E* is shown in *F*. *G-I,* the majority of the tomato-expressing cells in the distal portion of the INL are calsenilin-positive. The

tdTomato-expressing cells that do not show calsenilin staining are marked with arrowheads. The tdTomato-expressing retina was immunostained for PKCα in a retinal vertical section. The double-positive BCs are marked with arrows in the somas and arrowheads pointing to the axon terminals. *J-L*, The tdTomato-expressing retina was immunostained for PKARIIβ. Two double-positive cells are marked with stars. *M-R*, the tdTomato-expressing retinal BCs were not found to be labeled by antibodies for HCN4 in *M-O* and Syt-2 in *P-R*. Scale bars 50 μm.

Pcp2-cre mouse line

For the Pcp2-cre line, bright tdTomato-expressing cells were also observed throughout the retina. When examined in retinal vertical sections, the vast majority of the tdTomato-expressing cells were located in the INL, which were clearly all BCs based on their characteristic morphology (Fig. 8A). As shown in Figure 8A, the tdTomato-expressing BCs tend to form clusters. Some of the cells appeared to be RBCs based on their characteristic terminal buttons located in the proximal margin of the IPL (Fig. 8B; marked by white arrowheads). In addition, BCs with axon terminal stratification in the distal portion of the IPL (sublaminae 1 and 2; marked by yellow arrowheads) as well as in the proximal portion of the IPL (sublaminae 4 and 5; marked by blue arrowheads) were also observed, suggesting the presence of labeling in both ON and OFF CBCs. In retinal whole-mount, the tdTomato-expressing BC somas and axon terminals can also be visualized with the focal plane at the distal portion of the INL (Fig. 8C) and the proximal portion of the IPL to the ganglion cell layer (GCL) (Fig. 8D), respectively. In addition, sparsely distributed cells with their somas located in the ganglion cell layer were also labeled (marked by an arrowhead in Fig. 8D). The characterization of these ganglion cells has been reported (Ivanova, 2012).

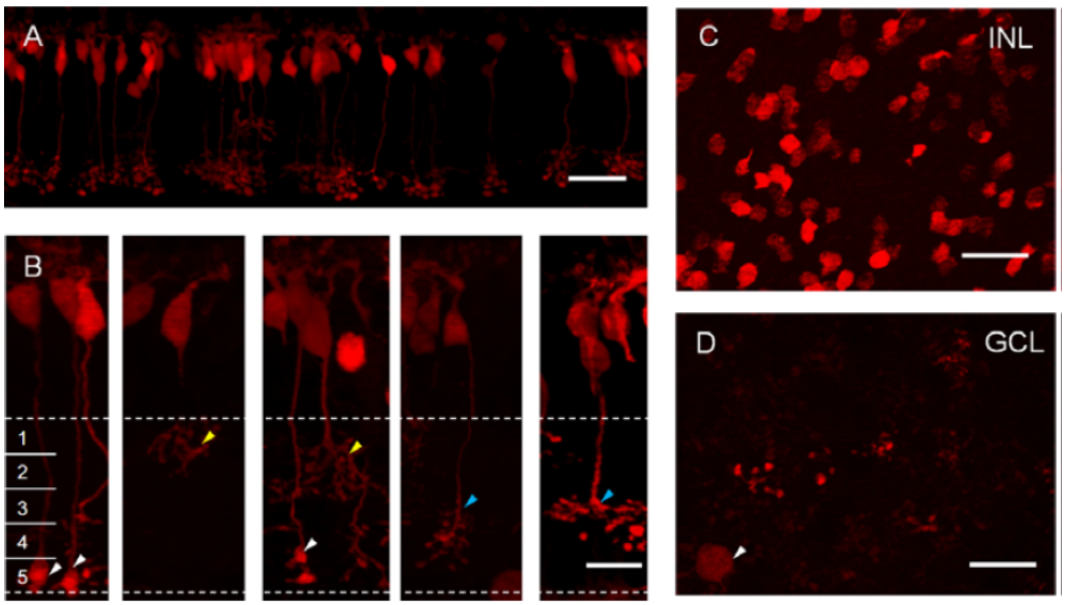

Figure 8. tdTomato-expressing cells in the Pcp2-cre transgenic mouse line. *A*, tdTomato-expressing cells viewed in a retinal vertical section. *B*, representative BCs in high magnification viewed in retinal vertical sections. The IPL was divided into 5 sublaminae. White arrowheads point to the axon terminals of RBCs. Yellow arrowheads point to the axon terminals of BCs stratified in the distal portion of IPL. Blue arrowheads point to the axon terminals of BCs stratified in the proximal portion of IPL. *C*, tdTomato-expressing cells viewed in a retinal whole-mount with the focal plane at the INL. *D*, whole-mount view of the axon terminals of the tdTomato-expressing BCs with the focal plane at the proximal portion of the IPL to ganglion cell layer. The arrowhead points to a weak tdTomato-expressing ganglion cell. The images in *C* and *D* were taken in the same field. Scale bars 25 µm in *A*, *C*, and *D* and 10 µm in *B*.

Bipolar cell type / Cre line	1	2/6	3a	3b	4	5	7-9	RBC
5-HTR2a-cre	-	0	few	0	69.5 ± 8.9%	-	-	4.5 ± 2.5%
Pcp2-cre	-	Many	0	0		-	-	75.5 ± 7.1%

Table 5. The summary of bipolar cell types identified in 5-HTR2a-cre and Pcpc2-cre mouse lines. The percentage value for each bipolar cell type was estimated based on the total tdTomato- expressing cells in the distal portion of the inner nuclear layer. Unexamined bipolar cell types are marked with "-."

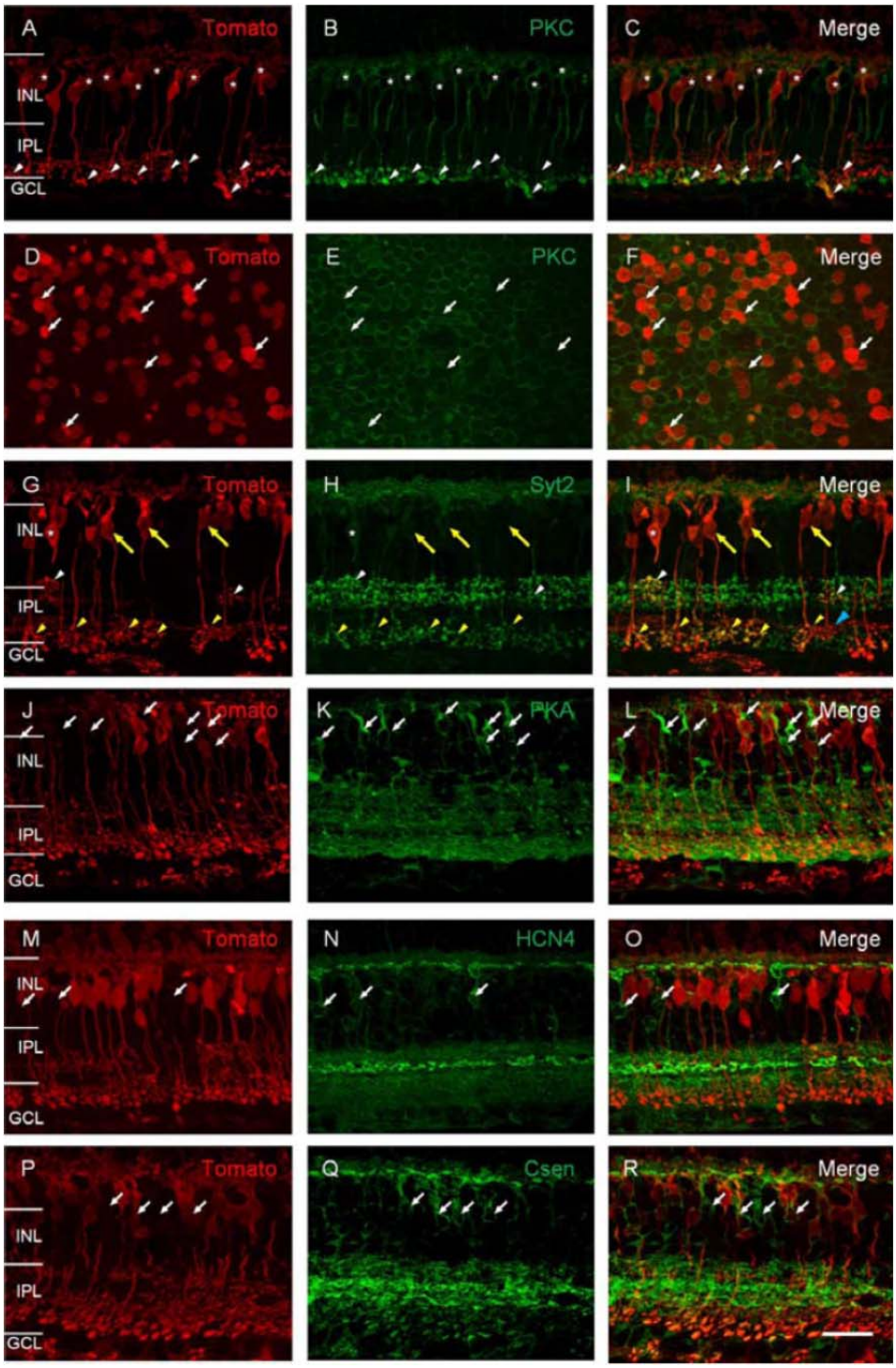

Figure 9. Immunolabeling of the tdTomato-expressing retinal BCs in the Pcp2-cre mouse line with bipolar-cell-type specific antibodies. *A-C,* in retinal vertical sections, the tdTomato-expressing retina was immunostained for PKCα in *B*. The overlay of *A* and *B* is shown in *C*. The double-positive BCs were marked with stars in the somas and with arrowheads pointing at the axon terminals. *D-F,* in retinal whole-mount with the focal plane in the INL, co-labeling with tdTomato and PKCα. PKCα-negative tdTomato-expressing cells are marked with arrows. *G-I,* The tdTomato-expressing retina was immunostained for Syt-2. The double-positive BCs with axon terminals stratified at the distal portion of the IPL (type 2 CBCs) are marked with white stars in the somas and with white arrowheads pointing at the axon terminals. The double-positive BCs with axon terminals stratified in the proximal portion of the IPL (type 6 CBCs) are marked with yellow arrows at the somas and yellow arrowheads at the axon terminals. A tdTomato-expressing BC with their axon terminals stratified slightly distal to Syt2-positive cells is marked with a blue arrowhead in *I*. *J-O,* the tdTomato-expressing retinal BCs were not found to be labeled by PKARIIβ in *J-L*, HCN4 in *M-O*, and calsenilin in *P-R*. Scale bars 50 µm.

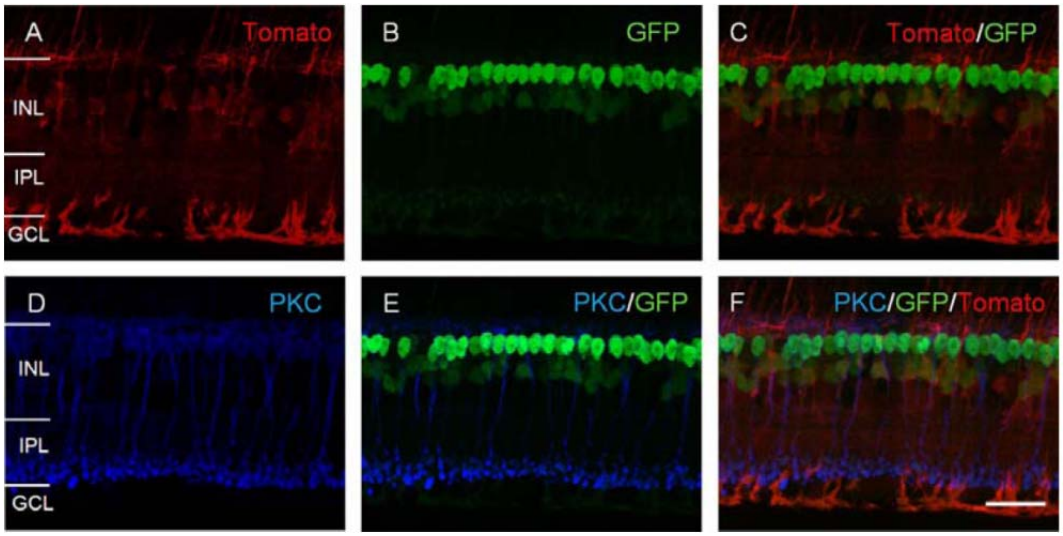

Figure 10. tdTomato-expressing pattern in the Chx10-cre transgenic mouse line. *A-C,* In a retinal vertical section, the expression pattern of tdTomato fluorescence is compared with that of GFP-cre. The GFP was enhanced with an antibody to GFP. The overlay of *A* and *B* is shown in *C*. *D-F,* In the same retinal vertical section, the expression pattern of PKC in *D*, which labels RBCs, is compared with that of GFP and tdTomato. The overlay of PKC and GFP labeling is show in *E*. The triple overlay of PKC, GFP, and tdTomato labeling is show in *F*. Scale bars 25 µm.

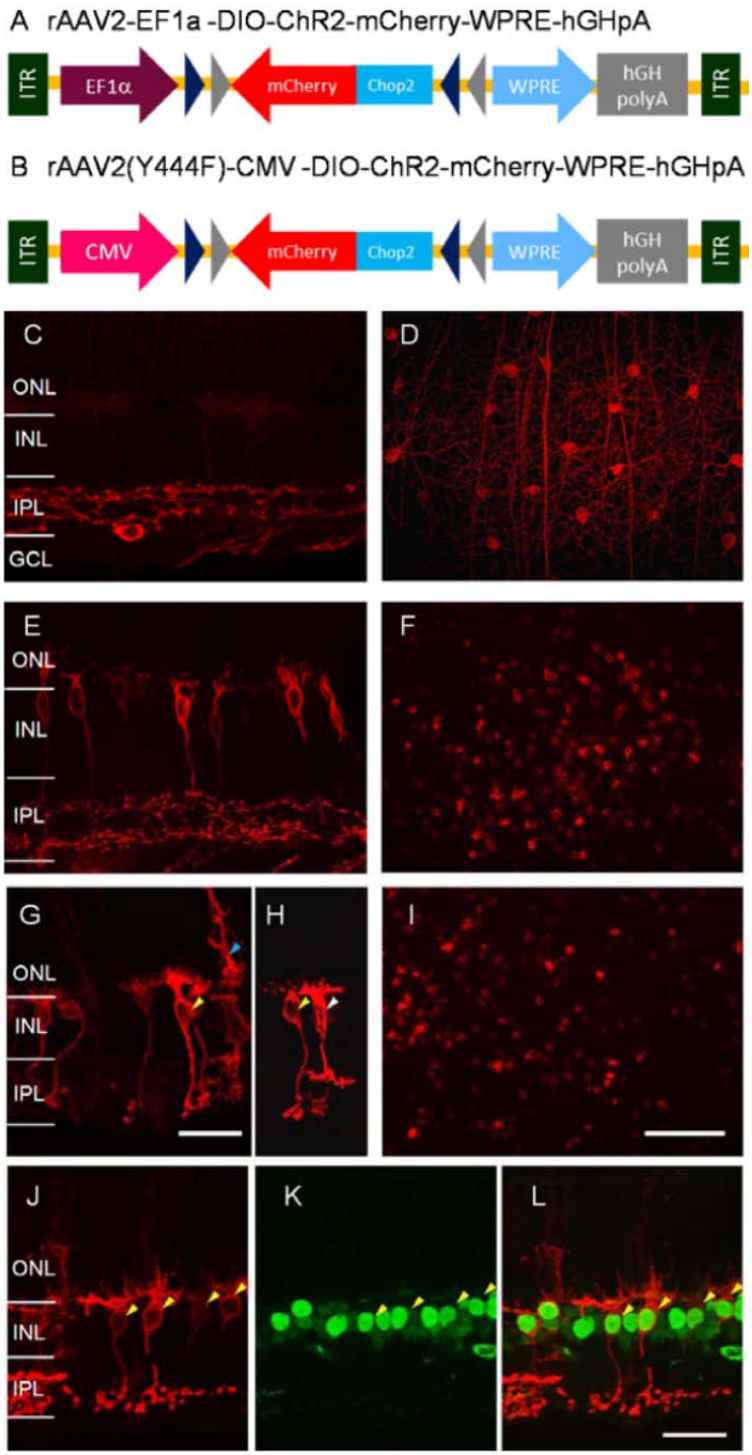

Figure 11. Cre-dependent rAAV-mediated transgene delivery to retinal BCs. *A-B,* The Cre-dependent rAAV2 virus vector cassettes that mediate the expression of a double-floxed inverted open-reading frame (DIO) encoding channelrhodopsin-2-mCherry (ChR2-mCherry) with ubiquitous neuronal promoter EF1α in *A* and with Y444F capsid mutation and a ubiquitous viral promoter, cytomegalovirus (CMV) in *B*. WPRE: woodchuck post-transcriptional regulatory element. hGHpA: a human growth hormone polyadenylation sequence. *C-D,* The expression of ChR2-mCherry mediated by virus vectors with the vector cassette shown in *A* in Pcp2-cre mice, viewed in retinal vertical section in *C* and in retinal whole mount with the focal plane at the GCL in *D*. *E-F,* The expression of ChR2-mCherry mediated by virus vectors with the vector cassette shown in *B* in Pcp2-cre mice, viewed in retinal vertical section in *E* and in retinal whole mount with the focal plane at the INL in *F*. *G-I,* The expression of ChR2-mCherry infected by virus vectors with the vector cassette shown in *B* in Chx10-cre mice, viewed in retinal vertical section in *G-H* and in retinal whole mount with the focal plane at the INL in *I*. *J-L*, in vertical retinal sections, co-labeling of GFP in *J* and mCherry in *K* of the virus infected retina in Chx10-cre mice. The overlay of *J* and *K* is shown in *L*. The double-positive BCs were marked with arrowheads. Scale bars 25 μm in *C, E, G, H,* and J-L and 100 μm in *D, F,* and *I*.

To identify the BC types in the Pcp2-cre line, we co-labeled the tdTomato-expressing cells with the BC-specific antibodies. First, many tdTomato-expressing cells were labeled with PKCα and, therefore, are RBCs as revealed in retinal vertical sections (Fig. 9A-C; marked by

stars in the somas and arrowheads at the axon terminals). The co-labeling of PKCα and tdTomato was also observed in retinal whole mounts (Fig. 9D-F). Approximately 75.5 ± 7.1% (Mean ± SEM; n = 6) of the tdTomato-expressing BCs were immunoreactive for PKCα, indicating that the majority of the tdTomato-expressing cells were RBCs, but the presence of PKCα negative tdTomato-expressing cells is also evident (marked by arrows in Fig. 9D-F). These results suggest that other BC types exist in addition to RBCs. Indeed, some tdTomato-expressing cells were immunoreactive for Syt2 (Fig. 9G-I). Among them, a few of these cells had their axon terminals stratified in the distal portion of the IPL (somas marked by white starts and axon terminals identified by white arrowheads) and, therefore, were most likely type 2 CBCs. The majority of the Syt2-positive cells had their axon terminals stratified in the proximal portion of the IPL (somas marked by yellow arrows and axon terminals marked by yellow arrowheads) and thus should be type 6 BCs. The percentage of these two cell types was not determined due to a weak labeling of Syt2 at the somas. On the other hand, the tdTomato-expressing cells were not labeled by antibodies against PKAIIβ (Fig. 9J-L), HCN4 (Fig. 9M-O), or calsenilin (Fig. 9P-R), indicating that there were no type 3 and type 4 tdTomato-expressing BCs. In addition, there were tdTomato-expressing BCs with axon terminals stratified slightly distal to Syt2-positive type 6 BCs (marked by a blue arrowhead in Fig. 9I). These cells might be type 5 and/or 7 CBCs.

Taken together, these results indicate that the majority of the tdTomato-expressing cells in the Pcp2-cre line are RBCs. The tdTomato-expressing cells also contain numerous type 6 CBCs, some type 2 CBCs, and possibly also type 5 or 7 CBCs, but not type 3 or 4 CBCs (see Table 5).

Chx10-cre mouse line

For the Chx10-cre line, very bright tdTomato fluorescence was observed through the entire retina in retinal whole-mount preparations (data not shown). In vertical sections, the tdTomato fluorescence was predominantly located in Müller cells, based on their characteristic morphology (Fig. 10A). Interestingly, this pattern does not fully resemble that of the GFP-cre (enhanced with GFP antibody) (Fig. 10B-C). In particular, the tdTomato fluorescence was absent in the strongest GFP-labeled cells, with their somas located in the distal portion of the INL and their axon terminals located in the proximal margin of the IPL. These strongest GFP-labeled cells were RBCs because they showed co-labeling with an antibody against PKC (Fig. 10D-F). The GFP-labeled cells including weakly labeled Müller cells were visible without antibody enhancement. Also, previous studies showed that the Cre and GFP immunostaining patterns are the same (Ivanova et al., 2010). The latter would be expected because the transgenic line was generated with a GFP-Cre fusion transgene (Rowan and Cepko, 2004). Therefore, the bright expression of tdTomato fluorescence in the Müller cells could be explained by a low level of Cre expression in these cells. The lack of tdTomato fluorescence in the strong GFP-Cre-expressing BCs, however, is unexpected. The examination of retinal BC types in this line, therefore, was not further performed.

Cre-dependent rAAV-mediated transgene delivery

We next evaluated the ability and efficiency of Cre-dependent rAAV-mediated gene delivery for targeting the transgene to Cre-expressing BCs in the retina. We first examined a rAAV2 vector construct carrying a double-floxed inverted open-reading frame (DIO) sequence encoding channelrhodopsin-2-mCherry (ChR2-mCherry) driven by a ubiquitous neuronal promoter, EFlα (see Fig. 11A). The viral vectors were injected intravitreally in the eyes of adult Pcp2-cre mice. This virus vector construct was found to be able to effectively deliver the

transgene to retinal ganglion cells but not BCs. As shown in retinal vertical sections (Fig. 11C), bright expression of ChR2-mCherry was observed in a population of Cre-expressing retinal ganglion cells, but its expression was barely detectable in retinal BCs. The bright expression of ChR2-mCherry in retinal ganglion cells was also evident in retinal whole mount with the focal plane at the GCL (Fig. 11D). Because a recent study reported that a capsid mutation of AAV2 (Y444F) can markedly increase the transduction efficacy in distal retinal neurons via intravitreal injection (Petrs-Silva et al., 2009), we replaced the virus construct with the capsid mutation. In addition, the EFlα promoter was replaced with a ubiquitous viral promoter, CMV (Fig. 11B), because rAAV2 vectors with CMV promoters were observed to show a better transduction efficacy in BCs (unpublished observations). Indeed, the virus vector with the combination of the Y444F capsid mutation and the CMV promoter resulted in bright expression of ChR2-mCherry in retinal BCs as well as in retinal ganglion cells (Fig. 11E). The expression of ChR2-mCherry in retinal BCs was also shown in retinal whole-mount with the focal plane at the INL (Fig. 11F).

We also examined the Cre recombination profile of the rAAV2 vectors with the combination of the Y444F capsid mutation and the CMV promoter in the Chx10-cre mouse line because of its unexpected Cre recombination profile with the reporter mouse line. The expression of ChR2-mCherry was observed in many BCs, as shown in retinal vertical sections (Fig. 11G and H), and in the retinal whole-mount, with the focal plane at the INL (Fig. 11I). Based on their morphological properties and terminal stratification, both RBCs (marked by yellow arrowheads in Fig. 11G and H) and CBCs (marked by a white arrowhead in Fig. 11H) were transfected, consistent with the expression of Cre in the multiple BC types reported in this line (Rowan and Cepko, 2004). In addition, the expression of ChR2-mCherry was also observed in some Müller cells (marked by a blue arrowhead in Fig. 11G). Furthermore, we performed the co-labeling of

GFP-cre and mCherry (Fig. 11J-L). The results confirm that mCherry indeed targeted to GFP-cre expressing BCs (marked by arrowheads).

DISCUSSION

In this study, we examined the Cre/LoxP recombination efficiency and expression patterns of three retinal BC-expressing Cre transgenic lines by crossing these lines with a strong Cre reporter line. We also examined the Cre-dependent rAAV-mediated gene delivery and reported a rAAV vector construct that is capable of delivering the transgene to BCs through intravitreal injection.

Our results show that, for the 5-HTR2a-cre and Pcp2-cre mouse lines, the expression pattern of the transgene in BCs mediated by the Cre recombination through the reporter line largely resembles the expression pattern of Cre. However, for both lines, this study revealed additional BC types that are involved in Cre recombination, as discussed below. For the 5-HTR2a-cre mouse line, our results show that the majority of the tdTomato-expressing BCs observed after crossing with the reporter line are type 4 CBCs, based on the co-labeling with antibodies against calsenilin. This result is similar to the previous reported result of a 5-HTR2a-GFP mouse line that was produced using the same BAC promoter construct (Lu et al., 2009). In addition, in both 5-HTR2a-cre and 5-HTR2a-GFP lines, a few of the labeled BCs were identified to be type 3b CBCs. Two discrepancies, however, were observed between the tdTomato expression pattern in the 5-HTR2a-cre line and the GFP expression pattern of 5-HTR2a-GFP. First, a small percentage of the tdTomato-expressing cells in the 5-HTR2a-cre line were observed to be RBCs. In addition, many bright tdTomato-expressing third-order neurons were observed in this line. These differences are likely to result from the combination of the highly sensitive Cre recombination and the strong Cre reporter line used in this study. In previous

studies of the 5-HTR2a-GFP line, barely visible GFP (after GFP enhancement) was observed in some ON type CBCs (Lu et al., 2009). The current study indicates at least some of these BCs are RBCs. Additionally, in the 5-HTR2a-GFP line, some weakly labeled cells were observed in the RGL. Therefore, the expression patterns of the transgene in these two lines, Cre and GFP, are likely to be similar, suggesting that the local chromatin environment does not significantly influence the transgene expression profile for the 5-HTR2a BAC promoter.

For the Pcp2-cre line, based on the GFP fluorescence, our previous study showed that the GFP/Cre-expressing BCs were mainly RBCs (Ivanova et al., 2010). The results of this study, obtained by crossing with the reporter line, also showed that the majority of the tdTomato-expressing BCs are RBCs, based on the co-labeling with an antibody against PKCα. In addition, the current study also revealed the expression of tdTomato in many type 6 CBCs as well as in some type 2 CBCs based on co-labeling with an antibody against Syt2. Furthermore, our results suggest that there are additional tdTomato labeled ON-type CBCs. Based on their terminal stratification level, these cells could be type 5 or 7 CBCs. The observation of these additional tdTomato-expressing BC types again suggests there is likely a weak expression of Cre recombinase in these cells. Although Pcp2 has been known to be rod-bipolar-cell specific, the expression of the transgene in other BC types in this mouse line is not totally surprising because the Pcp2-cre line was generated by pronuclear injection, in which the transgenic phenotype would be subject to the position effect.

For Chx10-cre, the expression pattern of tdTomato resulting from crossing with the Cre reporter mouse was found to be markedly different from that of the GFP/Cre. First, there is strong expression of tdTomato fluorescence in Müller cells although this is not too surprising because there is weak expression of GFP/Cre in Müller cells (Ivanova et al., 2010) (also see Fig.

10). The expression of Cre in a subset of Müller glia cells in the Chx10-cre line was also previously reported (Zhang et al., 2004). Surprisingly, however, the tdTomato fluorescence was absent in the strongest GFP/Cre-expressing retinal BCs. On the other hand, the transgene expression profile delivered via rAAV vectors is more consistent with the Cre expression in this line (Rowan and Cepko, 2004; Ivanova et al., 2010). We observed robust Cre-mediated transgene expression in multiple types of BCs as well as in some Müller cells in this line through Cre-dependent DIO virus vectors. The reason for the lack of Cre/loxP recombination in the GFP-Cre expressing BCs via the reporter line is not clear. It is possible that strong Cre expression causes rearrangement of genomic DNA or transgene silencing. In addition, the Chx10-cre line is well known to display mosaic expression in retinal progenitor cells (Rowan and Cepko, 2004). The mosaicism might contribute to the unexpected Cre recombination profile. It also remains to be determined whether this phenomenon is reporter mouse line dependent. Nevertheless, our results point to the importance of the validation of the expression profile through *in vivo* examination of reporter gene expression (Smith, 2011).

Together, by directly crossing with the Cre reporter mouse line and validating by immunostaining, our studies reveal the existence of multiple Cre-expressing BC types in two of the transgenic lines. These two Cre mouse lines could be valuable tools for gene targeting and manipulation of BCs in the mouse retina. On the other hand, our results suggest that the Chx10-cre mouse line may not be suitable for transgenic mouse line-based gene manipulation but can still be used for virus-based applications.

In this study, we also evaluated Cre-dependent virus mediated gene delivery to retinal BCs by intravitreal injection. Our results show that an AAV2 vector construct with the combination of the Y444F capsid mutation and CMV promoter can effectively target the

transgene to retinal BCs. Thus, double floxed inverted AAV2 vectors could provide another valuable tool for gene targeting and manipulation in BCs of Cre transgenic mouse lines. There are several advantages for using virus-mediated targeting or delivery. First, using virus-mediated gene delivery would allow time-dependent control of gene manipulation. Second, virus-mediated gene delivery could be less subject to the complex problems arising from crossing with reporter lines. As shown in this study, for the Chx10-cre line, the Cre-mediated recombination in retinal BCs could not be achieved by crossing with the reporter mouse line but still could be achieved through Cre-dependent rAAV vector delivery. Furthermore, combining with promoters and virus serotypes could allow differential targeting to different retinal cell populations/types in Cre-transgenic mouse lines.

CHAPTER 4 Heterogeneous expression of high-voltage-activated calcium channels in retina bipolar cells

SUMMARY

In this study, we performed whole-cell patch-clamp recordings to investigate the electrophysiological, pharmacological and molecular biological properties of high-voltage-activated (HVA) Ca^{2+} channels in retinal BCs in mice from retinal slice preparations. Ca^{2+} currents with different electrophysiological properties were observed among cone bipolar cells (CBCs), and between CBCs and rod bipolar cells (RBCs). First, large HVA Ca^{2+} currents were observed in OFF CBCs but not in ON-CBCs. Second, HVA Ca^{2+} currents among different BCs were found to show different activation potentials. Moreover, the HVA Ca^{2+} currents in RBCs display two components, a sustained and a transient component with the latter activated at more negative potentials. Our pharmacological results indicate the sustained and transient HVA Ca^{2+} currents originate from L- and P/Q type Ca^{2+} channels, respectively. Furthermore, using L-type Ca^{2+} channel knockout or deficient mouse lines, our results suggest that the L-type Ca^{2+} currents in RBCs are mediated mainly by α1C Ca^{2+} channels with a minor component from α1F Ca^{2+} channels. The findings of this study provide valuable insights into the role of voltage-gated Ca^{2+} channels in basic visual information processing in the retina as well as Ca^{2+} signaling and Ca^{2+} channel deficit-related diseases in the visual system.

INTRODUCTION

Retinal BCs, conveying visual information from photoreceptors to retinal third order neurons, are essential in segregating visual information into multiple parallel pathways in the

retina through their diversified cell types and physiological properties. BCs contained about ten types. Based on synaptic input, there is one single type of RBCs and multiple types of CBCs. BCs are also divided into ON and OFF types based on their light response polarity.

Voltage-gated Ca^{2+} channels that can influence neuronal excitability and trigger neurotransmitter release could be responsible for the diversified physiological properties of different retinal BCs. Retinal BCs in mammalian retinas have been known to process both high-voltage-activated (HVA) Ca^{2+} channels and low-voltage-activated (LVA) T-type Ca^{2+} channels. The HVA Ca^{2+} currents in retinal BCs, especially in mammalian RBCs, have been well studied and reported to be exclusively L-type. Immunostaining studies have reported a heterogeneous expression of four L-type Ca^{2+} channel α subunits, α1S ($Ca_V1.1$), α1C ($Ca_V1.2$), α1D ($Ca_V1.3$), and α1F ($Ca_V1.4$) in the retina, including in certain retinal BCs. Whether there are heterogeneous properties of HVA Ca^{2+} currents among different BCs still remains unclear. Also, the molecular composition of HVA Ca^{2+} current in retinal BCs, even in the most extensively studied RBCs, still remains elusive.

To understand the functional roles of voltage-gated Ca^{2+} currents in BC processing, in this study we investigated the electrophysiological, pharmacological, and molecular properties of HVA Ca^{2+} currents in retinal BCs, especially RBCs by performing whole-cell patch-clamp recordings from retinal slice preparations in mice. To facilitate BC identification in *in vitro* recordings, BC-type specific GFP or Cre transgenic mice were used.

METHODS

Animals

All animal handling procedures are approved by the Institutional Animal Care and Use Committee at Wayne State University and are in accordance with the NIH Guide for the Care

and Use of Laboratory Animals. All efforts were made to minimize the number of animals used and their suffering.

C57BL/6J, Pcp2-cre/GFP and the α1F mutant mice were purchased from Jackson Laboratory. 5-HTR2A-EGFP transgenic mice were obtained from Mutant Mouse Regional Resource centers (MMRRC; Line: DQ118). As described earlier, mainly RBCs and type 4 CBCs were labeled by GFP in the Pcp2-cre/GFP and 5-HTR2a-EGFP mouse lines, respectively. Gus-GFP mice were provided by Dr. Robert F. Margolskee at Mount Sinai School of Medicine in New York. In this mouse line, the type 7 CBCs are labeled by GFP.

The α1D knockout mice were kindly provided by Stressing's lab in Austria. This mouse line was generated through homologous recombination together with a multi-stop codon cassette sequence (Platzer et al., 2000).

The α1F mutant mouse line has been reported to be a naturally occurring null mutation for the α1F Ca^{2+} channel gene (Koschak et al., 2003). A recent study, however, reported the expression of a low level of α1F Ca^{2+} channel in this α1F mutant mouse strain due to alternative splicing (Doering et al., 2008). We will consider this fact in the interpretation of our experimental results.

The α1C conditional knockout mice were kindly provided by the Geoffrey G. Murphy group at the University of Michigan (White et al., 2008). Since the global deletion of the α1C gene is lethal (Seisenberger et al., 2000), this α1C conditional knockout line was generated by introducing a mutation cassette flanked by two loxP sites into the α1C gene.

To knockout the α1C gene, without affecting by animal development, the AAV2/2 vectors carrying Cre-GFP sequence were injected intravitreally into the eyes of adult α1C conditional knockout mice. Figure 12A shows an AAV2/2 construct,

mGluR6enhancers+mSV40P–Cre–GFP-hGHpA, which is capable of expressing Cre in retinal BCs (our unpublished studies). For identifying those cells with Cre expression and Cre-mediated recombination, a second AAV2/2 vector expression of a double-floxed inverted open-reading frame (DIO) encoding channelrhodopsin-2-mCherry (ChR2-mCherry) with a ubiquitous CMV promoter was also intravitreally injected simultaneously. Figure 12B shows the Virus vectors construct carrying mCherry-ChR2, rAAV2 (Y444F)-CMV-DIO-ChR2-mCherry. Therefore, the α1C gene will be knocked out in the cells expressing mCherry (Fig. 12C).

Virus Vector Injection

The virus intravitreal injection procedure was as previously described (Ivanova et al., 2010). Briefly, 1- to 2-month-old mice were anesthetized by intraperitoneal injection of a mixture of 120 mg/kg ketamine and 15 mg/kg xylazine. Under a dissection microscope, a small perforation was made in the temporal sclera region with a needle. A total of 1.5 μl of viral vector suspension in saline at a concentration of 1.3×10^{12} GC/ml and 5.6×10^{12} GC/ml for mGluR enhancer+mSV40P–Cre–GFP-hGHpA and rAAV2-(Y444F)-CMV-DIO-ChR2-mCherry, respectively, was injected into the intravitreal space through the perforation with a Hamilton syringe. The electrophysiogical recording was performed about 1 month after the injection.

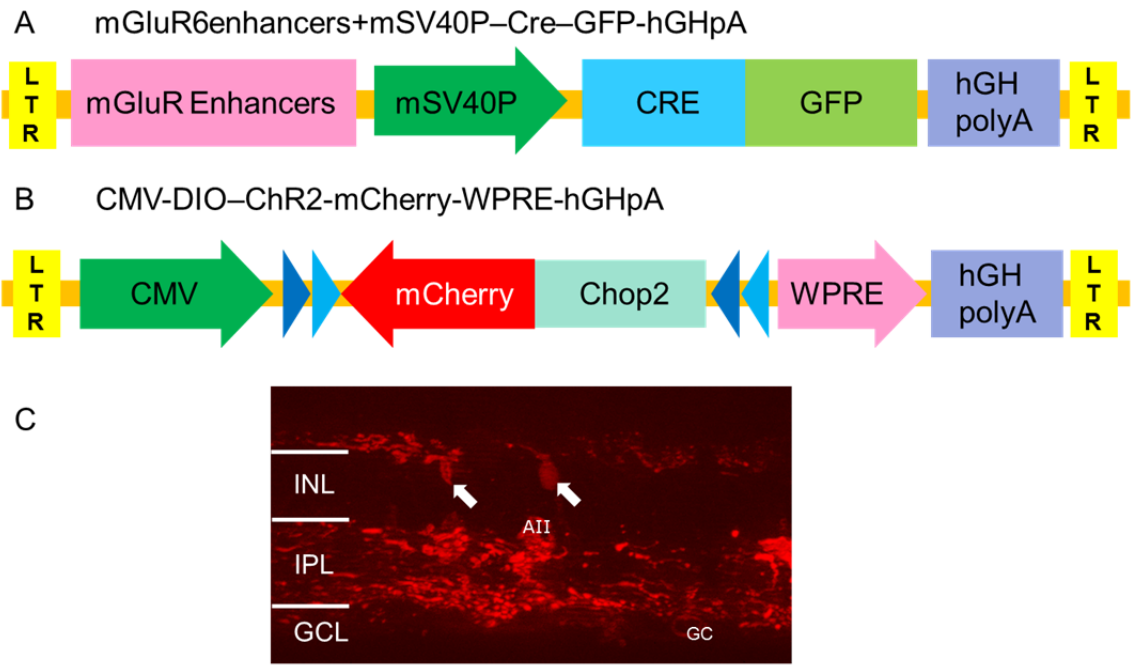

Figure 12. AAV2/2 Cre and reporter constructs *A*, AAV2/2 constructs carrying mGluR6 enhancers were inserted in the 5' end of Cre-GFP fusion protein and driven by a basal mSV40P promoter. Cre-GFP sequence is followed by hGHpolyA. Both sides are flanked by long terminal repeat (LTR). *B*, AAV2/2 serotype with a point mutation of capsid (Y444F) construct mediate expression of double-floxed inverted open reading frame (DIO) encoding channelrhodopsin-2-mCherry (ChR2-mCherry) with a ubiquitous promoter of CMV. *C*, The expression of mCherry mediated by the two virus vectors in a retinal vertical section. The positive BCs were marked with arrows. CMV: cytomegalovirus. WPRE: woodchuck post-transcriptional regulatory element. hGHpA: a human growth hormone polyadenylation sequence.

	Type 2	Type 3	Type 4	Type 6	Type 7	RBC
WT C57BL/6J	Axon terminal stratification					
Pcp2-cre-tdTomato						
5HT2aR-cre-tdTomato						
Gus-Thy1-GFP						
a1C conditional KO + AAV2/2-Cre						
a1D $^{-/-}$	Axon terminal stratification					
a1F$^{-/-}$ deficient	Axon terminal stratification					
CD15 labeling						

Table 6. List of animal lines for specific cell types recording. In wild type, α1D knockout, and α1F deficient animals the cell types were determined by axon terminal stratification in inner plexiform layer with dye filling. In Pcp2-cre-tdTomato line, type 2, 6 CBC and RBC can be identified with tdTomato expression. In

5HTR2a-cre-tdTomato line, type 4 CBC can be identified with tdTomato expression. In Gus-thy1-GFP line, type 7CBC can be identified with GFP expression. The type 2 CBC can also be labeled with CD15 antibody.

Dissociation of bipolar cells

BCs were dissociated from adult mice (C57/BL6J) 4 weeks of age by dissociation methods previously described (Pan and Lipton 1995). In brief, animals were deeply anesthetized with CO_2 and killed by decapitation. Retinas were removed and placed in a Hanks' solution (in mM): 138 NaCl, 1 $NaHCO_3$, 0.3 Na_2HPO_4, 5 KCl, 0.3 KH_2PO_4, 1.25 $CaCl_2$, 0.5 $MgSO_4$, 0.5 $MgCl_2$, 5 HEPES-NaOH, and 22.2 glucose, with phenol red, 0.001% vol/vol; adjusted to pH 7.2 with 0.3 N NaOH. The retinas were incubated for 50 min at 34–37°C in an enzyme solution that consisted of the normal Hanks' described above, supplemented with 0.2 mg/ml DL-cysteine, 0.2 mg/ml bovine serum albumin, and 1.6 U/ml papain, adjusted to pH 7.2 with 0.3 N NaOH. Following several rinses in Hanks' solution, the retinas were dissociated by gentle trituration with a glass pipette mechanically. The resulting cell suspension was plated onto culture dishes for settle down. Cells were kept at room temperature and used for recordings within 5 hours after dissociation.

Retinal slice preparation

In brief, animals were deeply anesthetized with CO_2 and killed by decapitation. The retina was dissected in carbongen-bubbled (95% O_2 / 5% CO_2) Ames's solution (Sigma-Aldrich, St. Louis MO, USA). The cornea, iris and lens of the animal eye were dissected away. The eyecup was inverted on a piece of filter (Whatman, VWR; 10402506) with the photoreceptor layer up. Vertical slices (150 μM) were cut together with the filter by a scalpel blade on a chopper. The slices were kept in darkness to minimize photo damage in Ames' solution at room temperature.

Whole-cell patch clamp recordings on dissociated cells

Recordings with patch electrodes in the whole-cell configuration were made by standard procedures (Hamill et al. 1981) at room temperature (20–25°C) with an EPC-9 amplifier and PULSE software (Heka Electronik, Lambrecht/Pfalz, Germany). Electrodes were fabricated from borosilicate microcapillary tubes (VWR Scientific, West Chester, PA, US), coated with silicone elastomer (Sylgard; Dow Corning, Midland, MI), and fire-polished. The resistance of the electrode was 7–10 MΩ. Series resistance ranged from 10 to 40 MΩ and was not routinely compensated because the Ca^{2+} currents were small (≤100 pA). Cell capacitance was automatically canceled and recorded by EPC-9 amplifier and PULSE software. Test pulses were delivered once every 5–10 s for all recordings.

To facilitate Ca^{2+} current recordings, voltage-activated K^+ currents were suppressed by the inclusion of Cs^+ and tetraethylammonium (TEA) in the recording electrode and extracellular solutions. Unless otherwise indicated, the recordings were performed in high- Ca^{2+} (10 mM) extracellular solution containing (in mM) 95 NaCl, 5 KCl, 10 CsCl, 20 TEA-Cl, 1 $MgCl_2$, 10 $CaCl_2$, 10 HEPES, and 22.2 glucose, with phenol red, 0.001% vol/vol; pH 7.2. The electrode solution contained (in mM) 120 CsCl, 20 TEA-Cl, 1 $MgCl_2$, 0.5 $CaCl_2$, 5 EGTA, 10 HEPES, 0.5 Na-GTP, and 2 Na-ATP, pH adjusted with CsOH to 7.4. Under these recording conditions, the voltage-activated K^+ currents in BCs were mostly blocked because no significant outward current was observed when Ca^{2+} (10 mM) in the extracellular solution was replaced by 4 mM Co^{2+} and 6 mM Mg^{2+}. The chloride reversal potential was around -20 mV using the above intracellular and extracellular recording solutions. Liquid junction potentials were measured to be 3 mV according to the procedure described by Neher (1992) and corrected.

Whole-cell patch clamp recordings on retinal slices

During recordings, the slices were placed on a recording chamber. The chamber was continuously superfused with bubbled Ames solution at a rate of 2 ml/min. The electrode solution was the same as in the recording of dissociated cells. The fluorescent dye Alexa 488 or 594 was added to the electrode solution at a concentration of 100 μM. The extracellular solution contained (in mM) 95 NaCl, 5 KCl, 10 $CaCl_2$, 10 CsCl, 20 TEA-Cl, 1 $MgCl_2$, 10 HEPES, and 22.2 glucose, with phenol red, 0.001% v/v, pH 7.2. In all recordings, 100 μM bicuculline, 100 μM TPMPA, 2 μM strychnine, and 1 μM tetrodotoxin (TTX) were included in the extracellular solutions.

The same electrode solution was used as described above. Liquid junction potential (3 mV) was corrected. Pipette resistances ranged from 7 to 10 MΩ. Whole cell input resistances of BCs were at least 1GΩ. Cells were voltage-clamped in whole cell mode. For recording HVA Ca^{2+} currents, the membrane potential of the cells was holding at -50 mV. The voltage-gated Ca^{2+} currents were activated by ramp stimulus from -50 mV to 20 mV at a speed of 100 mV/1S and by depolarizing steps ranging from -45 mV to -15 mV, with a 5 mV increment.

Identification of bipolar cell types in dissociated cell and slice preparations

In dissociated preparation, type 4 CBCs were identified based on GFP from the 5HTR2a-GFP transgenic mouse line. RBCs were identified based on GFP from the Pcp2-cre/GFP transgenic mouse line or their characteristic morphology.

In retinal slice preparation, we used the following three ways to identify the cell types: (1) stratifications of axon terminals in the IPL using recording pipettes filled with dye Alexa 488 or Alexa 594 dye (100 μM); (2) the expression of GFP using BC specific transgenic mouse lines; (3) for type 2 CBCs, live antibody staining with CD15 as described below.

The type 2 CBCs were identified by staining with a CD15 antibody as previously described (Jakobs et al., 2003). Briefly, the mouse monoclonal IgM antibody against the CD15 epitope (1:50, BD PharMingen, San Diego, CA, US) was dissolved in the extracellular solution. The retinal slices were immersed in the primary antibody solution for 2 hours, and then washed for 30 mins with perfusion of the extracellular solutions. Secondary antibody donkey anti mouse IgG Alexa 488 (1:200, green fluorescence, Molecular Probes, Invitrogen, Carlsbad, CA) was applied for 1 hour, and then washed away for 30 mins. The stained retinal slices were then ready for patch clamp recordings. The summary of BC type's identification methods is showed in table 6.

Chemicals

Nimodipine, nifedipine, BayK 8644, and tetrodotoxin (TTX) were purchased from Research Biochemicals (Natick, MA). The ω-Agatoxin IVA (RTA-500，ω-Conotoxin (C-300) and SNX482 (RTS-500) were purchased from Alomone (Alomone Labs, Har Hotzvim, Jerusalem, Israel). Mibefradil was a kind gift from F.Hoffmann (La Roche, Basel, Switzerland). Other chemicals were purchased from Sigma (St. Louis, MO). Chemical agents were applied by local perfusion. In the local perfusion, chemicals were applied to the cells by five-barreled gravity-driven superfusion pipettes (modified from Carbone and Lux 1987) placed about 200–300 μm away from the cell being recorded.

Statistical analysis

Data were analyzed off-line using PULSE-FIT (Heka Electronik) and ORIGIN programs (Microcal Software, Northampton, MA). One way ANOVA was used to compare data. In all results, the significance was accepted as $p < 0.05$. Date are presented as mean ± SEM.

RESULTS

Part 1. Comparison of HVA Ca^{2+} currents in acutely dissociated cell preparations

To assess the properties of voltage-gated Ca^{2+} currents in CBCs and RBCs, we first performed whole-cell patch-clamp recordings on acutely dissociated RBCs and type 4 CBC cells from the two BC specific-GFP transgenic mouse lines, pcp2-GFP for RBCs and 5HTR2a-GFP for type 4 CBCs as described above. The BCs were identified by their GFP fluorescence. In these recordings, voltage-gated Ca^{2+} channels were isolated by the blockade of other voltage-gated membrane channels (see Methods). The cell's membrane potential was held at -80 mV and depolarized by a voltage ramp from -80 to +40 mV at a speed of 100 mV/ s and by a series of 400 ms test pulses ranging from -60 mV to +30 mV. To isolate the Ca^{2+} currents, extracellular solutions contain 10 mM Cs^{+} and intracellular solutions contain 120 mM Cs^{+} to block K^{+} channels.

Figure 13A and B show the typical voltage-gated Ca^{2+} currents elicited from type 4 CBCs with ramp stimulus and step pulses, respectively. Interestingly, we did not observe any significant voltage-gated Ca^{2+} currents (n = 10). The results contrasted with those in retinal slice recordings in which both HVA and LVA Ca^{2+} currents were observed (see below).

Figure 13C and D show the voltage-gated Ca^{2+} currents recorded from RBCs. In RBCs, voltage-gated Ca^{2+} currents were evoked at around -60 mV and reached their peak around -40 mV to -30 mV. It should be noted that the observed currents in RBCs in dissociated cells are mainly T-type (Pan, 2000). Although RBCs also express L-type Ca^{2+} channels, the current is located at the axon terminals and only becomes apparent by the application of L-type Ca^{2+} channel agonist BayK8644.

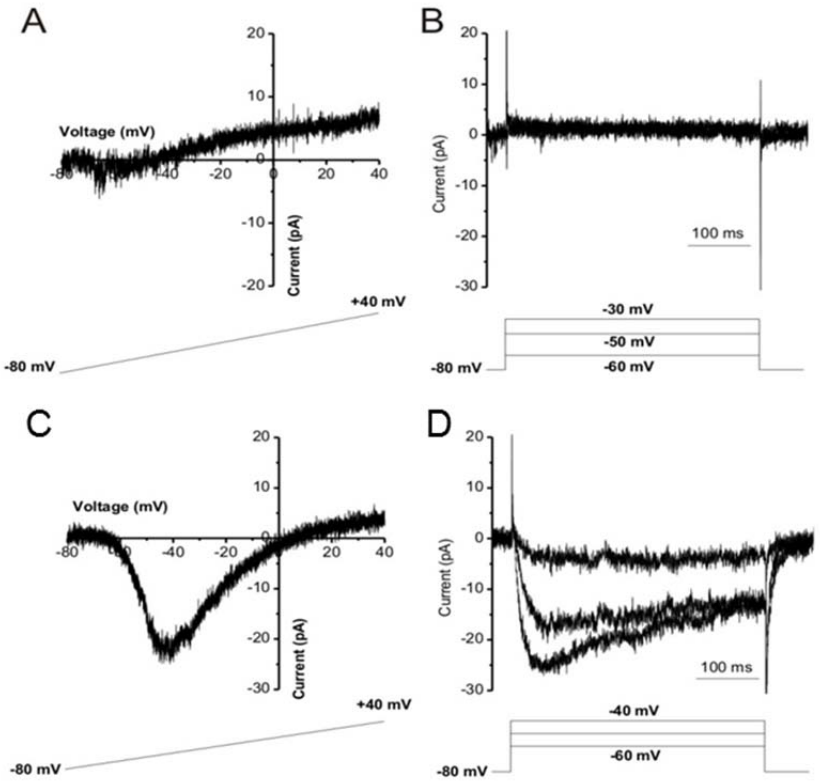

Figure 13. Voltage-activated Ca^{2+} currents of type 4 CBCs and RBCs recorded from acutely dissociated cell preparations. *A-B,* Type 4 CBCs show no apparent voltage gated Ca^{2+} currents. A: Currents were evoked by a voltage ramp ranging from -80 to 40 mV. B: Currents were evoked by three 400 ms test pulses from the holding potential of -80 mV to -60, -50, and -30 mV. *C-D,* Typical Ca^{2+} currents recorded from on RBCs. *C,* Ca^{2+} currents were evoked by a voltage ramp ranging from -80 to 40 mV. *D,* Ca^{2+} currents were evoked by three 400 ms test pulses from the holding potential of -80 mV to -60, -50, and -40 mV, respectively.

Part 2. Comparison of HVA Ca^{2+} currents among CBCs and RBCs in retinal slices

To investigate the properties of voltage-gated Ca^{2+} currents in retinal BCs under more physiological conditions, in all the following experiments, we performed whole-cell patch-clamp recordings to characterize the HVA Ca^{2+} currents in the CBCs and RBCs in retinal slice preparations.

To isolate the HVA Ca^{2+} currents from LVA in voltage ramp stimulation, the HVA Ca^{2+} currents were recorded from the holding potential of -50 mV to inactivate LVA T-type Ca^{2+} currents. The HVA Ca^{2+} currents among different BCs were evaluated by both ramp and step pulse stimulation protocols.

The heterogeneous properties of HVA Ca^{2+} currents were observed among the BCs. First, large HVA Ca^{2+} currents were observed in all recorded OFF-CBCs, type 2, type 3, type 4 (see Fig. 14A- F). In contrast, HVA Ca^{2+} currents in recorded ON-CBCs, type 6 and type 7, were found to be small (see Fig. 14G, H and J, K).

Second, although prominent HVA Ca^{2+} currents were also observed in RBCs (Fig. 14I, L, and M), the kinetics of the HVA Ca^{2+} currents of RBCs, were markedly different from those of CBCs. As shown in Fig, 14D, E, and F, the HVA calcium currents of OFF CBCs, type 2, 3, and type 4 CBCs do not show significant time-dependent inactivation. In contrast, the HVA Ca^{2+} currents of RBCs exhibit fast inactivation, especially at the relatively negative test potential (Fig. 14L).

Third, the voltage-dependent activation of HVA among CBCs was found to be different. This was particularly noticeable when the I-V relationships of type 2 and type 4 CBCs were compared both by ramp stimulus and test pulses (Fig. 15 A-D). Both the threshold and peak Ca^{2+}

current activation potentials of type 2 CBCs were significantly shifted to more positive potentials than that of type 4 CBCs (Fig. 15E).

Finally, it is also interesting to note that the large HVA Ca^{2+} currents in type 4 CBCs observed in slice preparations (see Fig. 15C) contrast to the results recorded from dissociated cells (Fig. 12A). The failure to detect voltage-gated Ca^{2+} currents in type 4 CBCs in acutely dissociated cell preparations appeared to be unique to this cell type, because T-type voltage-gated Ca^{2+} currents were observed in other BC types, such as RBCs (see below). A possible explanation is that all voltage-gated Ca^{2+} channels in type 4 CBCs are located at the axon terminals which could be lost during cell dissociation. Alternatively, the loss of voltage-gated Ca^{2+} currents could be due to a down-regulation mechanism, possibly related to the enzymatic treatment.

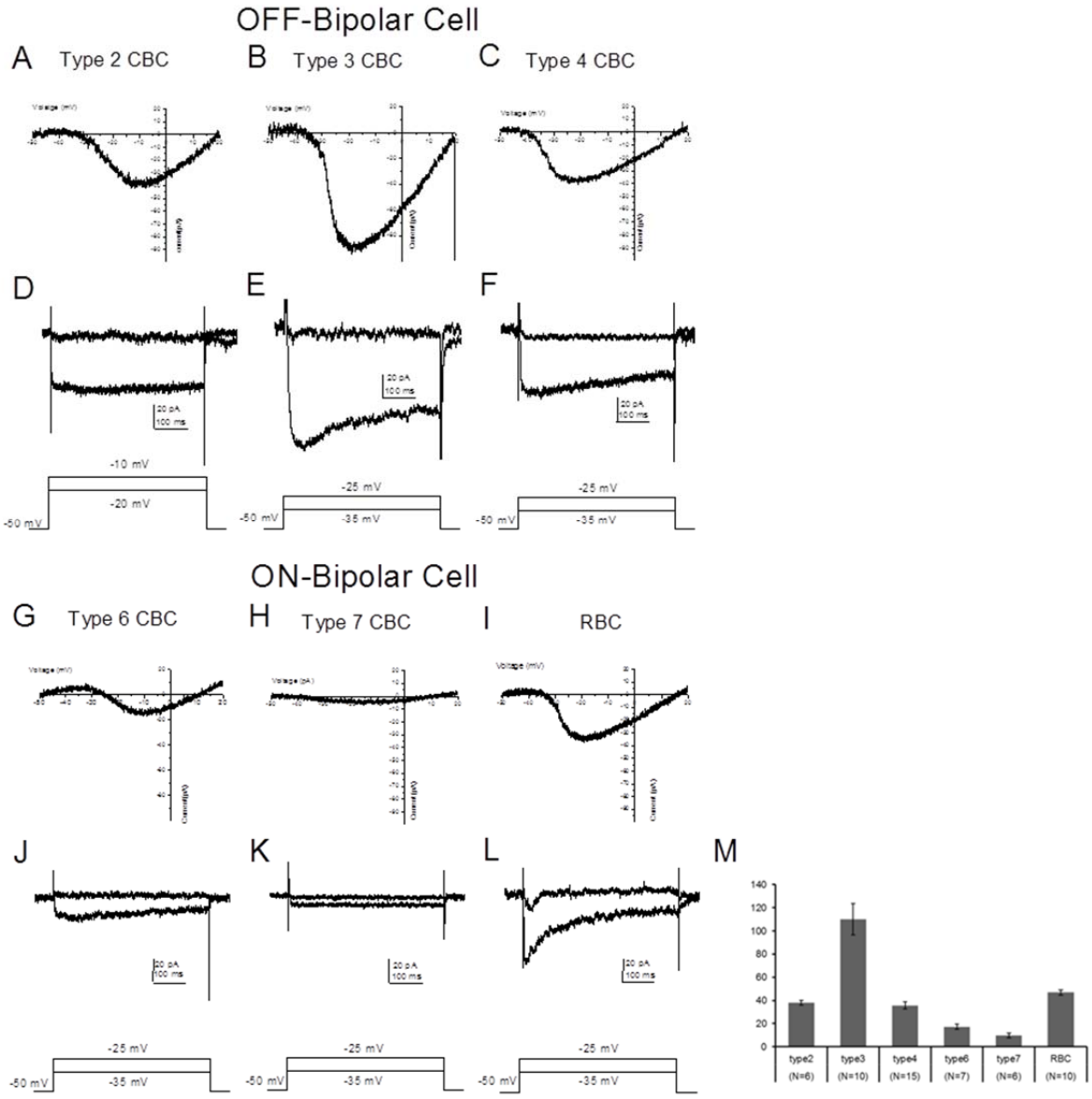

Figure 14. L-type voltage-gated Ca^{2+} currents recorded from different BCs. *A-C, G-I,* Ca^{2+} currents were evoked by a voltage ramp from -50 to 20 mV from the holding potential of -50 mV. *D-F, J-L,* Ca^{2+} currents were evoked by a series of 500 ms test pulses from the holding potential of -50 mV with an incremental step of 5 mV. *D,* Individual traces were shown evoked by test potential to -20 mV and -10mV at holding potential to -50 mV. *E, F, J-L,* Individual traces were shown evoked by test potential to -35 mV and -25 mV from the holding potential of -50 mV. *A, D,* type 2 CBCs. *B, E,* type 3 CBCs. *C, F,* type 4 CBCs. *G, J,* type 6 CBCs. *H, K,* type 7 CBCs. *I, L,* RBCs. *M,* Statistical data of the peak current amplitudes of HVA Ca^{2+} currents for BCs. The data were measured from the ramp stimulus.

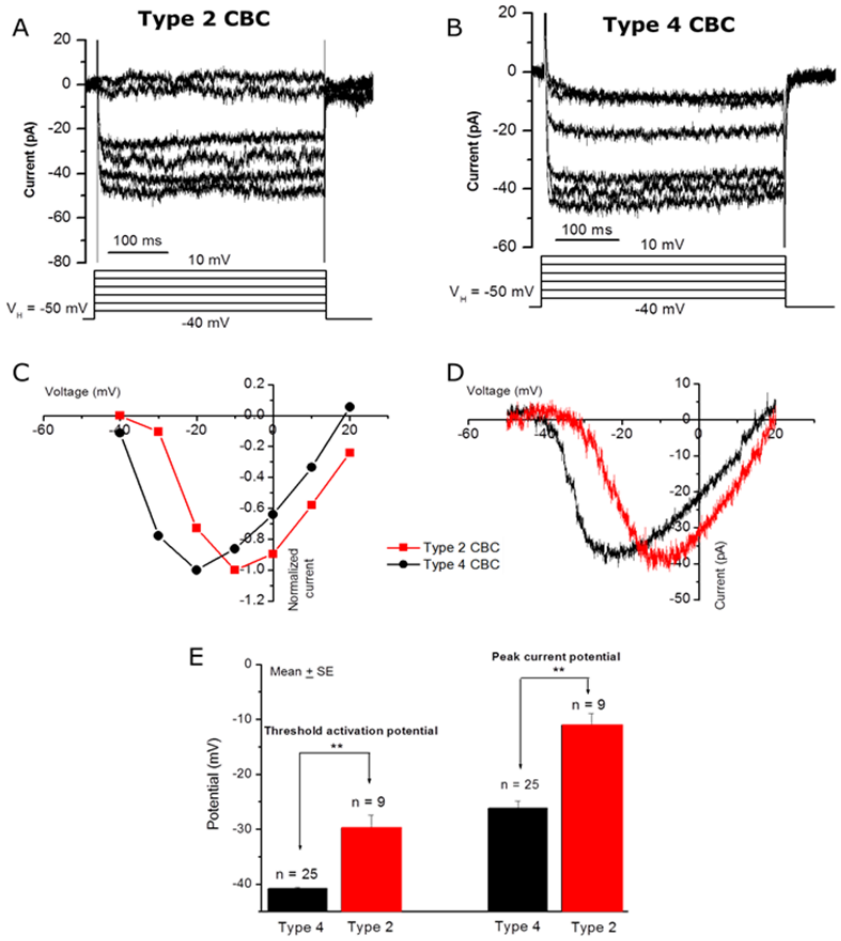

Figure 15. Comparison of voltage-dependent activation of HVA Ca^{2+} currents between type 2 and 4 CBCs. *A*, *B*, The representative recordings of HVA Ca^{2+} currents from type 2 in *A* and type 4 in *B* CBCs elicited by test pulses. *C*, The I-V plots for the Ca current for the recordings shown in *A* and *B*. *D*, Comparison of HVA Ca^{2+} currents between type 2 in *A* and type 4 in *B* CBCs elicited by ramp stimulus from -50 to 20 mV from the holding potential of -50 mV. *E*, Statistical data of the threshold and peak activation potentials of HVA Ca^{2+} currents for type 2 and type 4 CBCs. The data were measured from the ramp stimulus.

Part 3. Electrophysiology, pharmacology and molecular properties of HVA Ca^{2+} currents in RBCs

3-1. The HVA Ca^{2+} current of RBCs exhibits both sustained and transient components

Since the L-type Ca^{2+} current is usually known to display no or slow time-dependent inactivation, our finding of the fast inactivation of the HVA Ca^{2+} currents in RBCs contrasted with the common belief that HVA Ca^{2+} currents in all BCs including RBCs are L-type. This unexpected finding therefore prompted us to investigate in detail the properties of HVA Ca^{2+} currents in RBCs.

Again, to characterize the HVA Ca^{2+} currents in RBCs, HVA Ca^{2+} currents were evoked by a voltage ramp from -50 to +20 mV or by a series of 400 ms depolarizing test pulses ranging from -40 mV to +20 mV from the holding potential of -50 mV. Fig. 16 shows sample recordings of HVA Ca^{2+} currents of RBCs from the C57/BL6J mouse line. In ramp stimulation, a prominent HVA Ca^{2+} current was activated at the potential >-40 mV (Fig. 16A). The HVA Ca^{2+} currents elicited by test pulse stimuli show fast inactivation (Fig. 16B). The current-voltage (I-V) relationships of the inward HVA Ca^{2+} currents measured at the peak and the plateau (at the end of stimulation pulse) are shown in Figure 16C. As evidenced from Figure 16B and C, a transient current appeared at the relatively hyperpolarized test membrane potentials $\leq$ -30 mV and reached a peak around -20 mV. At more depolarized test potentials, a sustained component of current appeared. The sustained current reached a peak around -15 to -10 mV. The inactivation time constant obtained by fitting the current decay time course was found to be test-potential dependent but the time constant becomes slower at more depolarized test potentials (Fig. 16D

and E). These results suggest that the HVA Ca^{2+} currents of RBCs contain two components: a sustained component and a transient component.

The average peak Ca^{2+} current of RBCs is 48.6 pA ± 2.4 pA (n = 12) in step stimulations. The average Ca^{2+} currents of the sustained component at the end of the 500 ms step stimulation of RBCs is 31 pA ± 1.8 pA (n = 12) and the average whole cell capacitance of RBCs is 4.59 pF ± 0.6 pF (n = 24).

To investigate further the properties of these two components of the current, in the following experiments, the transient component of the Ca^{2+} current was evoked by the test pulse to -35 mV from the holding potential of -50 mV. The sustained component together with the transient one was evoked by the test pulse to -25 mV.

First, both the transient and sustained components of the current were not observed from RBCs without axon terminals (n = 9) (lost during the slice section). In contrast, the T-type Ca^{2+} currents were still present (see Fig. 17). This result suggests that both components of the HVA Ca^{2+} current in RBCs are located exclusively at the axon terminals, which is consistent with all previous reports.

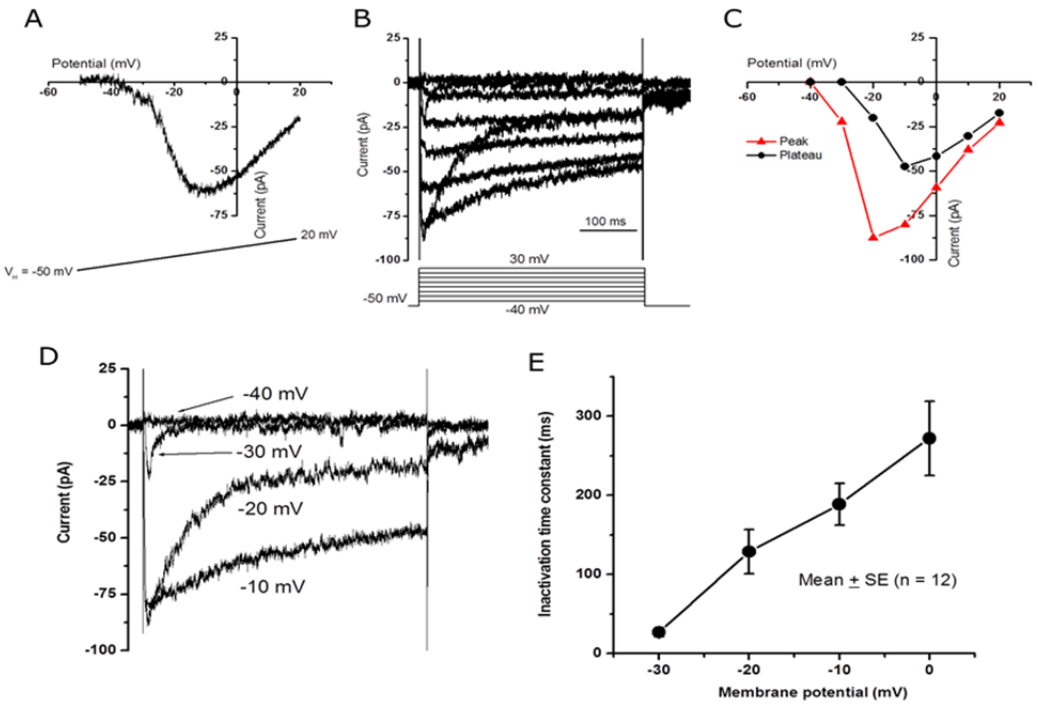

Figure 16. Voltage-gated Ca^{2+} currents recorded from the GFP labeled RBCs in the C57/BL6J mouse line. *A*, Ca^{2+} currents were evoked by a voltage ramp from -50 to 20 mV from the holding potential of -50 mV. *B*, Ca^{2+} currents were evoked by a series of 400 ms test pulses from the holding potential of -50 mV. *C*, The current-voltage (I-V) relationships of the inward HVA Ca^{2+} currents measured at the peak (red triangles) and the plateau (black circles; at the end of stimulation pulse) for the cell shown in B. *D*, Ca^{2+} currents were evoked by four test pulses of 400 ms test pulses of -40 mV to -10 mV from the holding potential of -50 mV. *E*, The relationship of inactivation time constant and test/potential. The inactivation time constants were obtained by fitting the decay phase of the currents with an exponential function.

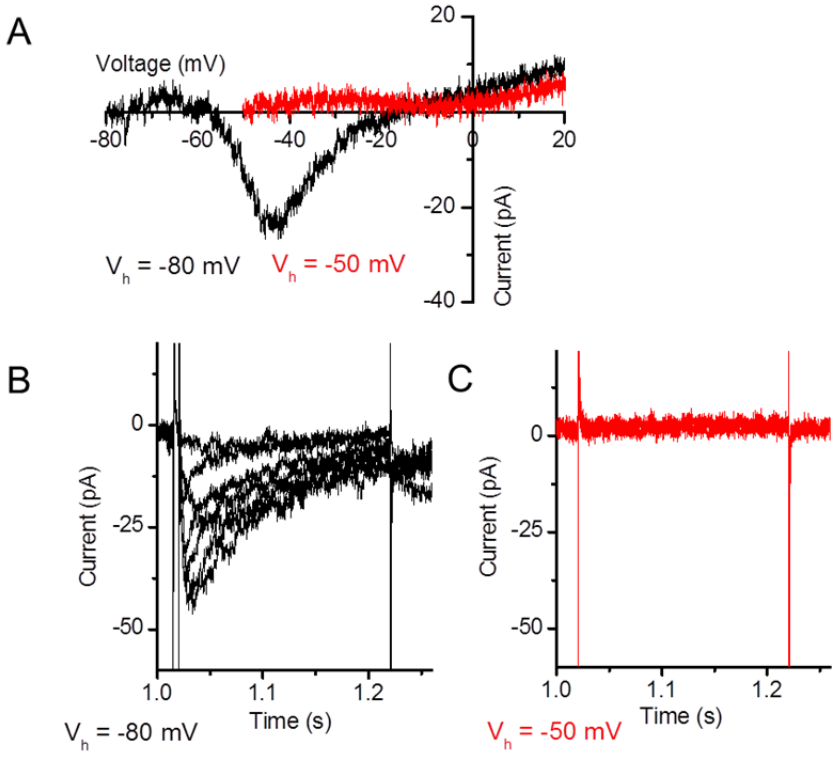

Figure 17. Voltage-activated Ca^{2+} currents from a soma of RBC without axon terminal. *A*, Currents were evoked by a voltage ramp from -80 to 20 mV from the holding potential of -80 mV (black line) and -50mV (red line). *B*, Individual traces evoked by 200 ms test pulses of -40 mV to 20 mV from the holding potential of -80 mV. In *A*-*B*, there were only T-type current on axonless RBCs. This means HVA Ca^{2+} channels expression exclusively at axon terminal of RBCs. In *C*, the single trace was shown evoked by of 200 ms test pulses of -40 mV from the holding potential of -50 mV.

We next examined the possibility of whether the transient component of the current could be contaminated by other currents including Ca^{2+} dependent currents or due to Ca^{2+} dependent inactivation. First, the transient current is TTX insensitive (data not shown). This excludes the possible involvement of voltage-dependent Na^{+} currents in RBCs. Second, we found that both components of the current are Ca^{2+} dependent because no inward current was observed in Ca^{2+}-free extracellular solutions (n = 10) (data not shown). In addition, both components of the current were blocked by 100 μM cadmium (n = 7) (Fig. 18). Furthermore, a similar pattern of Ca^{2+} currents were observed with an extracellular solution where Ca^{2+} was replaced by Ba^{2+} (n = 20) (Fig. 19), suggesting that the transient property of the Ca^{2+} current is unlikely due to Ca^{2+}-dependent inactivation or Ca^{2+} activated other currents. Furthermore, the transient current could not be mediated through the transient receptor potential-like channels (TRPM1) located in the dendrites of RBCs. This is because the current is absent in RBCs without terminals (see Fig. 17). Taken together, these results indicate that the observed HVA current in RBCs was the Ca^{2+} current.

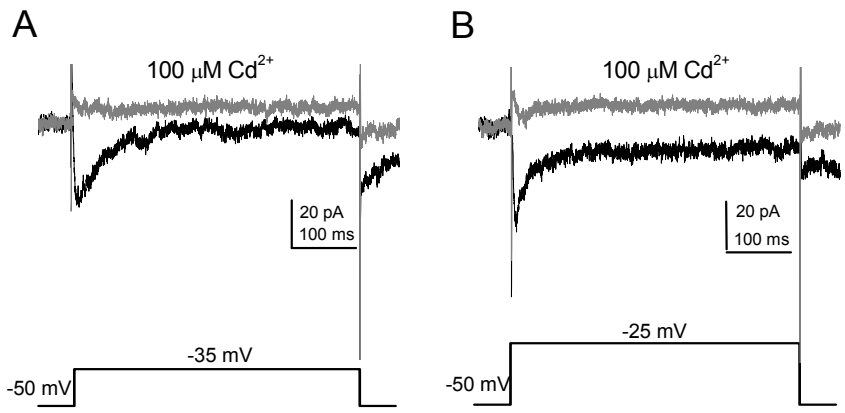

Figure 18. Effects of Cadmium on Ca^{2+} currents in RBCs. Ca^{2+} currents were evoked by the test potential of -35 mV in *A* and -25 mV in *B*. *A*, at the membrane potential of -35 mV, there was only transient component. The transient component can be totally blocked by 100 μM Cadmium. *B*, at the membrane potential of -25 mV, there were both transient and sustained component. Both of the transient and sustained components can be totally blocked by 100 μM cadmium.

3-2. The sustained component of Ca^{2+} current in RBCs was coming from L-type channels

Next, we examined the pharmacological properties of the two components of HVA Ca^{2+} currents in RBCs. It is known that L-type Ca^{2+} currents are DHP-sensitive (Carbone and Lux, 1984). For example, the current can be enhanced by DHP agonists, such as BayK8644, and blocked by DHP antagonists, such as nimodipine. We found that the sustained but not the transient component of Ca^{2+} currents was enhanced by 1 μM BayK-8644 (n = 14) (Fig. 20 A and B). Furthermore, the sustained but not the transient component of Ca^{2+} currents can be blocked by 100 μM nimodipine (n = 13) (Fig. 20 C and D). These results indicated that the sustained but not the transient component of the HVA Ca^{2+} currents was from L-type channels. These results are in part consistent with the early reports that RBCs process sustained L-type Ca^{2+} currents, but our results indicate RBCs also process a non-L-type Ca^{2+} current.

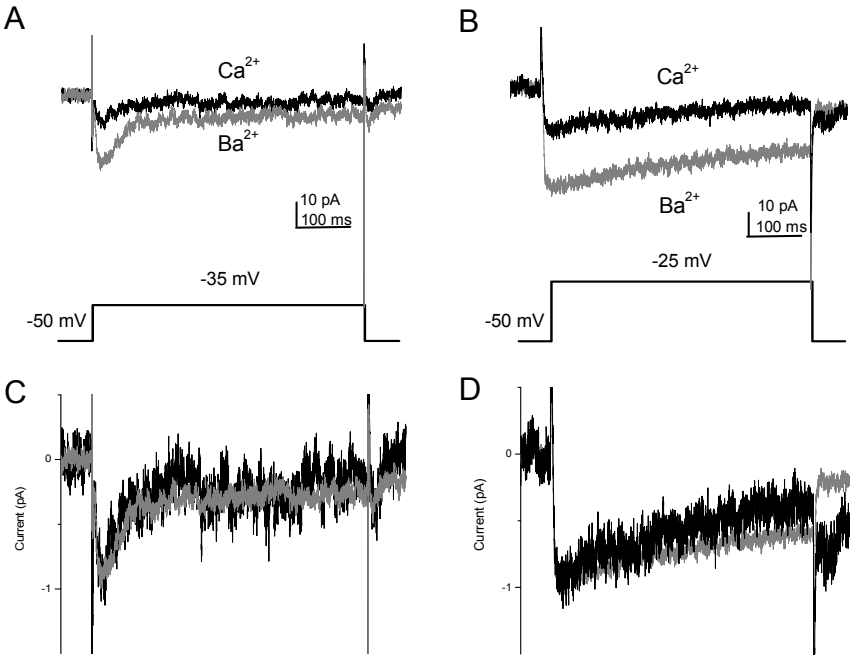

Figure 19. Comparison of Ba^{2+} and Ca^{2+} ion selectivity for the high voltage activated Ca^{2+} currents of RBCs. *A-D*, Currents were evoked by depolarizing to -35 mV from the holding potential of -50 mV. *A*, *C*, Currents were evoked by depolarizing to -35 mV from the holding potential of -50 mV. *B*, *D*, Currents were evoked by depolarizing to -25 mV from the holding potential of -50 mV. *A-B*, showed the original current amplitude. *C-D*, show normalized current based on recording in 10mM Ca^{2+} solution. In *A*, *B*, the currents were larger in 10mM Ba^{2+} comparing to 10 mM Ca^{2+}. But the inactivation properties of the current in 10mM Ba^{2+} were mostly the same as in 10 mM Ca^{2+}. Solutions containing 10 mM Ba^{2+} or 10 mM Ca^{2+} were applied by local perfusion.

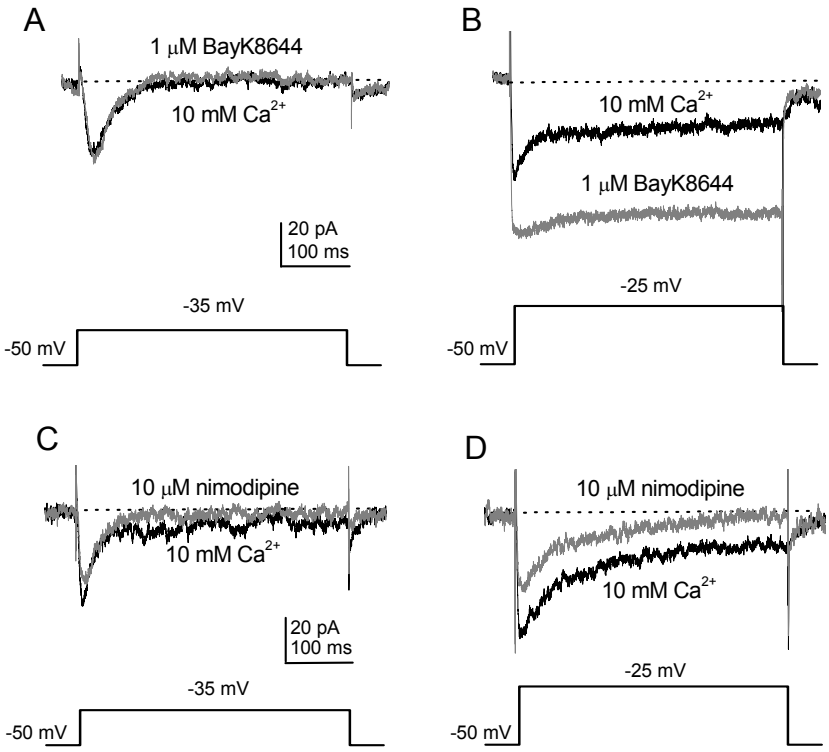

Figure 20. Comparison of the effect in nimodipine and BayK 8644 on the transient and sustained components of HVA Ca^{2+} currents on RBCs. *A* and *C*, Sample traces of Ca^{2+} currents evoked by 500 ms test potentials at -35 mV from the holding potential of -50 mV. *B* and *D*, Sample traces of Ca^{2+} currents evoked by 500 ms test potentials at -25 mV from the holding potential of -50 mV. *A* and *B* were recorded in 10mM Ca^{2+} solution in the presence of 1 μM BayK 8644. *C* and *D* were recorded in 10mM Ca^{2+} solution in the presence of 10 μM nimodipine.

3-3. The transient component of Ca^{2+} current in BCs was coming from P/Q-type channels

We further investigated the pharmacological properties of the transient component of the Ca^{2+} current. First, the transient component of the HVA current could not be blocked by the T-type channel blocker, mibefradil (2μM) (n =16) (Fig. 21A) although mibefradil at this concentration could mostly block the T-type Ca^{2+} current evoked from the RBCs from a more negative holding potential (Fig. 21B). Therefore, the transient component is not a T-type Ca^{2+} current.

Next, we examined non-DHP sensitive HVA Ca^{2+} channel blockers. We found that the transient component was not affected by the N-type Ca^{2+} channels blocker ω-conotoxin GVIA (n = 8) and the R-type Ca^{2+} channel blocker SNX482 (n = 7) (Fig. 22 A and B). On the other hand, the transient component but not the sustained component was largely blocked by a P/Q type Ca^{2+} channel blocker ω-agatoxin IVA (n = 13) (Fig. 22C and D). On average, 53.6% ± 1.8% of the currents was blocked by 200 nM ω-agatoxin IVA. Thus, our results indicate the transient component of the HVA originate from P/Q type Ca^{2+} channels. It should be noted that the voltage activation and the speed of inactivation properties of P/Q type Ca^{2+} channels are between L-type and T-type channels, (Nowycky et al., 1985; Fox et al., 1987). The transient component of HVA Ca^{2+} appears to show this feature.

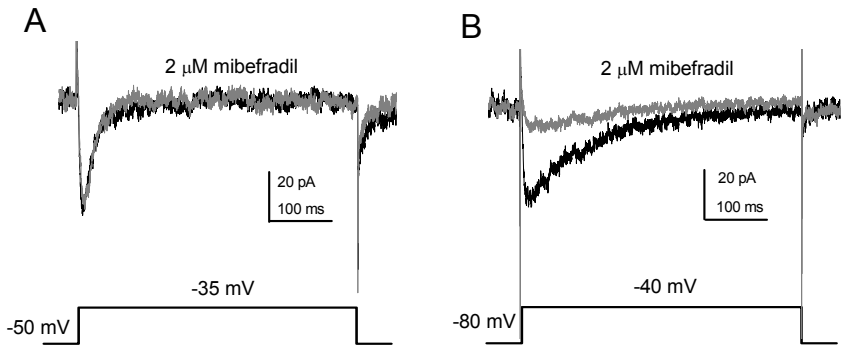

Figure 21. Effects of T-type channel blocker mibefradil on HVA Ca^{2+} currents in RBCs. *A*, Ca^{2+} currents were evoked by the test potential of -35 mV at membrane potential holding at -50 mV. At the membrane potential of -35 mV, there was only transient component. The transient component cannot be blocked by 2 μM mibefradil. *B*, Ca^{2+} currents were evoked by the test potential of -40 mV at membrane potential holding at -80 mV. At the membrane potential of -40 mV, there were only low voltage activated T-type Ca^{2+} currents. The T-type currents can be blocked by 2 μM mibefradil.

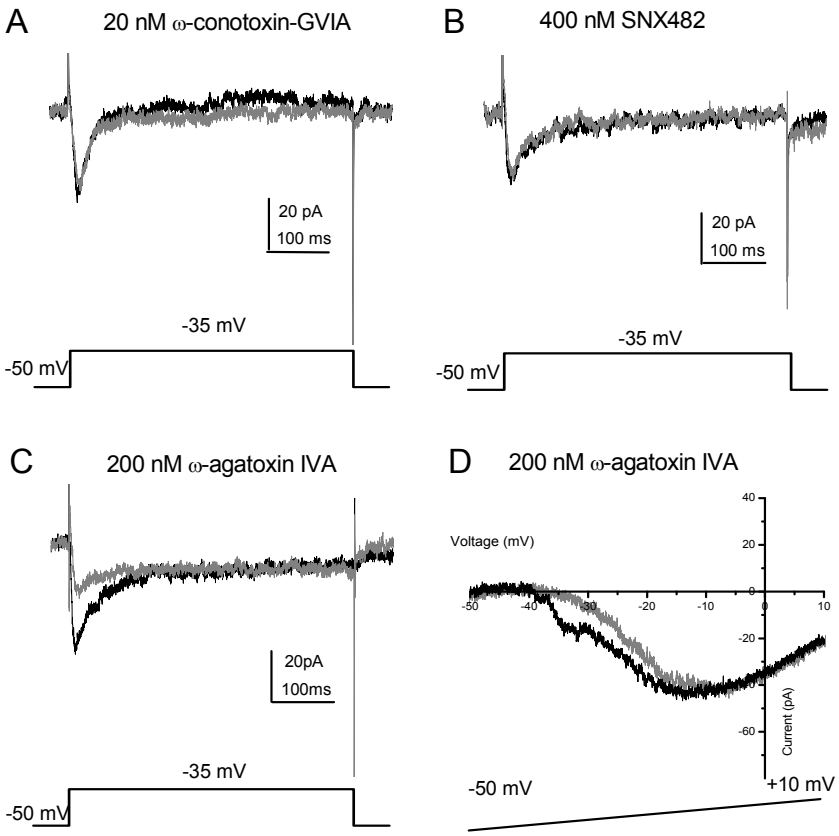

Figure 22. Effects of non-DHP channel blockers on HVA Ca^{2+} currents in RBCs. Sample traces of Ca^{2+} currents evoked by 500 ms test potentials at -35 mV from the holding potential of -50 mV. *A*, Currents were evoked in 10 mM Ca^{2+} (black) and 10 mM Ca^{2+} plus 20 nM N type blocker ω-conotoxin GVIA (grey). The ω-conotoxin cannot block the transient component. *B*, Currents were evoked in 10 mM Ca^{2+} (black) and 10 mM Ca^{2+} plus 400 nM R type blocker SNX482 (grey). SNX-482 cannot block the transient component either. *C*, Currents were evoked in 10 mM Ca^{2+} (black) and 10 mM Ca^{2+} plus 200 nM P/Q type blocker ω-agatoxin IVA (grey). The ω-agatoxin IVA can block the transient component. *D*, Currents were evoked by a voltage ramp from -50 to 10 mV from the holding potential of -50 mV in 10 mM Ca^{2+} (black), and 10 mM Ca^{2+} plus 200 nM P/Q type blocker ω-agatoxin IVA (grey).

Part 4. The molecular composition of L-type Ca^{2+} current in RBC

We then investigated the molecular composition of L-type Ca^{2+} currents in RBCs by using Ca^{2+} channel knockout or deficient mouse lines. In this set of experiments, the magnitude of L-type Ca^{2+} currents in RBCs was evaluated by the ramp stimulation from the holding potential of -50 mV. This is based on the observation that although RBCs process P/Q type Ca^{2+} current, the P/Q type Ca^{2+} current did not contribute significantly to the peak inward Ca^{2+} current evoked by the ramp stimulus. This is because the application of ω-agatoxin did not show significantly affecting the peak inward current evoked by ramp stimulation (shown in Fig. 22D). This would not be unexpected because the P/Q Ca^{2+} current shows relatively fast inactivation and the current is not prominent during slow ramp stimulation.

We first recorded the L-type Ca^{2+} current from a α1D knockout transgenic line and a α1F deficient mouse line. The global knockout α1D mice were generated through homologous recombination together with a multi stop codons cassette sequence (Platzer et al., 2000). The α1F mutant mouse line has been reported to be a naturally occurring null mutation for the α1F Ca^{2+} channel gene (Doering et al., 2008). In ramp stimulation, the magnitude of L-type Ca^{2+} currents recorded from the $\alpha1D^{-/-}$ knockout mice was not found to be different from that of wt mice (Fig. 23). On the other hand, the magnitude of L-type Ca^{2+} currents recorded from the α1F deficient mice knockout mice was found to be moderately reduced (Fig. 24). The average peak current from $\alpha1D^{-/-}$ knockout mice is 28.7 ± 2.8 pA (n = 27) which is significantly smaller than that of the wt mice (39.2 ± 1.9 pA; n = 36) (see Fig. 26). On the other hand, both sustained and transient HVA currents were observed in both Ca^{2+} knockout and deficient lines (Fig. 23B and 24B).

These results suggest at least a partial involvement of the α1F Ca^{2+} channel subunit but not the α1D Ca^{2+} channels in RBCs. However, since in both mouse lines, the gene is deleted

during development, the results could be complicated by possible gene replacement during the development. In addition, a more recent study reported that the α1F Ca^{2+} deficient mouse line used still presents a minor splicing variant of the α1F gene.

We further investigated the molecular composition of the L-type Ca^{2+} current in RBCs by using a α1C conditional knockout mouse line. The α1C conditional knockout line was generated by introducing a mutation cassette flanked by two loxP sites into α1C gene (White et al., 2008). To circumvent the possible gene replacement that could occur during development, the knockout of the α1C gene was achieved by injected an AAV2/2 vector carrying Cre-GFP sequence into the eye of $\alpha1C^{-/-}$ or $\alpha1C^{+/-}$ conditional knockout mice (see Methods). To facilitate the identification of Cre-positive cells with Cre-mediated recombination, a second virus vector carrying mCherry was co-injected. Both viruses can infect RBCs in the retina (see Methods; Fig. 12). The recordings were made from the mCherry positive RBCs.

The L-type Ca^{2+} current from the mCherry-positive RBCs in $\alpha1C^{-/-}$ or $\alpha1C^{+/-}$ conditional knockout mice was compared with that of RBCs from wt mice (C57B/6J), as well as from the mCherry negative RBCs in the virus injected α1C conditional knockout mice. Again, the L-type Ca^{2+} current was assessed by the ramp stimulation from the holding potential of -50 mV.

As assessed by ramp stimulus, the L-type Ca^{2+} currents from the mCherry-positive RBCs of both $\alpha1C^{-/-}$ or $\alpha1C^{+/-}$ knockout mice, especially $\alpha1C^{-/-}$ knockout mice, were markedly smaller than those of the control (Fig. 25 A-C). The average peak inward currents evoked of RBCs by ramp stimulus are 8.53 ± 0.7 pA (n = 9) for $\alpha1C^{-/-}$ and 23.3 ± 2.4 pA (n = 8) for $\alpha1C^{+/-}$ (see Fig. 26).

We also compared the L-type Ca^{2+} current evoked by test pulses among mCherry-expressing RBCs from $\alpha1C^{-/-}$ conditional knockout mice, RBCs in wt mice, the RBCs from

mCherry-negative $\alpha 1C^{-/-}$ conditional knockout mice. As shown in Figures 25D-F and 27, the sustained component of HVA Ca^{2+} current in the mCherry-positive RBCs were markedly reduced compared to the controls. The average peak current and the peak plateau current measured at the end of the 400 ms of the test potential were 26.3 ± 2.3 pA and 4.95 ± 0.89 pA (n = 6), respectively. The values are significantly smaller than those from both controls. From wt mice, the average peak total current and the peak plateau current are 50.6 ± 2.5 pA and 31 ± 2 pA (n = 12), respectively. From mCherry-negative $\alpha 1C^{-/-}$ conditional knockout mice, the average peak total current and the peak plateau current are 46.7 ± 3.3 pA and 30.2 ± 3.8 pA (n = 8), respectively.

Taken together, our results suggest that the majority of the L-type Ca^{2+} current in RBCs is from the α1C Ca^{2+} channels.

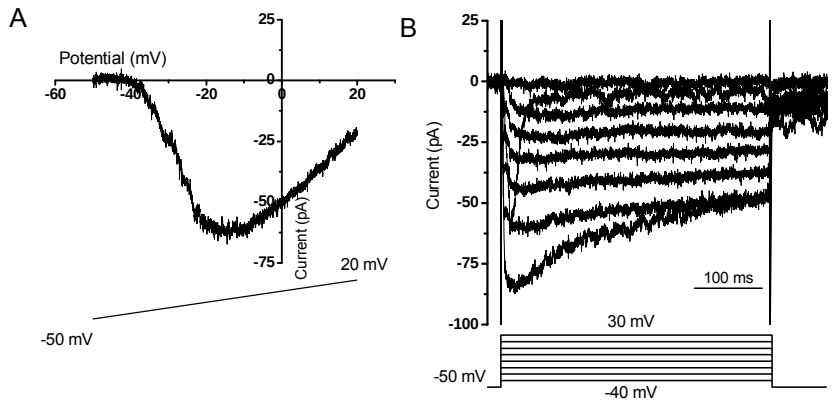

Figure 23. Voltage activated Ca^{2+} currents recorded from RBCs in the $\alpha 1D^{-/-}$ mouse line. *A*, Currents were evoked by a voltage ramp from -50 to 20 mV from the holding potential of -50 mV. *B*, Currents were evoked by a series of 500 ms test pulses from the holding potential of -50 mV.

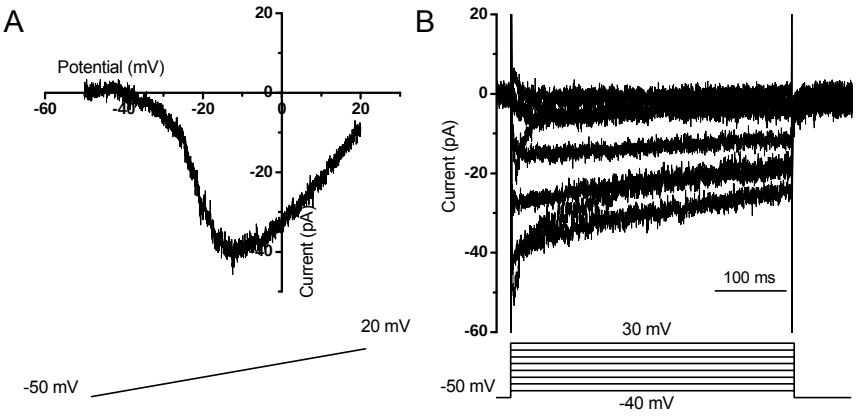

Figure 24. Voltage activated Ca^{2+} currents recorded from RBCs in the $\alpha 1F^{-/-}$ mouse line. *A*, Currents were evoked by a voltage ramp from -50 to 20 mV from the holding potential of -50 mV. *B*, Currents were evoked by a series of 500 ms test pulses from the holding potential of -50 mV.

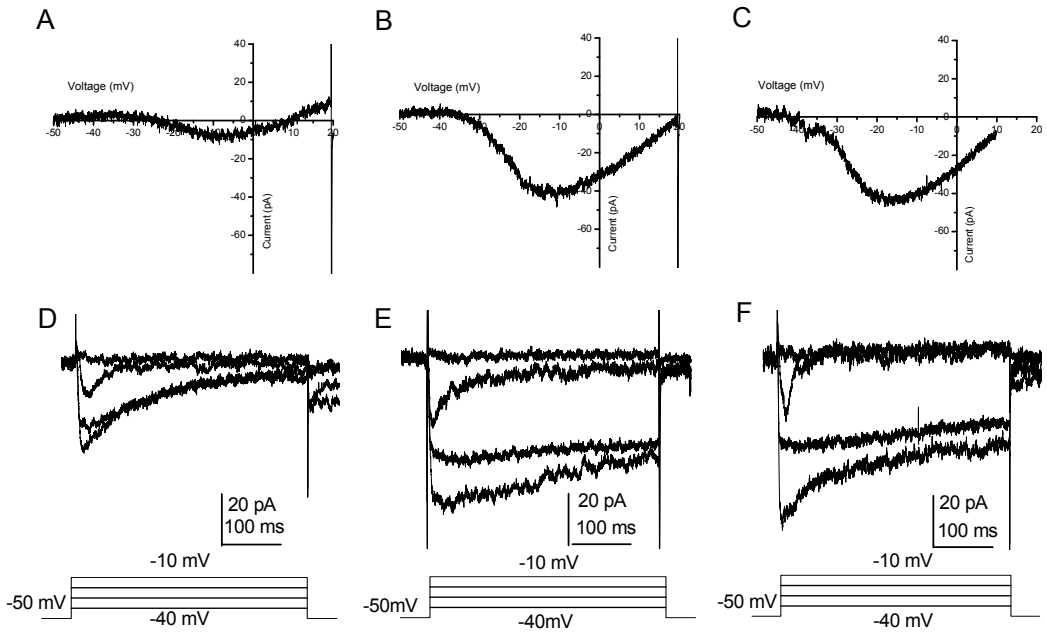

Figure 25. Voltage activated Ca^{2+} currents recorded from the Cre positive RBCs in the $\alpha1C^{-/-}$ mouse line. *A*, Currents were evoked by a voltage ramp from -50 to +20 mV from the holding potential of -50 mV in $\alpha1C^{-/-}$ RBCs. *B*, Currents were evoked by a voltage ramp from -50 to +20 mV from the holding potential of -50 mV in mCherry negative RBCs in α1C conditional knockout animals. Because these cells had no cre recombinase enzyme expression, these cells were recorded as control with normal α1C channels expression pattern as wild type control cells. *C*, Currents were evoked by a voltage ramp from -50 to +20 mV from the holding potential of -50 mV in WT RBCs. *D*, Currents were evoked by a series of 500 ms test pulses from the holding potential of -50 mV in Cre positive RBCs in α1C conditional knockout animals. In these cells the α1C channels were knockout. *E*, Currents were evoked by four test pulses of 500 ms test pulses from the holding potential of -50 mV in in Cre negative RBCs. *F*, Currents were evoked by four test pulses of 500 ms test pulses from the holding potential of -50 mV in wild type cells.

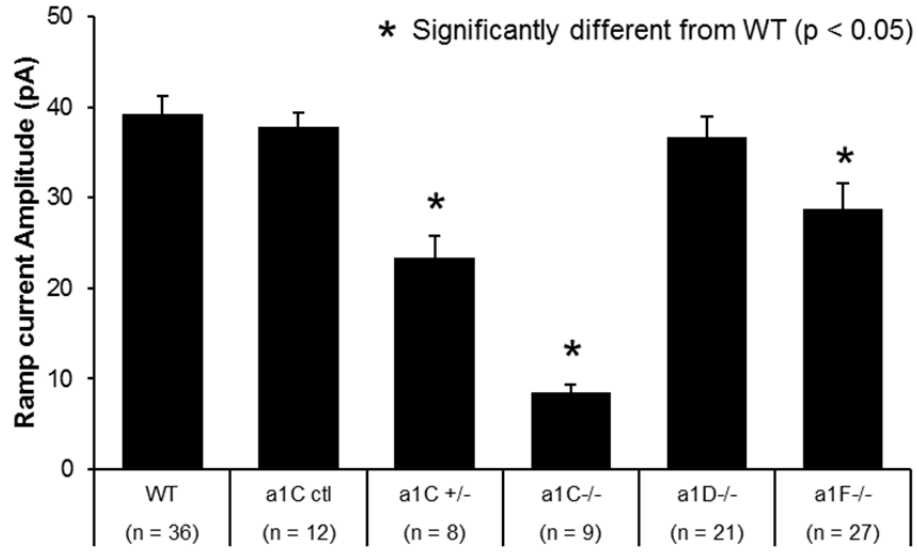

Figure 26. Average current amplitude of HVA Ca^{2+} currents recorded from the BCs with ramp stimulation in the Ca^{2+} channel knockout line and wild type animals. Comparison of current amplitude of HVA Ca^{2+} currents in WT, $\alpha 1C^{+/-}$, $\alpha 1C^{-/-}$, $\alpha 1D^{-/-}$, $\alpha 1F^{-/-}$ RBCs from ramp current. Ca^{2+} currents were evoked by a voltage ramp from -50 to 20 mV from the holding potential of -50 mV.

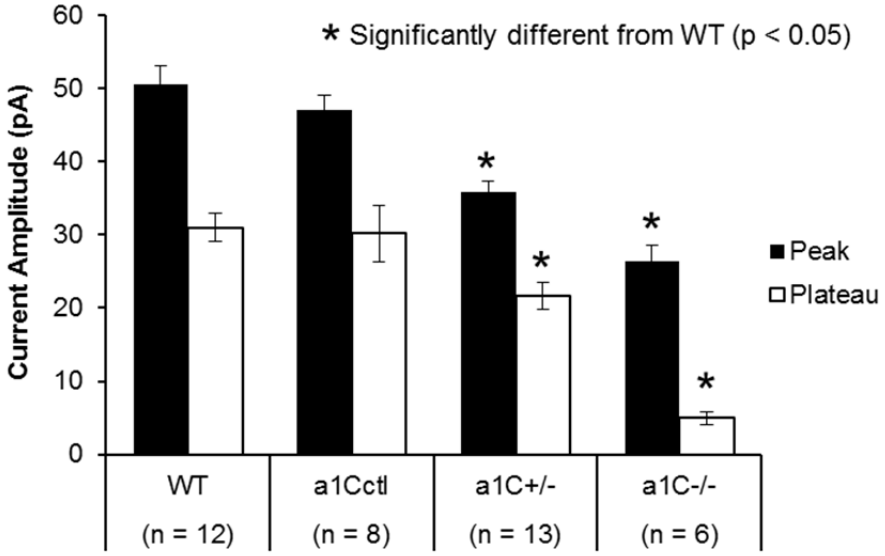

Figure 27. Mean current amplitude of HVA Ca^{2+} currents recorded from the RBCs in the α1C Ca^{2+} channel knockout and wild type animals. Mean peak current for WT mice, normal cells without cre recombinase in α1C conditional knockout mice, and α1C conditional knockout (-/-) mice obtained from the indicated number of cells. Currents were evoked by a series of 500 ms test pulses from the holding potential of -50 mV.

DISCUSSION

In this study, we made a number of new findings about the electrophysiological and molecular properties of HVA Ca^{2+} currents in retinal BCs. First, we revealed the heterogeneous properties of HVA Ca^{2+} currents among CBCs and between CBCs and RBCs. We found that OFF-CBCs as well as RBCs possess prominent HVA Ca^{2+} currents. In contrast, HVA Ca^{2+} currents in ON-CBCs were small or barely detectable in some cases. We also found that the voltage-dependent activation of HVA Ca^{2+} currents among OFF CBCs was different. In addition, the HVA Ca^{2+} currents in CBCs were found to be largely sustained. In contrast, the HVA Ca^{2+} current in RBCs exhibited two components, both sustained and transient. Furthermore, we found for the first time the RBCs in mouse retinas possess P/Q type of HVA Ca^{2+} channels in addition to L-type HVA Ca^{2+} channels. Finally, our results suggest that the L-type HVA Ca^{2+} currents in RBCs are mainly mediated by α1C Ca^{2+} channels.

Heterogeneous properties of HVA Ca^{2+} currents among BCs and functional implications

In this study, we found that all of the recorded OFF-CBCs, type 2, 3, and 4, show large HVA Ca^{2+} currents, which are particularly large in certain types of OFF CBCs, such as type 3 CBCs. In contrast, the HVA Ca^{2+} currents recorded from ON-CBCs, types 6 and 7, were found to be small or barely detectable in some cases. Relatively large HVA Ca^{2+} current was also observed in RBCs, which is an ON-type cell. Could the difference in the amplitude of HVA Ca^{2+} currents observed in electrophysiological recordings reflect their different cellular localization? For example, could it be possible that the Ca^{2+} channels localized at the distal terminal of BCs may not be detected with the patch-clamp recording on the cell soma? We consider this unlikely.

First, because the axons of BCs are relatively short, BCs in general have been considered to be largely isopotential. In addition, as also confirmed in this study, large HVA Ca^{2+} currents were recorded from RBCs although the HVA Ca^{2+} channels in RBCs are known to be present almost exclusively at the axon terminals. Similarly, large HVA Ca^{2+} currents were also observed in type 4 CBCs while our results suggest that HVA Ca^{2+} channels in type 4 CBCs are likely also localized at the axon terminals because no HVA Ca^{2+} current was observed in isolated preparations. In addition, type4 CBCs without terminals have no HVA Ca^{2+} currents in retinal slice preparations. Therefore, the different amplitudes of HVA Ca^{2+} currents observed among different BCs likely reflects the expression level of the HVA Ca^{2+} channels among these cells.

Retinal BCs of all types have been known to process both HVA Ca^{2+} currents and LVA T-type Ca^{2+} currents. Also, both Ca^{2+} currents have been reported to be capable of triggering transmitter release at the axon terminals. The different current amplitude of HVA Ca^{2+} currents observed between ON and OFF-CBCs may suggest that the neurotransmitter release from these two classes of BCs might be mediated by HVA Ca^{2+} channels and LVA T-type Ca^{2+} channels, respectively. Since HVA Ca^{2+} channels and LVA T-type Ca^{2+} channels differ in their voltage-dependent activation and time-dependent inactivation (Pan, 2000; Catterall et al., 2005), the potential differential involvement of these two types of Ca^{2+} currents in different BC classes could have significant functional consequence for regulating BCs' excitability and neurotransmitter release.

Furthermore, our results show the voltage-dependent activation of HVA Ca^{2+} currents among CBCs are different. Specifically, we found that the I-V curve of the HVA Ca^{2+} currents in type 2 CBCs was shifted to more positive potentials than that of type 4 CBCs. The average threshold potential and peak potential in type 2 CBCs are about 10 mV and 15 mV more positive

than that of type 4 CBCs, respectively. As commonly believed, the HVA Ca^{2+} currents in CBCs are likely to be L-type (Protti and Llano, 1998; Protti et al., 2000). L-type Ca^{2+} channels can be formed by four different α1 Ca^{2+} channel subunits, α1S ($Ca_V1.1$), α1C ($Ca_V1.2$), α1D ($Ca_V1.3$), and α1F ($Ca_V1.4$), along with other associated Ca^{2+} channel subunits, which are known to exhibit distinct properties, including voltage-dependent activation, reviewed in (Catterall, 1995, 2000). Our results thus imply the expression of different molecular compositions of L-type Ca^{2+} currents among CBCs. Again, the expression of different properties of HVA Ca^{2+} channels among different BCs, such as among CBCs, could have significant functional consequence for regulating BC excitability and neurotransmitter release.

Expression of P/Q type HVA Ca^{2+} channels in RBCs

An unexpected finding of this study is the expression of both the L-type and P/Q type calcium channels in RBCs. Up to the present time, all the HVA Ca^{2+} channels in retinal BCs, including RBCs, were reported to be L-type (Protti and Llano, 1998; Pan, 2000; Protti et al., 2000; Pan, 2001). Previously, all of the HVA Ca^{2+} currents in BCs were reported to exhibit slow or no time-dependent inactivation (von Gersdorff and Matthews, 1996; Shen et al., 2006). However, in this study in mice, we were surprised to observe a transient component of HVA Ca^{2+} current in RBCs in addition to a sustained one. Consistent with many previous reports our results indeed show that RBCs express L-type Ca^{2+} channels because a sustained Ca^{2+} current that was sensitive to DHP antagonist and agonist was observed. On the other hand, the transient component of the Ca^{2+} currents was activated at more negative membrane potential than the sustained one.

In this study, we demonstrate that the transient component of HVA Ca^{2+} current is mediated by P/Q Ca^{2+} channels. First, our results show that the transient current is not due to a

contamination of other currents or due to Ca^{2+}-dependent inactivation. Second, our pharmacological results show that the current is not blocked by L-, T-, N-, and R-type Ca^{2+} channel blocker but by P/Q-type Ca^{2+} channel selective blocker, ω-agatoxin. In addition, the expression of non-L-type Ca^{2+} channels in RBCs is also consistent with the results of Ca^{2+} channel knockout studies because the transient component of HVA Ca^{2+} current is persistent in all of L-type Ca^{2+} channel knockout or deficient mouse lines.

The P/Q type (Cav2.1) subfamily is a major component of Ca^{2+} channels in trigger transmitter release in neuromuscular junctions and CNS (Olivera et al., 1994). The non-DHP sensitive Ca^{2+} channels are highly rich in presynaptic terminals in CNS neurons (Catterall, 1998). The fast inactivation and blockage by ω-Agatoxin IVA are hallmarks of P/Q type Ca^{2+} currents (Mintz et al., 1992; Sather et al., 1993). P/Q type Ca^{2+} channels also possess intermediate voltage-dependent and Ca^{2+} -dependent properties between L- and T- type Ca^{2+} channels (Catterall et al., 2005).

It is worth mentioning that the P type α1 subunit and the Q- type subunit are two alternative splicing products of the same gene (Stea et al., 1994). The P-type seems to be the α1Ab splice variant and the Q-type is α1Aa. There are several different properties between these two subtypes. First, the blocking efficiency of ω-Agatoxin IVA is high to P-type (K_d = 1-3 nM) (Mintz et al., 1992) and lower to Q- type (K_d = 200 nM) (Randall and Tsien, 1995). Second, only Q-type exhibits a two-exponential function, an obvious peak and slow decline (Budde et al., 2002). Third, P-type channels are more sensitive to the T-type blocker Miberfradil than Q-type channels (Catterall et al., 2005). Based on our results, the transient component of RBCs is likely to be Q-type Ca^{2+} currents. It is possible that in RBCs of mice the P/Q type channels bind with different auxiliary subunits or they are regulated in different mechanisms.

Functional implications for the expression of P/Q Ca^{2+} channels in RBCs

What could be functional roles for the expression of P/Q Ca^{2+} channels in addition to L-type Ca^{2+} channels in RBCs? The RBCs convert synaptic inputs from rod photoreceptors to AII amacrine cells in the rod pathway which operate at dim light, scotopic vision. The rod pathway, which is extremely sensitive, is capable of encoding light luminance as well as contrast at different background light. Although RBCs exhibit a sustained change of membrane potential in response to light, the transmitter release from RBCs to AII amacrine cells was found to be biphasic, both sustained and transient (Singer and Diamond, 2003). The biphasic synaptic transmission has been proposed to be the synaptic mechanism underlining the encoding of light luminance and contrast at RBC-All synapses (Oesch and Diamond, 2011). In previous studies, the transient transmitter release was considered to be the result of depletion of a readily releasable vesicle pool at the terminals of RBCs (Mennerick and Matthews, 1996; von Gersdorff and Matthews, 1996; Singer and Diamond, 2006; Jackman et al., 2009).

The discovery of the expression of two types of HVA Ca^{2+} channels in RBCs in this study raises an alternative possible explanation of the biphasic transmitter release of RBCs. In fact, the P/Q type (Cav2.1) subfamily is a major component of Ca^{2+} channels in triggering transmitter release in neuromuscular junctions and the CNS (Olivera et al., 1994), which is capable of triggering fast synaptic transmission in the CNS (Catterall, 2011). It is also interesting to note that the involvement of L-type Ca^{2+} channels in triggering transmitter release has been considered to be unique to retinal photoreceptor cells and BCs neurons. Since our results show that both P/Q and L-type Ca^{2+} channels are localized at the axon terminals of RBCs, likely both Ca^{2+} channels are involved in synaptic transmission of RBCs. In particular, our results show that the transient component is activated at a more hyperpolarization potential than DHP-sensitive

Ca^{2+} currents. Therefore, the P/Q channels could induce transient Ca^{2+} influx with a small membrane depolarization while L-type Ca^{2+} channels mediate Ca^{2+} influx at stronger stimulus. Although the total calcium influx through P/Q channels is smaller than L-type Ca^{2+} channels, it has better temporal resolution and involve in sensitivity regulation. Further studies would be interesting to determine whether the two types of HVA Ca^{2+} current could also contribute to the encoding of light luminance and contrast at the RBC–AII cell synapses. The finding of the expression of two types of HVA Ca^{2+} channels at the axon terminal of RBCs could be provide new insights into the functional role of voltage-gated Ca^{2+} channels in BC processing.

Approaches for α1C channel conditional knockout

In theory, there are two ways to knockout the α1C gene. The first one is by crossing this mouse line with the Cre transgenic mouse; the expression of α1C in the Cre-expressing cells will be deleted. The other one is intravitreal injection of AAV2/2 virus carrying Cre sequence as used in this study (see methods).

However, the first approach was unsuccessful in our situation, because the Cre-transgenic lines do not express fluorescence protein themselves. For our purpose, the Cre-line needs to cross with two animal lines: one is Cre reporter line with fluorescence protein first, and the other one is the α1C conditional knockout line. The strong Cre reporter line, B6.Cg-Gt (ROSA) 26Sortm9 (CAG-tdTomato) Hze/J (referred to as tdTomato reporter line) harbors a combination of the CMV early enhancer element and chicken beta-actin (CAG) promoter-driven red fluorescent protein (RFP) variant, tdTomato, at the Gt (ROSA) 26Sor locus with a loxP-flanked STOP sequence. Then those cells with reporter fluorescence protein expression will indicate the Cre existence. Only in these Cre expressing cells, the α1C gene would be knocked out. Moreover, the offspring of the triple crossing must be α1C conditional knockout homozygous. Unfortunately,

the gene of α1C (MGI: 103013; Ch6; 55.86cm) is on the same chromosome with the reporter Gt (ROSA) 26 Sor (MGI: 104735; Ch6; 52.73cm) on Chromosome 6 of mouse. Due to their gene sequence locus, it is impossible to obtain offspring with $\alpha 1C^{-/-}$ and $ROSA26^{+/+}$.

For the reason mentioned above, the second approach to obtain $\alpha 1C^{-/-}$ is intravitreal injection of AAV2/2 virus carrying Cre-GFP sequence into α1C conditional knockout animal. Therefore, those cells transfected by AAV virus had Cre-GFP expression are $\alpha 1C^{-/-}$. We developed a virus construct using a modified mGluR6 promoter enhancer that can achieve the expression of transgene in BCs, including RBCs. Although the Cre construct carry GFP sequence, the fluorescence is too weak for slice recordings. To identify the Cre positive RBCs as well as Cre-mediated recombination, the Cre vector as co-injected another AAV virus carrying DIO-mCherry (Lu et al., 2013). In this way, those cells with mCherry expression indicate the Cre-mediated recombination and, likely, the deletion of α1C gene. Also importantly, this approach offers an advantage to eliminate the potential developmental compensation effects.

Molecular composition of L-type Ca^{2+} currents in RBCs

Voltage gated Ca^{2+} channels in presynaptic terminals trigger neurotransmitter release after depolarization. Among the ten types of BC in mouse retina, RBC is a very unique one. In morphology aspect, RBCs have large and round axon terminals, the boutons. Regarding to vision information processing aspect, RBCs do not directly connect with retinal ganglion cells; they superimpose on the existing cone bipolar pathway through AII amacrine cells and A17 amacrine cells.

Although RBCs have been known to express L-type HVA Ca^{2+} channels, the molecular properties of the L-type Ca^{2+} currents in RBCs still needed to be elucidated. Previous

immunostaining studies suggested that L-type Ca^{2+} channels in RBCs could be formed by α1F, α1C, or a1S Ca^{2+} channel subunits (Specht et al., 2009).

In this study, by using α1 Ca^{2+} channel knockout or deficient mouse lines, our results show that L-type HVA Ca^{2+} channels in RBCs are mainly mediated by α1C Ca^{2+} channels. First, we find that the L-type Ca^{2+} current in RBCs was not altered in α1D knockout mice while only moderately reduced in α1F deficient mice. The average current was reduced to 73% in α1F deficient mice compared to that of control in wild type. In contrast, the L-type Ca^{2+} current is markedly reduced in the α1C knock-out RBCs. The average current was reduced to 21.7% of the control. It should be noted that, the negative results from α1D knockout mice could not exclude the possible involvement of α1D in the Ca^{2+} current in RBCs, because of the potential gene compensation that could occur during development in global knockout mouse lines. Similarly, the moderate reduction of HVA Ca^{2+} current in the α1F deficient mice would suggest the α1F gene is at least in part involved. The latter could particularly the case because a recent study reported the presence of a minor splicing variant of the α1F gene in this α1F deficient mouse line. However, our studies of α1C gene knockout were carried out by virus mediated Cre recombination in adult α1C conditional knock-out mice. This would largely reduce the developmental related gene compensation. Thus, the results from α1C knockout studies suggest that the α1C subunit contributes a major component of the L-type Ca^{2+} current in RBCs. Furthermore, considering the results of α1C conditional knockout data, our results suggest that the moderate reduction of the Ca^{2+} current in the α1F deficient mouse line should reflect a small contribution of the α1F subunit to the L-type Ca^{2+} current in RBCs.

A previous immunostaining study reported the positive staining of the α1S Ca^{2+} channel in the OPL (Specht et al., 2009). A more recent study reported that the α1S Ca^{2+} subunit in the retina was a novel isoform co-localized with mGluR6 receptors in the dendritic processes of RBCs. However, the same study by qRT-PCR and RNA sequencing reported but the isoform only contains transmembrane domains III and IV (Ray et al., 2013) (see Scheme 3). This truncated isoform, therefore, is incapable of forming a functional calcium channel. Therefore, the expression of functional α1S Ca^{2+} channels in RBCs is unlikely, consistency with my patch clamp recording data and many earlier reports (Pan, 2000; Protti et al., 2000) that RBCs without axon terminal have no HVA Ca^{2+} currents.

Our results are consistent with the earlier immunostaining results that RBCs express both α1C and α1F calcium channel subunits. However, it is worth to point out that the immunostaining studies of α1C previously showed that α1C is expressed throughout RBCs, including cell soma and dendrites in rats (Xu et al., 2002). The latter was not consistent with the electrophysiological recordings reported by many earlier studies as well as this study in mice.

Mutations in the human α1F-subunit cause X-linked congenital stationary night blindness (Koschak et al., 2003). The cellular pathophysiology of the disease has been suggested to be originate in rod photoreceptors and, also possibly, in RBCs. Since α1F only contributes a small component of Ca^{2+} current in RBCs, our results suggest that the deficiency in α1F mutation is mainly at the level of photoreceptors.

Contribution of Ca^{2+} channels to BC diversity

The voltage gated Ca^{2+} channels in presynaptic terminals are known to play an important role in mediating neuronal excitability and neurotransmitter release. Retinal BCs of different

types have both HVA Ca^{2+} currents and LVA Ca^{2+} currents. Previous studies reported the heterogeneous expression of LVA T-type Ca^{2+} channels among different retinal BCs (Pan, 2000). The major finding of this study is the disclosure of the heterogeneous expression of HVA Ca^{2+} channels in BCs. Our results suggest that the differential expression of HVA Ca^{2+} channels may also contribute to the diversity of synaptic transmission in BCs. Our studies provide new insights into the roles of voltage-gated Ca^{2+} channels of BC in retinal processing as well as the molecular mechanisms of retinal diseases/disorders that could occur from genetic mutations of voltage-gated Ca^{2+} channels.

REFERENCES

Adachi-Akahane S, Cleemann L, Morad M (1999) BAY K 8644 modifies Ca2+ cross signaling between DHP and ryanodine receptors in rat ventricular myocytes. Am J Physiol 276:H1178-1189.

Atasoy D, Aponte Y, Su HH, Sternson SM (2008) A FLEX switch targets Channelrhodopsin-2 to multiple cell types for imaging and long-range circuit mapping. J Neurosci 28:7025-7030.

Awatramani GB, Slaughter MM (2000) Origin of transient and sustained responses in ganglion cells of the retina. J Neurosci 20:7087-7095.

Ball SL, Powers PA, Shin HS, Morgans CW, Peachey NS, Gregg RG (2002) Role of the beta(2) subunit of voltage-dependent calcium channels in the retinal outer plexiform layer. Invest Ophthalmol Vis Sci 43:1595-1603.

Barbour B, Keller BU, Llano I, Marty A (1994) Prolonged presence of glutamate during excitatory synaptic transmission to cerebellar Purkinje cells. Neuron 12:1331-1343.

Barski JJ, Dethleffsen K, Meyer M (2000) Cre recombinase expression in cerebellar Purkinje cells. Genesis 28:93-98.

Berntson A, Taylor WR (2000) Response characteristics and receptive field widths of on-bipolar cells in the mouse retina. J Physiol 524 Pt 3:879-889.

Berntson A, Taylor WR, Morgans CW (2003) Molecular identity, synaptic localization, and physiology of calcium channels in retinal bipolar cells. J Neurosci Res 71:146-151.

Boycott BB, Kolb H (1973) The connections between bipolar cells and photoreceptors in the retina of the domestic cat. J Comp Neurol 148:91-114.

Branda CS, Dymecki SM (2004) Talking about a revolution: The impact of site-specific recombinases on genetic analyses in mice. Dev Cell 6:7-28.

Budde T, Meuth S, Pape HC (2002) Calcium-dependent inactivation of neuronal calcium channels. Nat Rev Neurosci 3:873-883.

Burrone J, Lagnado L (1997) Electrical resonance and Ca2+ influx in the synaptic terminal of depolarizing bipolar cells from the goldfish retina. J Physiol 505 (Pt 3):571-584.

Calin-Jageman I, Lee A (2008) Ca(v)1 L-type Ca2+ channel signaling complexes in neurons. J Neurochem 105:573-583.

Carbone E, Lux HD (1984) A low voltage-activated, fully inactivating Ca channel in vertebrate sensory neurones. Nature 310:501-502.

Catterall WA (1995) Structure and function of voltage-gated ion channels. Annual review of biochemistry 64:493-531.

Catterall WA (1998) Structure and function of neuronal Ca2+ channels and their role in neurotransmitter release. Cell Calcium 24:307-323.

Catterall WA (2000) Structure and regulation of voltage-gated Ca2+ channels. Annu Rev Cell Dev Biol 16:521-555.

Catterall WA (2011) Voltage-gated calcium channels. Cold Spring Harbor perspectives in biology 3:a003947.

Catterall WA, Leal K, Nanou E (2013) Calcium channels and short-term synaptic plasticity. J Biol Chem 288:10742-10749.

Catterall WA, Perez-Reyes E, Snutch TP, Striessnig J (2005) International Union of Pharmacology. XLVIII. Nomenclature and structure-function relationships of voltage-gated calcium channels. Pharmacol Rev 57:411-425.

Catterall WA, Cestele S, Yarov-Yarovoy V, Yu FH, Konoki K, Scheuer T (2007) Voltage-gated ion channels and gating modifier toxins. Toxicon 49:124-141.

Chien AJ, Hosey MM (1998) Post-translational modifications of beta subunits of voltage-dependent calcium channels. J Bioenerg Biomembr 30:377-386.

Cui J, Pan ZH (2008) Two types of cone bipolar cells express voltage-gated Na+ channels in the rat retina. Vis Neurosci 25:635-645.

D'Hooge R, Van de Vijver G, Van Bogaert PP, Marescau B, Vanholder R, De Deyn PP (2003) Involvement of voltage- and ligand-gated Ca2+ channels in the neuroexcitatory and synergistic effects of putative uremic neurotoxins. Kidney Int 63:1764-1775.

Dacheux RF, Raviola E (1986) The rod pathway in the rabbit retina: a depolarizing bipolar and amacrine cell. J Neurosci 6:331-345.

Dascal N, Snutch TP, Lubbert H, Davidson N, Lester HA (1986) Expression and modulation of voltage-gated calcium channels after RNA injection in Xenopus oocytes. Science 231:1147-1150.

de la Villa P, Vaquero CF, Kaneko A (1998) Two types of calcium currents of the mouse bipolar cells recorded in the retinal slice preparation. Eur J Neurosci 10:317-323.

DeVries SH (2000) Bipolar cells use kainate and AMPA receptors to filter visual information into separate channels. Neuron 28:847-856.

Dhingra A, Sulaiman P, Xu Y, Fina ME, Veh RW, Vardi N (2008) Probing neurochemical structure and function of retinal ON bipolar cells with a transgenic mouse. J Comp Neurol 510:484-496.

Doering CJ, Rehak R, Bonfield S, Peloquin JB, Stell WK, Mema SC, Sauve Y, McRory JE (2008) Modified Ca(v)1.4 expression in the Cacnα1F(nob2) mouse due to alternative splicing of an ETn inserted in exon 2. PLoS One 3:e2538.

Dolphin AC (2003) G protein modulation of voltage-gated calcium channels. Pharmacol Rev 55:607-627.

Dowling JE, Boycott BB (1969) Retinal ganglion cells: a correlation of anatomical and physiological approaches. UCLA forum in medical sciences 8:145-161.

Duebel J, Haverkamp S, Schleich W, Feng G, Augustine GJ, Kuner T, Euler T (2006) Two-photon imaging reveals somatodendritic chloride gradient in retinal ON-type bipolar cells expressing the biosensor Clomeleon. Neuron 49:81-94.

Ertel EA, Campbell KP, Harpold MM, Hofmann F, Mori Y, Perez-Reyes E, Schwartz A, Snutch TP, Tanabe T, Birnbaumer L, Tsien RW, Catterall WA (2000) Nomenclature of voltage-gated calcium channels. Neuron 25:533-535.

Euler T, Wassle H (1995) Immunocytochemical identification of cone bipolar cells in the rat retina. J Comp Neurol 361:461-478.

Euler T, Masland RH (2000) Light-evoked responses of bipolar cells in a mammalian retina. J Neurophysiol 83:1817-1829.

Evans RM, Zamponi GW (2006) Presynaptic Ca2+ channels--integration centers for neuronal signaling pathways. Trends Neurosci 29:617-624.

Famiglietti EV, Jr. (1981) Functional architecture of cone bipolar cells in mammalian retina. Vision Res 21:1559-1563.

Fisher R, Johnston D (1990) Differential modulation of single voltage-gated calcium channels by cholinergic and adrenergic agonists in adult hippocampal neurons. J Neurophysiol 64:1291-1302.

Fox AP, Nowycky MC, Tsien RW (1987) Single-channel recordings of three types of calcium channels in chick sensory neurones. J Physiol 394:173-200.

Fox MA, Sanes JR (2007) Synaptotagmin I and II are present in distinct subsets of central synapses. J Comp Neurol 503:280-296.

Fyk-Kolodziej B, Pourcho RG (2007) Differential distribution of hyperpolarization-activated and cyclic nucleotide-gated channels in cone bipolar cells of the rat retina. J Comp Neurol 501:891-903.

Gaveriaux-Ruff C, Kieffer BL (2007) Conditional gene targeting in the mouse nervous system: Insights into brain function and diseases. Pharmacol Ther 113:619-634.

Ghosh KK, Bujan S, Haverkamp S, Feigenspan A, Wassle H (2004) Types of bipolar cells in the mouse retina. J Comp Neurol 469:70-82.

Gong S, Doughty M, Harbaugh CR, Cummins A, Hatten ME, Heintz N, Gerfen CR (2007) Targeting Cre recombinase to specific neuron populations with bacterial artificial chromosome constructs. J Neurosci 27:9817-9823.

Gong S, Zheng C, Doughty ML, Losos K, Didkovsky N, Schambra UB, Nowak NJ, Joyner A, Leblanc G, Hatten ME, Heintz N (2003) A gene expression atlas of the central nervous system based on bacterial artificial chromosomes. Nature 425:917-925.

Graef IA, Mermelstein PG, Stankunas K, Neilson JR, Deisseroth K, Tsien RW, Crabtree GR (1999) L-type calcium channels and GSK-3 regulate the activity of NF-ATc4 in hippocampal neurons. Nature 401:703-708.

Grover LM, Teyler TJ (1990) Two components of long-term potentiation induced by different patterns of afferent activation. Nature 347:477-479.

Han L, Zhong YM, Yang XL (2007) 5-HT2A receptors are differentially expressed in bullfrog and rat retinas: a comparative study. Brain Res Bull 73:273-277.

Han Y, Massey SC (2005) Electrical synapses in retinal ON cone bipolar cells: subtype-specific expression of connexins. Proc Natl Acad Sci U S A 102:13313-13318.

Hartveit E (1999) Reciprocal synaptic interactions between rod bipolar cells and amacrine cells in the rat retina. J Neurophysiol 81:2923-2936.

Haverkamp S, Ghosh KK, Hirano AA, Wassle H (2003) Immunocytochemical description of five bipolar cell types of the mouse retina. J Comp Neurol 455:463-476.

Haverkamp S, Inta D, Monyer H, Wassle H (2009) Expression analysis of green fluorescent protein in retinal neurons of four transgenic mouse lines. Neuroscience 160:126-139.

Haverkamp S, Wassle H, Duebel J, Kuner T, Augustine GJ, Feng G, Euler T (2005) The primordial, blue-cone color system of the mouse retina. J Neurosci 25:5438-5445.

Haverkamp S, Specht D, Majumdar S, Zaidi NF, Brandstatter JH, Wasco W, Wassle H, Tom Dieck S (2008) Type 4 OFF cone bipolar cells of the mouse retina express calsenilin and contact cones as well as rods. J Comp Neurol 507:1087-1101.

Heidelberger R, Matthews G (1992) Calcium influx and calcium current in single synaptic terminals of goldfish retinal bipolar neurons. J Physiol 447:235-256.

Hess P, Lansman JB, Tsien RW (1984) Different modes of Ca channel gating behaviour favoured by dihydropyridine Ca agonists and antagonists. Nature 311:538-544.

Hille B (2001) Ion Channels of Excitable Membranes, Third Edition.

Hofmann F, Biel M, Flockerzi V (1994) Molecular basis for Ca2+ channel diversity. Annu Rev Neurosci 17:399-418.

Hu HJ, Pan ZH (2002) Differential expression of K+ currents in mammalian retinal bipolar cells. Vis Neurosci 19:163-173.

Huang L, Max M, Margolskee RF, Su H, Masland RH, Euler T (2003) G protein subunit G gamma 13 is coexpressed with G alpha o, G beta 3, and G beta 4 in retinal ON bipolar cells. J Comp Neurol 455:1-10.

Ivanova E, Muller F (2006) Retinal bipolar cell types differ in their inventory of ion channels. Vis Neurosci 23:143-154.

Ivanova E, Hwang GS, Pan ZH (2010) Characterization of transgenic mouse lines expressing Cre recombinase in the retina. Neuroscience 165:233-243.

Ivanova E, Lee, P., and Pan, Z.-H. (2012) Characterization of multiple bistratified retinal ganglion cells in a purkinje cell protein 2-cre transgenic mouse line. J Comp Neurol.

Jackman SL, Choi SY, Thoreson WB, Rabl K, Bartoletti TM, Kramer RH (2009) Role of the synaptic ribbon in transmitting the cone light response. Nat Neurosci 12:303-310.

Jakobs TC, Ben Y, Masland RH (2003) CD15 immunoreactive amacrine cells in the mouse retina. J Comp Neurol 465:361-371.

Kaneko A, Suzuki S, Pinto LH, Tachibana M (1991) Membrane currents and pharmacology of retinal bipolar cells: a comparative study on goldfish and mouse. Comp Biochem Physiol C 98:115-127.

Kolb H, Nelson R, Mariani A (1981) Amacrine cells, bipolar cells and ganglion cells of the cat retina: a Golgi study. Vision Res 21:1081-1114.

Kollmar R, Montgomery LG, Fak J, Henry LJ, Hudspeth AJ (1997) Predominance of the alphα1D subunit in L-type voltage-gated Ca2+ channels of hair cells in the chicken's cochlea. Proc Natl Acad Sci U S A 94:14883-14888.

Koschak A, Reimer D, Walter D, Hoda JC, Heinzle T, Grabner M, Striessnig J (2003) Cav1.4alpha1 subunits can form slowly inactivating dihydropyridine-sensitive L-type Ca2+ channels lacking Ca2+-dependent inactivation. J Neurosci 23:6041-6049.

Kuhlman SJ, Huang ZJ (2008) High-resolution labeling and functional manipulation of specific neuron types in mouse brain by Cre-activated viral gene expression. PLoS One 3:e2005.

Lacinova L (2005) Voltage-dependent calcium channels. Gen Physiol Biophys 24 Suppl 1:1-78.

Le YZ (2011) Conditional gene targeting: dissecting the cellular mechanisms of retinal degenerations. Journal of ophthalmology 2011:806783.

Lewis PM, Gritli-Linde A, Smeyne R, Kottmann A, McMahon AP (2004) Sonic hedgehog signaling is required for expansion of granule neuron precursors and patterning of the mouse cerebellum. Dev Biol 270:393-410.

Light AC, Zhu Y, Shi J, Saszik S, Lindstrom S, Davidson L, Li X, Chiodo VA, Hauswirth WW, Li W, DeVries SH (2012) Organizational motifs for ground squirrel cone bipolar cells. J Comp Neurol 520:2864-2887.

Lin B, Jakobs TC, Masland RH (2005) Different functional types of bipolar cells use different gap-junctional proteins. J Neurosci 25:6696-6701.

Lipscombe D, Pan JQ, Gray AC (2002) Functional diversity in neuronal voltage-gated calcium channels by alternative splicing of Ca(v)alpha1. Mol Neurobiol 26:21-44.

Lonchamp E, Dupont JL, Doussau F, Shin HS, Poulain B, Bossu JL (2009) Deletion of Cav2.1(alpha1(A)) subunit of Ca2+-channels impairs synaptic GABA and glutamate release in the mouse cerebellar cortex in cultured slices. Eur J Neurosci 30:2293-2307.

Lu Q, Ivanova E, Pan ZH (2009) Characterization of green fluorescent protein-expressing retinal cone bipolar cells in a 5-hydroxytryptamine receptor 2a transgenic mouse line. Neuroscience 163:662-668.

Ma YP, Pan ZH (2003) Spontaneous regenerative activity in mammalian retinal bipolar cells: roles of multiple subtypes of voltage-dependent Ca2+ channels. Vis Neurosci 20:131-139.

Ma YP, Cui J, Pan ZH (2005) Heterogeneous expression of voltage-dependent Na+ and K+ channels in mammalian retinal bipolar cells. Vis Neurosci 22:119-133.

Ma YP, Cui J, Hu HJ, Pan ZH (2003) Mammalian retinal bipolar cells express inwardly rectifying K+ currents (IKir) with a different distribution than that of Ih. J Neurophysiol 90:3479-3489.

Madisen L, Zwingman TA, Sunkin SM, Oh SW, Zariwala HA, Gu H, Ng LL, Palmiter RD, Hawrylycz MJ, Jones AR, Lein ES, Zeng H (2010) A robust and high-throughput Cre reporting and characterization system for the whole mouse brain. Nat Neurosci 13:133-140.

Maguire G, Maple B, Lukasiewicz P, Werblin F (1989) Gamma-aminobutyrate type B receptor modulation of L-type calcium channel current at bipolar cell terminals in the retina of the tiger salamander. Proc Natl Acad Sci U S A 86:10144-10147.

Mao BQ, MacLeish PR, Victor JD (1998) The intrinsic dynamics of retinal bipolar cells isolated from tiger salamander. Vis Neurosci 15:425-438.

Mataruga A, Kremmer E, Muller F (2007) Type 3a and type 3b OFF cone bipolar cells provide for the alternative rod pathway in the mouse retina. J Comp Neurol 502:1123-1137.

McCleskey EW, Fox AP, Feldman DH, Cruz LJ, Olivera BM, Tsien RW, Yoshikami D (1987) Omega-conotoxin: direct and persistent blockade of specific types of calcium channels in neurons but not muscle. Proc Natl Acad Sci U S A 84:4327-4331.

Mennerick S, Matthews G (1996) Ultrafast exocytosis elicited by calcium current in synaptic terminals of retinal bipolar neurons. Neuron 17:1241-1249.

Miller ED, Tran MN, Wong GK, Oakley DM, Wong RO (1999) Morphological differentiation of bipolar cells in the ferret retina. Vis Neurosci 16:1133-1144.

Milot E, Strouboulis J, Trimborn T, Wijgerde M, de Boer E, Langeveld A, Tan-Un K, Vergeer W, Yannoutsos N, Grosveld F, Fraser P (1996) Heterochromatin effects on the frequency and duration of LCR-mediated gene transcription. Cell 87:105-114.

Mintz IM, Venema VJ, Swiderek KM, Lee TD, Bean BP, Adams ME (1992) P-type calcium channels blocked by the spider toxin omega-Aga-IVA. Nature 355:827-829.

Miyake Y, Yagasaki K, Horiguchi M, Kawase Y, Kanda T (1986) Congenital stationary night blindness with negative electroretinogram. A new classification. Arch Ophthalmol 104:1013-1020.

Moosmang S, Kleppisch T, Wegener J, Welling A, Hofmann F (2007) Analysis of calcium channels by conditional mutagenesis. Handb Exp Pharmacol:469-490.

Morgans CW (1999) Calcium channel heterogeneity among cone photoreceptors in the tree shrew retina. Eur J Neurosci 11:2989-2993.

Morgans CW, Gaughwin P, Maleszka R (2001) Expression of the alphα1F calcium channel subunit by photoreceptors in the rat retina. Mol Vis 7:202-209.

Morgans CW, Ren G, Akileswaran L (2006) Localization of nyctalopin in the mammalian retina. Eur J Neurosci 23:1163-1171.

Morgans CW, Bayley PR, Oesch NW, Ren G, Akileswaran L, Taylor WR (2005) Photoreceptor calcium channels: insight from night blindness. Vis Neurosci 22:561-568.

Muller F, Scholten A, Ivanova E, Haverkamp S, Kremmer E, Kaupp UB (2003) HCN channels are expressed differentially in retinal bipolar cells and concentrated at synaptic terminals. Eur J Neurosci 17:2084-2096.

Murbartian J, Arias JM, Lee JH, Gomora JC, Perez-Reyes E (2002) Alternative splicing of the rat Ca(v)3.3 T-type calcium channel gene produces variants with distinct functional properties(1). FEBS Lett 528:272-278.

Nagy A (2000) Cre recombinase: the universal reagent for genome tailoring. Genesis 26:99-109.

Neely A, Wei X, Olcese R, Birnbaumer L, Stefani E (1993) Potentiation by the beta subunit of the ratio of the ionic current to the charge movement in the cardiac calcium channel. Science 262:575-578.

Nickerson PE, Ronellenfitch K, McEwan J, Kim H, McInnes RR, Chow RL (2011) A transgenic mouse line expressing cre recombinase in undifferentiated postmitotic mouse retinal bipolar cell precursors. PLoS One 6:e27145.

Nowycky MC, Fox AP, Tsien RW (1985) Three types of neuronal calcium channel with different calcium agonist sensitivity. Nature 316:440-443.

Oberdick J, Smeyne RJ, Mann JR, Zackson S, Morgan JI (1990) A promoter that drives transgene expression in cerebellar Purkinje and retinal bipolar neurons. Science 248:223-226.

Olivera BM, Miljanich GP, Ramachandran J, Adams ME (1994) Calcium channel diversity and neurotransmitter release: the omega-conotoxins and omega-agatoxins. Annual review of biochemistry 63:823-867.

Oltedal L, Hartveit E (2010) Transient release kinetics of rod bipolar cells revealed by capacitance measurement of exocytosis from axon terminals in rat retinal slices. J Physiol 588:1469-1487.

Pan ZH (2000) Differential expression of high- and two types of low-voltage-activated calcium currents in rod and cone bipolar cells of the rat retina. J Neurophysiol 83:513-527.

Pan ZH (2001) Voltage-activated Ca2+ channels and ionotropic GABA receptors localized at axon terminals of mammalian retinal bipolar cells. Vis Neurosci 18:279-288.

Pan ZH, Hu HJ (2000) Voltage-dependent Na(+) currents in mammalian retinal cone bipolar cells. J Neurophysiol 84:2564-2571.

Perez-Reyes E (2003) Molecular physiology of low-voltage-activated t-type calcium channels. Physiol Rev 83:117-161.

Perez De Sevilla Muller L, Shelley J, Weiler R (2007) Displaced amacrine cells of the mouse retina. J Comp Neurol 505:177-189.

Petrs-Silva H, Dinculescu A, Li Q, Min SH, Chiodo V, Pang JJ, Zhong L, Zolotukhin S, Srivastava A, Lewin AS, Hauswirth WW (2009) High-efficiency transduction of the mouse retina by tyrosine-mutant AAV serotype vectors. Mol Ther 17:463-471.

Pignatelli V, Strettoi E (2004) Bipolar cells of the mouse retina: a gene gun, morphological study. J Comp Neurol 476:254-266.

Platzer J, Engel J, Schrott-Fischer A, Stephan K, Bova S, Chen H, Zheng H, Striessnig J (2000) Congenital deafness and sinoatrial node dysfunction in mice lacking class D L-type Ca2+ channels. Cell 102:89-97.

Pootanakit K, Prior KJ, Hunter DD, Brunken WJ (1999) 5-HT2a receptors in the rabbit retina: potential presynaptic modulators. Vis Neurosci 16:221-230.

Pourcho RG, Goebel DJ (1987) A combined Golgi and autoradiographic study of 3H-glycine-accumulating cone bipolar cells in the cat retina. J Neurosci 7:1178-1188.

Protti DA, Llano I (1998) Calcium currents and calcium signaling in rod bipolar cells of rat retinal slices. J Neurosci 18:3715-3724.

Protti DA, Flores-Herr N, von Gersdorff H (2000) Light evokes Ca2+ spikes in the axon terminal of a retinal bipolar cell. Neuron 25:215-227.

Randall A, Tsien RW (1995) Pharmacological dissection of multiple types of Ca2+ channel currents in rat cerebellar granule neurons. J Neurosci 15:2995-3012.

Rowan S, Cepko CL (2004) Genetic analysis of the homeodomain transcription factor Chx10 in the retina using a novel multifunctional BAC transgenic mouse reporter. Dev Biol 271:388-402.

Saito H, Tsumura H, Otake S, Nishida A, Furukawa T, Suzuki N (2005) L7/Pcp-2-specific expression of Cre recombinase using knock-in approach. Biochem Biophys Res Commun 331:1216-1221.

Sather WA, Tanabe T, Zhang JF, Mori Y, Adams ME, Tsien RW (1993) Distinctive biophysical and pharmacological properties of class A (BI) calcium channel alpha 1 subunits. Neuron 11:291-303.

Schnutgen F, Doerflinger N, Calleja C, Wendling O, Chambon P, Ghyselinck NB (2003) A directional strategy for monitoring Cre-mediated recombination at the cellular level in the mouse. Nature biotechnology 21:562-565.

Seisenberger C, Specht V, Welling A, Platzer J, Pfeifer A, Kuhbandner S, Striessnig J, Klugbauer N, Feil R, Hofmann F (2000) Functional embryonic cardiomyocytes after disruption of the L-type alphα1C (Cav1.2) calcium channel gene in the mouse. J Biol Chem 275:39193-39199.

Shen Y, Yu D, Hiel H, Liao P, Yue DT, Fuchs PA, Soong TW (2006) Alternative splicing of the Ca(v)1.3 channel IQ domain, a molecular switch for Ca2+-dependent inactivation within auditory hair cells. J Neurosci 26:10690-10699.

Singer JH, Diamond JS (2003) Sustained Ca2+ entry elicits transient postsynaptic currents at a retinal ribbon synapse. J Neurosci 23:10923-10933.

Singer JH, Diamond JS (2006) Vesicle depletion and synaptic depression at a mammalian ribbon synapse. J Neurophysiol 95:3191-3198.

Sinnegger-Brauns MJ, Huber IG, Koschak A, Wild C, Obermair GJ, Einzinger U, Hoda JC, Sartori SB, Striessnig J (2009) Expression and 1,4-dihydropyridine-binding properties of brain L-type calcium channel isoforms. Mol Pharmacol 75:407-414.

Smith L (2011) Good planning and serendipity: exploiting the Cre/Lox system in the testis. Reproduction 141:151-161.

Specht D, Wu SB, Turner P, Dearden P, Koentgen F, Wolfrum U, Maw M, Brandstatter JH, tom Dieck S (2009) Effects of presynaptic mutations on a postsynaptic Cacna1s calcium channel colocalized with mGluR6 at mouse photoreceptor ribbon synapses. Invest Ophthalmol Vis Sci 50:505-515.

Stea A, Tomlinson WJ, Soong TW, Bourinet E, Dubel SJ, Vincent SR, Snutch TP (1994) Localization and functional properties of a rat brain alpha 1A calcium channel reflect similarities to neuronal Q- and P-type channels. Proc Natl Acad Sci U S A 91:10576-10580.

Strettoi E, Pignatelli V (2000) Modifications of retinal neurons in a mouse model of retinitis pigmentosa. Proc Natl Acad Sci U S A 97:11020-11025.

Surace EM, Auricchio A (2008) Versatility of AAV vectors for retinal gene transfer. Vision Res 48:353-359.

Tang ZZ, Hong X, Wang J, Soong TW (2007) Signature combinatorial splicing profiles of rat cardiac- and smooth-muscle Cav1.2 channels with distinct biophysical properties. Cell Calcium 41:417-428.

Tang ZZ, Liang MC, Lu S, Yu D, Yu CY, Yue DT, Soong TW (2004) Transcript scanning reveals novel and extensive splice variations in human l-type voltage-gated calcium channel, Cav1.2 alpha1 subunit. J Biol Chem 279:44335-44343.

Tareilus E, Roux M, Qin N, Olcese R, Zhou J, Stefani E, Birnbaumer L (1997) A Xenopus oocyte beta subunit: evidence for a role in the assembly/expression of voltage-gated calcium channels that is separate from its role as a regulatory subunit. Proc Natl Acad Sci U S A 94:1703-1708.

von Gersdorff H, Matthews G (1996) Calcium-dependent inactivation of calcium current in synaptic terminals of retinal bipolar neurons. J Neurosci 16:115-122.

Wang HG, George MS, Kim J, Wang C, Pitt GS (2007) Ca2+/calmodulin regulates trafficking of Ca(V)1.2 Ca2+ channels in cultured hippocampal neurons. J Neurosci 27:9086-9093.

Wassle H (2004) Parallel processing in the mammalian retina. Nat Rev Neurosci 5:747-757.

Wassle H, Puller C, Muller F, Haverkamp S (2009) Cone contacts, mosaics, and territories of bipolar cells in the mouse retina. J Neurosci 29:106-117.

Weiergraber M, Henry M, Radhakrishnan K, Hescheler J, Schneider T (2007) Hippocampal seizure resistance and reduced neuronal excitotoxicity in mice lacking the Cav2.3 E/R-type voltage-gated calcium channel. J Neurophysiol 97:3660-3669.

West AE, Chen WG, Dalva MB, Dolmetsch RE, Kornhauser JM, Shaywitz AJ, Takasu MA, Tao X, Greenberg ME (2001) Calcium regulation of neuronal gene expression. Proc Natl Acad Sci U S A 98:11024-11031.

Westenbroek RE, Hell JW, Warner C, Dubel SJ, Snutch TP, Catterall WA (1992) Biochemical properties and subcellular distribution of an N-type calcium channel alpha 1 subunit. Neuron 9:1099-1115.

Wheeler DB, Randall A, Sather WA, Tsien RW (1995) Neuronal calcium channels encoded by the alpha 1A subunit and their contribution to excitatory synaptic transmission in the CNS. Prog Brain Res 105:65-78.

White JA, McKinney BC, John MC, Powers PA, Kamp TJ, Murphy GG (2008) Conditional forebrain deletion of the L-type calcium channel Ca V 1.2 disrupts remote spatial memories in mice. Learn Mem 15:1-5.

Wilkinson MF, Barnes S (1996) The dihydropyridine-sensitive calcium channel subtype in cone photoreceptors. J Gen Physiol 107:621-630.

Williams A, Harker N, Ktistaki E, Veiga-Fernandes H, Roderick K, Tolaini M, Norton T, Williams K, Kioussis D (2008) Position effect variegation and imprinting of transgenes in lymphocytes. Nucleic Acids Res 36:2320-2329.

Wiser O, Bennett MK, Atlas D (1996) Functional interaction of syntaxin and SNAP-25 with voltage-sensitive L- and N-type Ca2+ channels. EMBO J 15:4100-4110.

Wiser O, Trus M, Hernandez A, Renstrom E, Barg S, Rorsman P, Atlas D (1999) The voltage sensitive Lc-type Ca2+ channel is functionally coupled to the exocytotic machinery. Proc Natl Acad Sci U S A 96:248-253.

Wong GT, Ruiz-Avila L, Margolskee RF (1999) Directing gene expression to gustducin-positive taste receptor cells. J Neurosci 19:5802-5809.

Wu J, Marmorstein AD, Striessnig J, Peachey NS (2007) Voltage-dependent calcium channel CaV1.3 subunits regulate the light peak of the electroretinogram. J Neurophysiol 97:3731-3735.

Wu SM, Gao F, Maple BR (2000) Functional architecture of synapses in the inner retina: segregation of visual signals by stratification of bipolar cell axon terminals. J Neurosci 20:4462-4470.

Xiao H, Chen X, Steele EC, Jr. (2007) Abundant L-type calcium channel Ca(v)1.3 (alphα1D) subunit mRNA is detected in rod photoreceptors of the mouse retina via in situ hybridization. Mol Vis 13:764-771.

Xu HP, Zhao JW, Yang XL (2002) Expression of voltage-dependent calcium channel subunits in the rat retina. Neurosci Lett 329:297-300.

Yasuda T, Chen L, Barr W, McRory JE, Lewis RJ, Adams DJ, Zamponi GW (2004) Auxiliary subunit regulation of high-voltage activated calcium channels expressed in mammalian cells. Eur J Neurosci 20:1-13.

Zhang J, Schweers B, Dyer MA (2004) The first knockout mouse model of retinoblastoma. Cell cycle 3:952-959.

Zhang XM, Chen BY, Ng AH, Tanner JA, Tay D, So KF, Rachel RA, Copeland NG, Jenkins NA, Huang JD (2005) Transgenic mice expressing Cre-recombinase specifically in retinal rod bipolar neurons. Invest Ophthalmol Vis Sci 46:3515-3520.

ABSTRACT

CHARACTERIZATION OF HIGH-VOLTAGE-ACTIVATED CALCIUM CHANNELS IN RETINAL BIPOLAR CELLS

by

QI LU

August 2013

Advisor: Dr. Zhuo-Hua Pan

Major: Anatomy and Cell Biology

Degree: Doctor of Philosophy

Retinal bipolar cells, conveying visual information from photoreceptors to ganglion cells, segregate visual information into multiple parallel pathways through their diversified cell types and physiological properties. Voltage-gated Ca^{2+} channels could be particularly important underlying the diversified physiological properties of different BCs. In this dissertation, I investigated high-voltage-activated (HVA) calcium currents in retinal bipolar cells in mice. In the first part of my dissertation, I characterized multiple bipolar cell-expressing GFP and/or Cre transgenic mouse lines. In the second part of my dissertation, by performing whole-cell patch-clamp recordings, I examined the electrophysiological properties of HVA calcium currents among CBCs and between CBCs and RBCs. In particular, the second part of my study focused on the investigation of electrophysiological, pharmacological, and molecular properties of HVA calcium currents in RBCs. The results of my studies showed that the HVA Ca^{2+} currents with different electrophysiological properties were observed among CBCs, and between CBCs and RBCs. First, large HVA Ca^{2+} currents were observed in OFF CBCs but not in ON-CBCs. Second, HVA Ca^{2+} currents among different bipolar cells were found to show different activation

potentials. Furthermore, the HVA Ca^{2+} currents in RBCs exhibited two components, a sustained and a transient component with the latter activated at more negative potentials. My pharmacological results indicated that sustained and transient HVA Ca^{2+} currents originated from L- and P/Q type Ca^{2+} channels, respectively. Using L-type Ca^{2+} channel knockout or deficient mouse lines, my results suggest that the L-type Ca^{2+} currents in RBCs are mediated mainly by α1C Ca^{2+} channels with a minor component from α1F Ca^{2+} channels. The studies will advance our understanding of the role of voltage-gated Ca^{2+} channels in basic visual information processing in the retina as well as Ca^{2+} signaling and Ca^{2+} channel deficit-related diseases in the visual system.

AUTOBIOGRAPHICAL STATEMENT

I was born and raised in China. I attended Fudan University, where I received a Bachelor degree of Science in Biology. As an undergraduate student, I had an opportunity to rotate in research laboratories in the School of Life Sciences. There, I learned that the life and study style in lab is completely different from being a student. The overwhelming joy and excitement, which I experienced after weeks of heavy experiments, made a big impression on me. I have never been so excited by anything else. From that point, my goal was to become a research scientist.

I initially chose to study mechanisms of learning and memory. However, during my time in the Institute of Neurobiology I became more interested in the research of the lab next door, whose research interest was the retina. For Chinese culture rules and conventions, it is almost impossible to transfer to other labs especially within the same institute. After successfully applying for PhD program in the US, my new life began in Detroit in 2008, when I join in the lab of Dr. Zhuo-Hua Pan, at Wayne State University School of Medicine. There I start my fascinating research work on visual signal processing and vision restoration.

I have experienced so much during my PhD training. I Mastered patch clamp techniques, deciphered mistakes and figure out improvements. All of these made me stronger. As Elena Ivanova said: "Never, never give up. Never, never stop." I wrote this message on my laboratory bench and imprinted in my heart. The five years of my PhD training was mixed with desperation, confusion, luck and most memorable joy. I look forward to the road ahead, where I will continue pursue happiness as a researcher.